Semiconductor nanostructures have recently attracted growing attention due to their peculiar electronic and optical properties. Questions related to the electronic structure of quantum dots, many-particle effects, and the carrier dynamics are central issues not only from a fundamental point of view, but also for future devices. Electronic and opto-electronic applications depend on the quantum dot energy levels and carrier emission time constants.

Here, the adaption of depletion-layer capacitance spectroscopy for the investigation of self-organized quantum dots is introduced. Quantum dots in two material systems (InAs/GaAs and Ge/Si) are experimentally examined by this method for the first time. Besides clarifying the carrier emission mechanisms, ground state and quantization energies are determined. Good agreement with theoretical predictions for the quantum dot level structure is obtained. The influence of many-particle effects is studied and Coulomb charging and state filling effects are found to dominate for large quantum dots. Furthermore, a microstate description for the carrier dynamics in quantum dot systems is presented, which allows a detailed analysis of the experimental observations.

22,00 €

ISBN 3-89820-238-0

Carrier Emission and Electronic Properties of Quantum Dots

C. Kapteyn

Christian Kapteyn

Carrier Emission and Electronic Properties of Self-Organized Semiconductor Quantum Dots

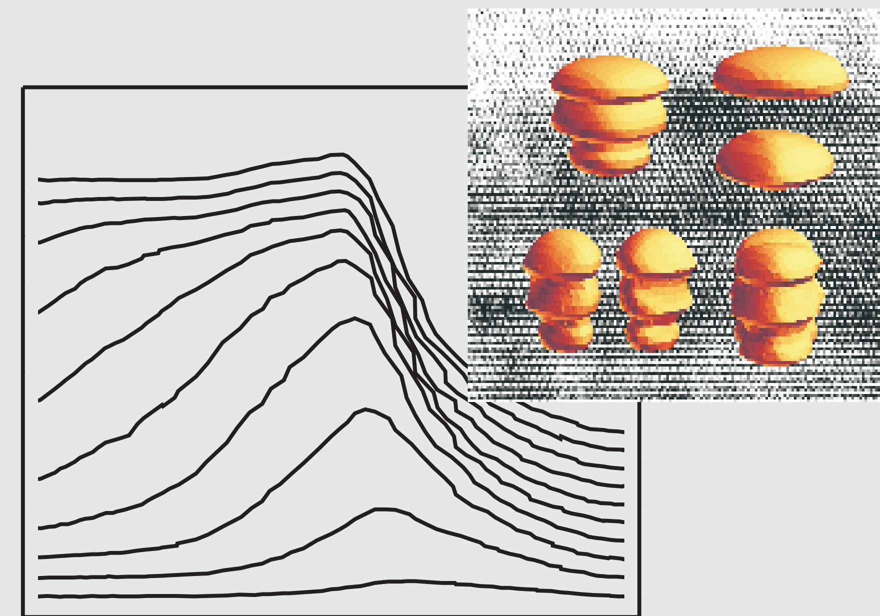

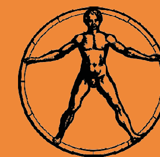

Mensch & Buch Verlag

Carrier Emission and Electronic Properties of Self-Organized Semiconductor Quantum Dots

von

Dipl.-Phys. Christian Kapteyn

aus Berlin

Von der Fakultät II
– Mathematik und Naturwissenschaften –
der Technischen Universität Berlin
zur Erlangung des akademischen Grades

Doktor der Naturwissenschaften
– Dr. rer. nat. –

genehmigte Dissertation

Promotions-Ausschuß:
Prof. Dr. Peter Zimmermann
Prof. Dr. Dieter Bimberg
Prof. Dr. Eckehard Schöll

Tag der wissenschaftlichen Aussprache:
10.5.2001

Berlin 2001

D 83

Die Deutsche Bibliothek - CIP-Einheitsaufnahme

Kapteyn, Christian:

Carrier Emission and Electronic Properties of Self-Organized Semiconductor Quantum Dots / von Christian Kapteyn.

- Berlin : Mensch-und-Buch-Verl., 2001

Zugl.: Berlin, Techn. Univ., Diss., 2001

ISBN 3-89820-238-0

Alle Rechte vorbehalten. Ohne ausdrückliche Genehmigung des Verlages ist es nicht gestattet, das Buch oder Teile daraus zu vervielfältigen.

© MENSCH & BUCH VERLAG, Berlin 2001
Sprengelstr. 4-5, 13353 Berlin • ☎ 030 - 45 49 48 66
http://www.menschundbuch.de • info@menschundbuch.de

Carrier Emission and Electronic Properties of Self-Organized Semiconductor Quantum Dots

Christian Kapteyn

Mensch&Buch Verlag
Berlin

The White Rabbit put on his spectacles.
"Where shall I begin, please your Majesty?" he asked.
"Begin at the beginning," the King said gravely,
"and go on till you come to the end; then stop."

Lewis Carroll, Alice's Adventures in Wonderland

JABBERWOCKY

'Twas brillig, and the slithy toves
Did gyre and gimble in the wabe;
All mimsy were the borogoves,
And the mome raths outgrabe.

"Beware the Jabberwock, my son!
The jaws that bite, the claws that catch!
Beware the Jubjub bird, and shun
The frumious Bandersnatch!"

He took his vorpal sword in hand:
Long time the manxome foe he sought —
So rested he by the Tumtum tree,
And stood awhile in thought.

And as in uffish thought he stood,
The Jabberwock, with eyes of flame,
Came whiffling though the tulgey wood,
And burbled as it came!

One, two! One, two! And through and through
The vorpal blade went snicker-snack!
He left it dead, and with its head
He went galumphing back.

"And hast thou slain the Jabberwock?
Come to my arms, my beamish boy!
O frabjous day! Callooh! Callay!"
He chortled in his joy.

'Twas brillig, and the slithy toves
Did gyre and gimble in the wabe;
All mimsy were the borogoves,
And the mome raths outgrabe.

Lewis Carroll, Through the Looking-Glass

Abstract

In this work, the carrier dynamics and electronic properties of self-organized semiconductor quantum dots are studied by depletion-layer capacitance transient spectroscopy (or deep level transient spectroscopy – DLTS). The first experimental investigations of carrier escape from InAs/GaAs and Ge/Si quantum dots by this method are reported.

In the emission of electrons from a triple-layer of InAs/GaAs quantum dots, thermal activation and tunnel escape from the ground state are clearly identified. The thermally activated process with an activation energy of 94 meV is attributed to the transition from the electron ground state to the first excited state. For single-layer samples an activation energy of 82 meV for electron escape for the same transition is determined. Hole emission from such quantum dots is found to be solely due to thermal activation from the quantum dot hole ground state to the matrix valence band. The activation energy of 194 meV is hence much larger than in the case of electrons. The absence of tunneling in the hole escape process is explained by the larger effective mass, which leads to a decreased tunneling probability. The derived quantum dot energy level scheme agrees well with results from optical investigations, admittance spectroscopy, and predictions based on eight-band $\mathbf{k}\cdot\mathbf{p}$ theory including strain and piezoelectricity. Furthermore, the influence of the electric field and the position of the Fermi level on the emission process is studied.

From the investigation of hole escape from multiply-charged Ge/Si quantum dots, a ground state activation energy of 350 meV was obtained, in good agreement with results from photoluminescence and admittance spectroscopy. Furthermore, hole emission with an activation energy of about 100 meV is observed, which is attributed to carrier escape from the Ge wetting layer. It is demonstrated, that by adjusting filling pulse bias and reverse bias, the quantum dots can be partly filled or emptied. This is reflected also by the activation energy.

From these observations it is concluded that many-particle effects dominate the electronic structure, and thus the carrier capture and emission processes in self-organized quantum dots. By simulating DLTS spectra of carrier escape from quantum dots with help of a microstate model developed in this work, a strong dependence on the electronic structure is revealed. The presented experimental and theoretical results demonstrate the capabilities of capacitance techniques for investigating quantum dot systems.

Zusammenfassung

Ladungsträgerdynamik und elektronische Eigenschaften von selbstorganisierten Quantenpunkten werden in der vorliegenden Arbeit mit Hilfe von Kapazitätstransientenspektroskopie (deep level transient spectroscopy – DLTS) untersucht. Es wird über die ersten mit dieser Methode überhaupt durchgeführten Studien an InAs/GaAs und Ge/Si Quantenpunkten berichtet.

Beim Emissionsprozeß von Elektronen aus einer Dreifachschicht von InAs/GaAs Quantenpunkten werden thermische Aktivierung und Tunnelemission beobachtet. Die Aktivierungsenergie in Höhe von 94 meV wird als Energiedifferenz zwischen Elektronengrundzustand und erstem angeregten Zustand interpretiert. Proben mit einer Einzelschicht InAs/GaAs Quantenpunkte weisen eine Aktivierungsenergie von 82 meV für den entsprechenden Übergang auf. Löcheremission in solchen Quantenpunkten erfolgt ausschließlich aufgrund thermischer Aktivierung vom Quantenpunkt-Grundzustand in das Valenzband des GaAs. Die zugehörige Aktivierungsenergie, 194 meV, ist dementsprechend deutlich größer als diejenige der Elektronen. Tunnelemission für Löcher wird nicht beobachtet, da die wesentlich größere effektive Masse zu einer verminderten Tunnelwahrscheinlichkeit führt. Das aus den Messungen abgeleitete Quantenpunkt-Termschema stimmt gut mit Ergebnissen optischer Untersuchungen, admittanzspektroskopischer Messungen und Berechnungen mit Hilfe der 8-Band $\mathbf{k}\cdot\mathbf{p}$ Theorie überein. Zudem wurde der Einfluss des elektrischen Feldes und der Fermilevel-Position auf den Emissionsprozeß untersucht.

Die Löcheremission aus mehrfach geladenen Ge/Si Quantenpunkten weist eine Grundzustands-Aktivierungsenergie von 350 meV auf, was mit Ergebnissen von Photolumineszenz- und Admittanz-Messungen übereinstimmt. Löcheremission mit einer Aktivierungsenergie von etwa 100 meV wird Ladungsträgern aus dem Wetting-Layer zugeordnet. Es wird gezeigt, daß durch Wahl geeigneter Füllpuls- und Detektionsspannung Quantenpunkte auch nur teilweise geladen oder entleert werden können. Dies spiegelt sich unter anderem in der Aktivierungsenergie wider.

Aus den hier berichteten Beobachtungen ergibt sich, daß Vielteilcheneffekte die elektronischen Eigenschaften und damit die Ladungsträgeremissionsprozesse in selbstorganisierten Quantenpunkten wesentlich beeinflussen. Ein in dieser Arbeit entwickeltes Microstate-Modell erlaubt die Berechnung von DLTS-Spektren der Ladungsträgeremission aus Quantenpunkten. Dabei zeigt sich eine starke Abhängigkeit des DLTS-Signals von der elektronischen Struktur der Quantenpunkte. Die hier präsentierten experimentellen und theoretischen Ergebnisse demonstrieren die besondere Eignung kapazitätsspektroskopischer Methoden für die Untersuchung von Quantenpunkten.

Contents

1 Introduction **1**
- 1.1 General Background . . . 1
- 1.2 Quantum Dots . . . 2
- 1.3 Capacitance Spectroscopy . . . 4
- 1.4 This Work . . . 4

2 Depletion Layer Capacitance Spectroscopy **7**
- 2.1 Depletion Region . . . 8
  - 2.1.1 Schottky Contact . . . 8
  - 2.1.2 p-n Junction . . . 10
  - 2.1.3 Depletion Width . . . 11
  - 2.1.4 Depletion Capacitance . . . 13
- 2.2 Capacitance-Voltage Profiling . . . 14
- 2.3 Deep Levels in Semiconductors . . . 15
  - 2.3.1 Carrier Capture and Emission . . . 16
  - 2.3.2 Detailed Balance Condition in Thermal Equilibrium 17
  - 2.3.3 Majority and Minority Carrier Traps . . . 19
  - 2.3.4 Capture Barrier for Point Defects . . . 19
  - 2.3.5 Temperature Dependence of Emission Rate . . . 20
  - 2.3.6 Influence of the Electric Field . . . 21
  - 2.3.7 Transient Response . . . 24
- 2.4 Capacitance Transient Spectroscopy . . . 26
  - 2.4.1 Work Cycle . . . 26
  - 2.4.2 Capacitance Transients . . . 27
  - 2.4.3 Evaluation of Transient Data . . . 28
- 2.5 Quantum Wells . . . 31
  - 2.5.1 Capacitance-Voltage Characteristic . . . 31

2.5.2 Capacitance Transient Spectroscopy 33
2.6 Quantum Dots 36
2.6.1 Capacitance-Voltage Characteristic 36
2.6.2 Modeling the Capacitance-Voltage Characteristic . 37
2.6.3 Capacitance Transient Spectroscopy 43

3 Carrier Escape Mechanisms in InAs/GaAs Quantum Dots 47
3.1 Electron Emission 47
3.1.1 Samples 48
3.1.2 Capacitance-Voltage Characteristics 51
3.1.3 DLTS Measurements 54
3.1.4 Numerical Calculations of QD Energy Levels . . . 60
3.1.5 Discussion 62
3.2 Comparison of Electron and Hole Emission 66
3.2.1 Samples 66
3.2.2 Capacitance-Voltage Characteristics 69
3.2.3 DLTS Measurements 70
3.2.4 Discussion 75

4 Hole Emission from Many-Particle States in Ge/Si Quantum Dots 81
4.1 Samples 82
4.2 DLTS Experiments and Discussion 85
4.2.1 Partial Filling by Variation of Pulse Bias 86
4.2.2 Partial Emptying by Variation of Reverse Bias . . . 88
4.2.3 Simulations 90
4.3 Summary of the Results 92

5 Carrier Dynamics in Quantum Dots 97
5.1 Two-Level System 98
5.1.1 Emission Transients in a Two-Level System 98
5.1.2 Two-Level System with Electric Field 100
5.1.3 Carrier Relaxation Processes in Quantum Dots . . 101
5.2 Microstate Model 104
5.2.1 Basic Assumptions 105
5.2.2 Master Equation 110
5.2.3 Pure Emission 111
5.2.4 Microstate Model for Optical Carrier Excitation . . 112
5.3 DLTS Simulations 114

5.3.1 QD Dimensions and Filling 115
5.3.2 Microstate Model vs. Conventional Rate Equations 116
5.3.3 Discussion 117

Summary **123**

Outlook **127**

A Experimental Details **129**
A.1 Setup 129
A.2 Sample Processing 130

References **135**

Publications **151**

Acknowledgements **155**

Physical Constants

Symbol	Description	Value	Unit
h	Planck constant	$6.626069 \cdot 10^{-34}$	Js
$\hbar$	$h/2\pi$	$1.05458 \cdot 10^{-34}$	Js
k_B	Boltzmann constant	$1.38066 \cdot 10^{-23}$	J/K
e	Elementary charge	$1.60219 \cdot 10^{-19}$	C
m_0	Electron rest mass	$9.109382 \cdot 10^{-31}$	kg
ε_0	Vacuum permittivity	$8.85418 \cdot 10^{-12}$	F/m

Material Properties

Symbol	Description	Value	Unit
ε_{GaAs}	Relative permittivity of GaAs	13.18	
$m^*_{GaAs,e}$	Effective mass of electrons in GaAs	0.063	m_0
$m^*_{GaAs,lh}$	Effective mass of light holes in GaAs	0.076	m_0
$m^*_{GaAs,hh}$	Effective mass of heavy holes in GaAs	0.5	m_0
$E_{g,GaAs}$	GaAs band gap (at 300 K)	1.424	eV
ε_{InAs}	Relative permittivity of InAs	15.15	
$m^*_{InAs,e}$	Effective mass of electrons in InAs	0.0239	m_0
$m^*_{InAs,lh}$	Effective mass of light holes in InAs	0.026	m_0
$m^*_{InAs,hh}$	Effective mass of heavy holes in InAs	0.35	m_0
$E_{g,InAs}$	InAs band gap (at 300 K)	0.354	eV
ε_{Si}	Relative permittivity of Si	11.9	
$m^*_{Si,hh}$	Effective mass of heavy holes in Si	0.49	m_0
$E_{g,Si}$	Si band gap (at 300 K, indirect)	1.1242	eV
ε_{Ge}	Relative permittivity of Ge	16.2	
$m^*_{Ge,hh}$	Effective mass of heavy holes in Ge	0.284	m_0
$E_{g,Ge}$	Ge band gap (at 300 K, indirect)	0.664	eV

(Source: [LB882, LB887]. All values for room temperature.)

Chapter 1

Introduction

1.1 General Background

The importance of information technology is an outcome of the tremendous progress in semiconductor physics and technology over the last decades. In order to increase computation speed and memory capacity, while simultaneously decreasing power consumption and costs, smaller and smaller structures of integrated circuitry were developed. This process has lead to an exponentially progressing reduction in feature size, which was realized in 1965 by G. Moore [Moo65]. His prediction, known nowadays as ”Moore’s Law”, is commonly rephrased: ”The number of transistors per unit area on a chip doubles about every 18 months.” This prediction has continued to remain valid ever since.

The ongoing demand for further miniaturization of functional semiconductor structures has lead to a typical feature size of about 200 nm; dimensions nowadays realized in commercial computer chips, which were earlier predicted to be beyond physical limits [Hoe72, Sug76]. A slowing-down in the ongoing miniaturization is not in sight. In this process however, one is currently touching the size regime in which quantum mechanics begins to dominate the physical properties, replacing conventional ”bulk” physics. It was realized that lithographically defined structures below a certain size may be regarded as ”artificial atoms”. This term was coined, since such structures exhibit properties similar to those of natural atoms as, e.g. a strong influence from Coulomb interaction on the addition energy spectrum and a δ-function-like density of states [Ash92, Ash93, Kas93, Ash96]. In the magnetic-field depen-

dence of the addition energies, spin effects similar to those known from atomic physics (e.g. Hund's rule) were revealed [Tar96]. The properties of such devices can easily be tailored due to the degrees of freedom of the artificial production process, which opened up a new field of basic research and lead to a wealth of novel applications; e.g. in opto-electronics (semiconductor lasers), electronics (single-electron transistors and memories), and quantum computing. Structures which can controllably confine and release particular electrons are the culmination point of conventional microelectronics. Non-volatile single-electron memory devices may therefore soon be available [Sze99]. First experimental realizations of floating-gate single-electron memory structures have recently been reported [Guo97, Nak97, Wel97].

To allow for operation of single-electron devices at room temperature, structures with dimensions of about 10 nm are necessary. The fabrication of such small structures however, turns out to be technologically extremely challenging, which leads to an second relation, sometimes referred to as "Moore's Second Law": "The cost of a chip-factory also doubles about every 18 months." Taking into account that the cost of such a factory in 1995 was roughly 10^9\$, one obviously approaches a dilemma. The origin of the exponential growth of the equipment costs lies in the nature of the technological production processes. The "top-down" approach realized so far depends on explicit definition and structuring of the semiconductor crystal starting from a macroscopic piece of material. With decreasing feature size, the requirements in machinery precision and resolution increase dramatically.

It is realized, that so-called "bottom-up" approaches may help avoiding the dilemma resulting from the increasing costs of the "top-down" processing. Nature provides innumerable examples of self-organized generation of structures with a complexity and precision, which human-developed technology is not even close to. The application of such "natural" self-organization processes in combination with conventional technology has just begun. The physics of self-organization phenomena in semiconductor crystal growth is hence a topic gaining considerable attention at the moment (see e.g. [Shc99] and references therein).

1.2 Quantum Dots

Modern epitaxial techniques allow the formation of semiconductor crystal layers with atomic precision. The major objective over the past decades has been to create absolutely smooth layers with perfect interfaces.

Strained layer growth however, resulting from the wetting of a plain crystal surface of a matrix material with a substance of different lattice constant, may under certain circumstances lead to the formation of tiny droplets. The resulting structures can be extremely small (typically a few up to several hundred nanometers) and very regular in size and shape (with ensemble-fluctuations of less than 10%), and may appear with very high surface-densities (see [Bim98] and references therein). After covering such a layer with the matrix material, a sheet of tiny inclusions is hence formed. Interestingly, such a self-organized growth-mode has been described already in 1938 by Stranski and Krastanow [Str38b, Str38a]. Only about a decade ago however, the first realizations of semiconductor heterostructures by this method were reported [Eag90, Mo90, Guh90]. These droplets, which may confine carriers in all three spatial dimensions, are commonly referred to as *self-organized*, self-assembled, or self-ordered *quantum dots* (QDs).[1]

Field-effect transistor concepts based on charge-storage in QDs have recently been demonstrated [Tiw96a, Tiw96b, Koi00, Kim00]. A very intriguing approach is the charging of such structures by optical illumination [Ima95, Yus97, Yus98, Fin98, Fin99, Hei00]. By this method, wavelength-domain multiplexing [Mut95] and spectral hole burning in QD ensembles [Sug98] were also recently reported.

For all kinds of applications however, detailed understanding of the electronic properties of the QDs and the processes of carrier capture and exchange with the matrix material is of essential importance. Up to now, mainly optical techniques have been applied to study the properties of self-organized QDs (see [Wog97, Bim98, Jac98, Yof01] and references therein). Such experiments are limited to the detection of light emission due to excitonic recombination and can hence not reveal direct information on the energy levels of electrons and holes in QDs. From the observation of luminescence only indirect conclusions on the carrier dynamics of carriers can be drawn. The determination of emission rates of both types of carriers individually is therefore almost impossible. Finally, the presence of charge, which is the fundamental ingredient of all electronic applications, can not be detected at all by optical techniques. A method capable of accounting for these effects is consequently called for.

[1]Such self-organized QDs, mainly those in the InAs/GaAs material system, were found to exhibit superb optical properties. The application of such QDs for semiconductor lasers has already made tremendous progress (see [Gru00, Led00] and references therein) since the first realization of this concept [Kir94]. QD lasers are currently about to prove their superiority over conventional quantum well technology [Liu99] as was earlier predicted [Ara82].

1.3 Capacitance Spectroscopy

The capacitance is – by definition – an ideal measure for charge. Techniques based on capacitance measurements of depletion layers in semiconductors are therfore widely used in the investigation of electrically active levels due to impurities or point defects [Lan79a, Blo92, Gri81, Bou83, Rho88].[2] Besides information on the electronic properties of such levels, the carrier capture and emission processes can be directly studied by time-resolved capacitance spectroscopy, which is also referred to as ”capacitance transient spectroscopy” or ”deep level transient spectroscopy” (DLTS) [Lan74].

Static capacitance measurements of samples resembling a plate-capacitor with a sheet of QDs embedded close to one of its electrodes were recently reported [Dre94, MR95]. These investigations lead to a direct observation of the quantization of electron and hole levels in self-organized InAs/GaAs QDs. By improving the sensitivity of this approach, the Coulomb charging energy could be determined [MR97b, MR97a]. From studies of the magnetic-field dependence of the addition energy spectra in these structures, similarities to spin-pairing effects in atomic spectra were concluded [Woj96, Fri96, Mil97].

The use of time-resolved capacitance spectroscopy for the investigation of the electronic properties and the carrier dynamics of QDs is a logical step forward. Up until the stage of the commencement of the work presented here however, only a first application of DLTS on GaInP structures with InP QDs embedded was reported [Ana95]. The interpretation of capacitance transient experiments on QDs is significantly more difficult than for investigations of deep levels. This is because of the spatially extent nature of the QDs and the fact that charged QDs represent multi-level many-particle systems.

1.4 This Work

Here, the first comprehensive and systematic studies of self-organized semiconductor QDs with capacitance transient spectroscopy are reported. Two different material systems are investigated; InAs QDs in GaAs and Ge QDs in Si. From the temperature-dependence of the emission rates, the determined activation energies, and the dependence of the DLTS signal on the bias conditions, conclusions are drawn on the emission processes and the QD level

[2]Capacitance techniques have also successfully been employed for the determination of band offsets in semiconductor heterostructures [Kro80] and in the investigation of quantum wells [Deb89, Let91b, Wan96, Lu96, Bro96].

schemes. Furthermore, the particularities of capacitance spectroscopy of QD systems are elucidated and a model for the carrier dynamics of QDs is presented.

In Chapter 2, the basics of depletion-layer capacitance spectroscopy are summarized. After briefly revisiting the fundamentals of static capacitance-voltage measurements, capacitance transient experiments, and the carrier dynamics of deep levels in semiconductors in the first sections, the necessary extension of these concepts is discussed for investigating devices with layers of QDs embedded. In the last section of this chapter, the experimental capacitance-voltage characteristic of a p-n diode containing QDs is also discussed in detail. In the following two chapters, the experimental results are presented. Chapter 3 deals with the carrier escape processes of electrons and holes in InAs/GaAs QDs. In the first part, the contributions of tunneling and thermal activation to electron emission are clarified; in the second part, the differences of the emission mechanisms of electrons and holes are studied. Chapter 4 investigates the particularities of hole emission from Ge/Si QDs. The influence of many-particle effects is clearly revealed. In Chapter 5, a suitable general description of the carrier dynamics in QDs is developed. After summarizing the results of the analysis of a two-level system, a microstate approach is outlined. Based on this model, DLTS measurements are simulated in order to study the correlation between the QD level structure and the DLTS spectra. Finally, the main results are recapitulated and perspectives for possible future investigations are indicated in the Summary.

Chapter 2

Depletion Layer Capacitance Spectroscopy

In this chapter, the underlying physical concepts of the work presented in the remaining part of this work are briefly revisited. To begin with, the basic physics of the capacitance associated with the depletion region of a Schottky barrier or a p-n junction, and the concept of capacitance-voltage profiling in such structures are summarized in Sections 2.1 and 2.2, respectively. Then, carrier capture and emission of a deep level in a semiconductor are discussed and the common procedure of deriving the thermal emission rate from a detailed balance argument is presented in Section 2.3. The investigation of such processes with help of capacitance transient spectroscopy is explained, Section 2.4, before the application of capacitance techniques to the investigation of quantum well and QD structures is adressed in Sections 2.5 and 2.6. Within the latter, the numerical simulation of the capacitance-voltage characteristic of a device with QDs embedded is described and the application of this method to experimental data is demonstrated.

2.1 Depletion Region

The energy of electrons in a metal and a semiconductor (or two differently doped semiconductors) with respect to the vacuum level will not generally be the same. If a metal and a semiconductor (or two differently doped semiconductors) are brought in electric contact, charge in the form of free carriers will flow until both parts are in thermodynamic equilibrium and the Fermi energy E_F is equal throughout the whole structure. As a consequence, ionized donors or acceptors are left behind in the semiconductor leading to a local violation of charge neutrality in the vicinity of the interface. The layer depleted of free carriers is usually referred to as the ”depletion region” [Sze81, Sze85, Blo92].

The width of the depletion region depends on the doping concentration and the potential difference, of which the latter can easily be modified by an externally applied bias. Due to the absence of free carriers, the depletion region is electrically isolating and the origin of the rectifying properties of such semiconductor diode devices.

A metal-semiconductor contact can be described by the Schottky model and is therefore commonly referred to as ”Schottky contact”; a junction of p-doped and n-doped semiconductor material is usually called a ”p-n junction”. The physical picture of the depletion region is briefly sketched in the following sections.

2.1.1 Schottky Contact

Actual metal-semiconductor contacts are usually described in the framework of the Schottky model, as they can be characterized by a barrier height ϕ_b which is essentially independent of an applied external bias.

According to the Schottky model the energy band diagram is constructed by reference to the vacuum level. The work function of the metal ϕ_m and the electron affinity of the semiconductor χ_s are defined as the energies required to remove an electron from the Fermi level or semiconductor conduction band edge, respectively, to the vacuum level. These values are supposed to be material properties, and it is further assumed that the vacuum level is continuous across the interface.

Since at the interface the vacuum level is the same for the two materials, there must be a step between the Fermi level of the metal and the conduction band of the semiconductor due to the difference between ϕ_m and χ_s as depicted in Figure 2.1.

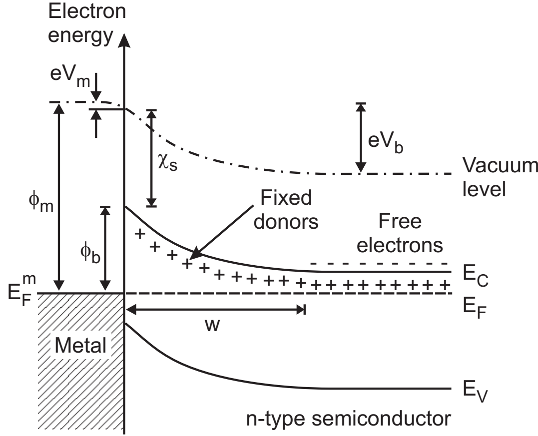

Figure 2.1: *Energy band diagram of a metal-semiconductor Schottky contact.*

The band bending in the metal V_m is very small due to the large electron density and can therefore be neglected. The Schottky barrier at the interface is thus given by

$$\phi_b = \phi_m - \chi_s. \tag{2.1}$$

Moving away from the interface, the conduction band energy changes such that it matches the ”bulk” value E_C with respect to the Fermi level at a certain distance from the contact. The resulting band bending is an effect of the removed free electrons leaving behind a distribution of fixed positive charge due to ionized donors. Where the bands become flat and the associated electric field vanishes, the depletion region ends.

The thickness of the depletion region, the depletion width w, is determined by the net ionized charge density according to Poisson’s equation (see Section 2.1.3). The total zero bias band bending of a Schottky contact, also referred to as ”built-in potential” V_b, can be written

$$eV_b = \phi_m - \chi_s - (E_C - E_F) = \phi_b - (E_C - E_F), \tag{2.2}$$

where e denotes the electron charge.Experimental values for various metal Schottky contacts on GaAs can be found in [Myb98].

2.1.2 p-n Junction

The band diagram of an abrupt p-n junction is considered in a similar manner. Since χ_s is the same for both parts of the junction, the conduction band is continuous. As a consequence, the band bending is caused entirely by the difference in the Fermi level with respect to the conduction band of the two materials. The resulting band scheme is depicted in Figure 2.2, and one obtains for zero external bias

$$\left(E_C^p - E_F\right) + \chi_s = eV_b + \chi_s + \left(E_C^n - E_F\right), \tag{2.3}$$

where the superscripts ”n” and ”p” denote values in the n- or p-doped region of the junction, respectively. The built-in voltage is hence given by

$$eV_b = E_g - \left(E_F - E_V^p\right) - \left(E_C^n - E_F\right), \tag{2.4}$$

where E_g is the energy gap of the semiconductor, i.e. the difference of the conduction band energy E_C and the valence band energy E_V.

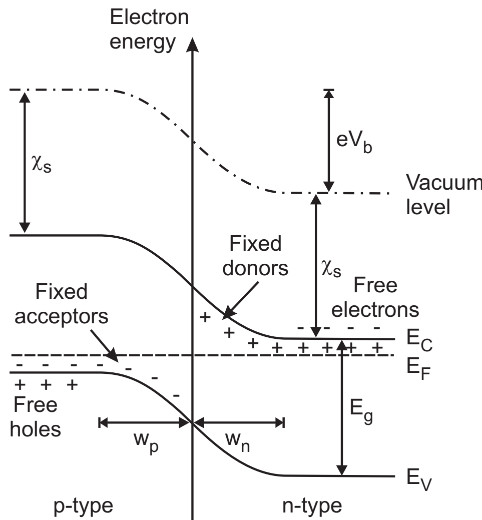

Figure 2.2: *Energy band diagram of a p-n junction.*

In the case of the p-n junction, depletion regions on each side of the contact emerge, where the fixed donor and acceptor charges of density N_d and N_a lead to the band-bending. Due to charge neutrality

$$N_a w_p = N_d w_n \tag{2.5}$$

must hold.

For similar doping concentrations the depletion widths will hence be comparable. For the purpose of capacitance experiments however, the doping is usually chosen such that the depletion region is situated almost entirely on one side of the contact. The depletion region hence resembles the depletion region of a Schottky contact. Such junctions are referred to as ”asymmetrical” p-n junctions, or briefly as p^+-n or n^+-p junctions, for $N_a \gg N_d$ or $N_d \gg N_a$, respectively.

2.1.3 Depletion Width

The total band bending across the depletion region is the sum of the built-in voltage of the contact V_b, defined by Equation (2.2) or (2.4), and the applied external bias V_a in reverse direction.

$$V = V_b + V_a. \tag{2.6}$$

The depletion layer width is calculated from the charge density $\rho(x)$ by integrating Poisson's equation. Here, we consider the simple case of constant doping in the semiconductor, which leads to a constant charge density in the depletion region

$$\rho(x) = eN_d. \tag{2.7}$$

The electrostatic potential ψ is given by Poisson's equation

$$-\frac{\partial^2\psi}{\partial x^2} = \frac{\partial F}{\partial x} = \frac{\rho(x)}{\varepsilon\varepsilon_0} \tag{2.8}$$

or

$$-\frac{\partial^2\psi}{\partial x^2} = \frac{eN_d}{\varepsilon\varepsilon_0} \qquad \text{for} \quad 0 \le x \le w, \tag{2.9}$$

where F is the electric field, ε_0 the vacuum dielectric constant, and ε the dielectric constant of the semiconductor material.

For a Schottky contact or an abrupt asymmetric p^+-n junction, integration of Equation (2.8) gives

$$F(x) = F_0 + \frac{eN_d x}{\varepsilon\varepsilon_0} \qquad \text{for} \quad 0 \le x \le w, \tag{2.10}$$

and $F(x) = 0$ for $x < 0$ or $x > w$. The integration constant F_0 is determined by the boundary condition of vanishing band bending at the edge of the depletion region, i.e. $-\frac{\partial\psi}{\partial x}\Big|_w = F(w) = 0$,

$$F_0 = -\frac{eN_d\,w}{\varepsilon\varepsilon_0} \tag{2.11}$$

and represents the electric field at the interface $F(0)$, where it has its maximum. Therefore

$$F(x) = \frac{eN_d}{\varepsilon\varepsilon_0}(x-w). \tag{2.12}$$

As boundary condition for integrating Equation (2.10), one notices that the band bending in the present approximation occurs only on the right-hand side of the junction. The contact potential is therefore equal to the total band bending $\psi(0) = -V$. The potential distribution along the depletion region is hence given by

$$\psi(x) = \frac{eN_d\,w}{\varepsilon\varepsilon_0}\left(x - \frac{x^2}{2w}\right) - V \qquad \text{for} \quad 0 \le x \le w, \tag{2.13}$$

with $\psi(x) = 0$ for $x > w$, and $\psi(x) = -V$ for $x < w$. Since the potential on the right edge of the depletion region is set to zero, $\psi(w) = 0$, one obtains

$$V = \frac{eN_d}{2\varepsilon\varepsilon_0}w^2, \tag{2.14}$$

or the expression for the depletion width

$$w = \sqrt{\frac{2\varepsilon\varepsilon_0}{eN_d}V}. \tag{2.15}$$

Beyond the Depletion Approximation

The assumption of an abrupt depletion layer edge, the so-called ”depletion approximation”, is not generally true. In a neutral non-degenerate n-type semiconductor in thermal equilibrium, the free carrier density n is given by the Boltzmann relation as function of the temperature T and the conduction band edge relative to the Fermi energy

$$n = N_C \exp\left(-\frac{E_C - E_F}{k_B T}\right), \tag{2.16}$$

where k_B is the Boltzmann constant and N_C the effective density of conduction band states. In the same manner one obtains for a non-degenerate free hole concentration

$$p = N_V \exp\left(-\frac{E_F - E_V}{k_B T}\right), \tag{2.17}$$

where N_V is the effective density of valence band states.

Equation (2.7) can thus be rewritten using Equation (2.16)

$$\rho(x) = e\left(N_d - n(x)\right). \tag{2.18}$$

With the first order approximation for $n(x)$ from Equation (2.16) the charge density may be written [Blo92]

$$\rho(x) = eN_d \left\{1 - \exp\left[-\frac{1}{2}\left(\frac{w-x}{L_D}\right)^2\right]\right\}, \tag{2.19}$$

where the Debye length L_D is given by

$$L_D = \sqrt{\frac{\varepsilon\varepsilon_0 k_B T}{e^2 N_d}}. \tag{2.20}$$

L_D represents the distance over which free electrons redistribute themselves in the vicinity of a fixed charge. The essence of the depletion approximation is thus, that the errors involved in the assumption of an abrupt depletion layer edge are small provided $w \gg L_D$ or $V \gg k_B T/2e$.

2.1.4 Depletion Capacitance

The capacitance associated with the depletion region is known as the depletion capacitance. It arises from the fixed space charge of the ionized donors or acceptors. When the applied reverse bias is increased by a small increment ΔV the depletion width increases leading to an increase in fixed charge per area ΔQ. The associated capacitance per area for a small bias signal ΔV is therefore given by

$$C = \lim_{\Delta V \to 0} \frac{\Delta Q}{\Delta V} = \frac{dQ}{dV}. \tag{2.21}$$

Note, that throughout this work C and Q are always given per unit area. With Equation (2.6) one notices that $dV = dV_b + dV_a = dV_a$, since V_b is constant.

In order to calculate the total charge Q stored in the depletion region in terms of the total band bending V, Poisson's equation is integrated and then Gauss' theorem is applied. This procedure [Blo92] yields the capacitance per area[1]

$$C = \sqrt{\frac{\varepsilon\varepsilon_0 e N_d}{2V}} = \frac{\varepsilon\varepsilon_0}{w} \qquad \text{for} \quad V \gg k_B T/e, \tag{2.22}$$

The depletion capacitance as given by Equation (2.22) hence resembles the capacitance per unit area of a plate capacitor with a distance of w between the plates and a dielectric with relative permitivity ε, although the charge is actually stored in the *volume* rather than on the edges of the depletion region.

2.2 Capacitance-Voltage Profiling

In the previous section the dependence of the capacitance on the width of the depletion region, i.e. the doping concentration and the applied bias, was derived. Due to this dependence, capacitance-voltage measurements (C-V) are widely used for measuring depth profiles of the apparent doping concentration in semiconductor devices.

From rewriting Equation (2.22) with help of Equation (2.15)

$$\frac{1}{C^2} = \frac{2V}{\varepsilon\varepsilon_0 e N_d} \tag{2.23}$$

it becomes apparent that plotting $1/C^2$ versus V yields a straight line for constant doping. The apparent doping concentration N_d^{CV} can hence be determined from

$$N_d^{CV} = \frac{2}{\varepsilon\varepsilon_0 e}\left(\frac{d(1/C^2)}{dV}\right)^{-1}. \tag{2.24}$$

Furthermore, the applied bias for which $\frac{1}{C^2} = 0$ corresponds to the built-in voltage.

Even for a varying doping density, Equation (2.24) remains valid, since in the depletion layer approximation the charge fluctuations only occur at the

[1]The expression for the capacitance can also be obtained from the following argument: From Equation (2.7) it is obvious that for constant doping the increment in charge depends on an increment in the depletion width as $dQ = eN_d dw$. The change in voltage is determined from Equation (2.15) as $dV = \frac{eN_d}{\varepsilon\varepsilon_0} w\,dw$. The capacitance is hence $C = \frac{dQ}{dV} = \frac{\varepsilon\varepsilon_0}{w}$.

depletion layer edge. With help of Equation (2.24) an apparent doping-voltage profile $N_d^{CV}(V)$ and with

$$w = \frac{\varepsilon\varepsilon_0}{C(V)} \tag{2.25}$$

a depth profile of the doping density $N_d^{CV}(w)$ can hence be determined from a measurement of the capacitance as function of the applied reverse voltage.

The values however, of the depletion width w and therefore the capacitance C cannot be given anymore in the simple shape of Equation (2.15), since ρ is not constant and depends on the depth. The depletion width is hence determined by the more general expression for the total potential drop in the abrupt junction case

$$V = \frac{1}{\varepsilon\varepsilon_0} \int_0^w x\rho(x)dx. \tag{2.26}$$

From the discussion of the depletion approximation it is clear, that the depth resolution of the capacitance-voltage profiling method presented here has a fundamental limit of about $\pm L_D$. Reference [Blo92] gives a more detailed discussion of this method, its limitations, and the interpretation of capacitance-voltage profiles.

2.3 Deep Levels in Semiconductors

So far, only the properties of semiconductors being dominated by an effective doping due to shallow states close to the band edges were considered; these states are effectively ionized for practical temperatures. Capacitance spectroscopy however, is widely used to study deeper states. Electron or hole states are usually referred to as ”deep” if their binding energy relative to the conduction band or valence band, respectively, is larger than several k_BT.

Bound states in QDs can be treated – in some respect – as deep levels, since they can confine and exchange carriers with the surrounding material in a similar way as common defects. In this section, the basic description of the carrier dynamics of such a deep level system is developed in a conventional rate equation approach. The discussion of carrier dynamics in this section will hence generally refer to deep levels or more briefly ”traps”, without taking into account the particularities of QD systems, which are discussed in Chapter 5.2.

2.3.1 Carrier Capture and Emission

A trap level in the band gap of a semiconductor can change its state by four different dynamic processes, namely the individual capture and emission processes for electrons and holes. The efficiency of the capture process is characterized by a capture cross-section σ times the carrier flux, which is determined by the density of carriers n, Equation (2.16), times the root-mean-square thermal carrier velocity $<v>$. If the total trap density per volume is N_t and a fraction $f \in [0,1]$ of these are occupied at any instant t, there are hence $1-f$ empty states, which can capture electrons. The change of the occupation due to capture is therefore given by

$$\frac{df}{dt} := \frac{\partial f}{\partial t} = \sigma_n <v_n> n(1-f), \tag{2.27}$$

where the subscripts "n" and "p" denote electron- and hole-related properties, respectively. The electron capture rate is defined as

$$c_n = \frac{\frac{df}{dt}}{1-f}, \tag{2.28}$$

and therefore

$$c_n = \sigma_n <v_n> n. \tag{2.29}$$

The hole capture rate is accordingly

$$c_p = \frac{\frac{\partial(1-f)}{\partial t}}{f} = -\frac{\frac{df}{dt}}{f} = \sigma_p <v_p> p. \tag{2.30}$$

The occupancy of the deep level is determined by the interplay of the emission and capture processes of electrons and holes as depicted in Figure 2.3 for an n-type material. With the emission rate for electrons and holes, e_n and e_p, respectively, the net rate of change in the electron occupancy of the trap is[2]

$$\frac{df}{dt} = (c_n + e_p)(1-f) - (e_n + c_p)f, \tag{2.31}$$

since holes can be emitted and electrons captured at the $1-f$ states unoccupied with electrons, while electrons can be emitted and holes captured at the f states occupied with electrons.

[2]The emission rates e_n and e_p represent the probability per unit time that a particular electron or hole is emitted.

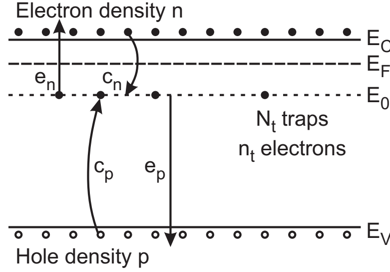

Figure 2.3: *Electron and hole capture and emission processes for a trap with energy level E_0 and volume density N_t being occupied with an electron density of n_t in an n-type semiconductor.*

For a weak concentration of deep states N_t compared to the net doping $N_d - N_a$, the influence of the trap on the free carrier concentrations n and p in the semiconductor are negligible. Therefore n and p can be considered constant and solutions to the rate Equation (2.31) may be obtained subject to the boundary conditions.

2.3.2 Detailed Balance Condition in Thermal Equilibrium

For the following examination of the time-dependent behaviour of the occupancy of the deep states, it is noted, that whatever the initial conditions might be the system will strive to reach thermodynamic equilibrium, which implies the principle of detailed balance. Therefore the capture and emission rate of electrons must be equal and the same must hold for the capture and emission rate of holes. These requirements have to be fulfilled in addition to the steady state condition of $\frac{df}{dt} = 0$. Thus

$$e_n f = c_n(1-f) \tag{2.32}$$

and

$$e_p(1-f) = c_p f. \tag{2.33}$$

These equations allow to derive the trap occupancy in thermal equilibrium $\tilde{f}$

$$\tilde{f} = \frac{c_n}{c_n + e_n} = \frac{e_p}{e_p + c_p}. \tag{2.34}$$

The occupancy of a trap in thermal equilibrium is on the other hand defined by the Fermi-Dirac distribution function [Kit80]. For a deep level of energy E_0, with degeneracy g_0 if empty, and g_1 when occupied, the occupancy is [Lan81, Bou83]

$$\tilde{f} = \frac{1}{1 + \frac{g_0}{g_1} \exp\left(\frac{E_0 - E_F}{k_B T}\right)}. \tag{2.35}$$

For a common spin-degenerate level holds $\frac{g_0}{g_1} = \frac{1}{2}$. Combining Equation (2.34) and Equation (2.35) hence yields for electrons

$$\frac{e_n}{c_n} = \frac{g_0}{g_1} \exp\left(\frac{E_0 - E_F}{k_B T}\right) \tag{2.36}$$

and analogously for holes

$$\frac{e_p}{c_p} = \frac{g_1}{g_0} \exp\left(\frac{E_F - E_0}{k_B T}\right). \tag{2.37}$$

Equations (2.36) and (2.37) imply for $E_0 < E_F$ that $c_n > e_n$ and $e_p > c_p$ so that the state in equilibrium will be occupied by electrons. From $E_0 > E_F$ results that $c_n < e_n$ and $e_p < c_p$, and conclusively the state in equilibrium will be occupied by holes.

It is important to notice here, that the *dynamic* quantities of the capture and emission rates according to Equations (2.36) and (2.37) are determined by the *equilibrium* occupancy of the deep level given through E_0, E_F, and Equation (2.35). This can only hold true of course, as long as E_0 does not depend on the trap occupation.

It is also worth noticing that the capture rates c_n and c_p depend on the doping concentration, whereas the capture cross-sections σ_n and σ_p, as well as the emission rates e_n and e_p, are intrinsic properties of the deep level.

In a non-degenerate semiconductor, i.e. $n < N_C$, the free electron concentration is determined by the Boltzmann relation, Equation (2.16), whereas the occupancy of the deep level is given by the Fermi-Dirac distribution function, Equation (2.35), since f may be as large as 1. Substituting Equation (2.29) into Equation (2.36) yields for the electron emission rate

$$e_n = \sigma_n <v_n> n \, \frac{g_0}{g_1} \exp\left(\frac{E_0 - E_F}{k_B T}\right), \tag{2.38}$$

and with Equation (2.16)

$$e_n = \sigma_n <v_n> \frac{g_0}{g_1} N_C \exp\left(-\frac{E_C - E_0}{k_B T}\right). \tag{2.39}$$

Substituting Equations (2.30) and (2.17) into Equation (2.37) results in

$$e_p = \sigma_p <v_p> \frac{g_1}{g_0} N_V \exp\left(-\frac{E_0 - E_V}{k_B T}\right). \tag{2.40}$$

2.3.3 Majority and Minority Carrier Traps

From Equations (2.39) and (2.40) it is clear that trap states in the upper half of the band gap have $e_n > e_p$, since $E_C - E_0 < E_0 - E_V$. For trap states in the lower half of the band gap consequently holds the opposite, $e_p > e_n$. In the former case the deep level is referred to as an *electron trap* and in the latter as a *hole trap*.[3] Equation (2.31) hence simplifies for an electron trap to

$$\frac{df}{dt} = c_n(1-f) - e_n f. \tag{2.41}$$

Without further going into detail, in an n-type semiconductor, an electron trap captures the predominant carrier type and is therefore commonly referred to as *majority carrier trap*, whereas a hole trap would be a *minority carrier trap*. In a p-type semiconductor, a hole trap must hence be referred to as a majority carrier trap and an electron trap as a minority carrier trap.

2.3.4 Capture Barrier for Point Defects

The charge in an occupied trap may lead to a local band bending E_α, which decreases the local density of states in the majority carrier band of the matrix material around the trap.[4] As a consequence according to Equation (2.29), the capture rate is reduced. E_α is hence referred to as the capture barrier. In an n-type semiconductor with an electron trap, E_C is locally increased in linear approximation by fE_α and n (and hence c_n) is accordingly reduced by a factor $\exp(-fE_\alpha/k_B T)$. Therefore Equation (2.41) has to be rewritten

$$\frac{df}{dt} = c_n \exp\left(\frac{-fE_\alpha}{k_B T}\right)(1-f) - e_n f, \tag{2.42}$$

---

[3] More precisely, one refers to an electron trap if $E_0 > \tilde{E}$, where $\tilde{E} = E_{iF} + \frac{kt}{2} \ln\left(\frac{\sigma_p <v_p> g_1/g_0}{\sigma_n <v_n> g_0/g_1}\right)$, and to a hole trap for $E_0 < \tilde{E}$. The Fermi level in intrinsic material E_{iF} is determined by $n = p$, which must be fulfilled in the absence of dopants. With Equations (2.16) and (2.17) $E_{iF} = \frac{1}{2}(E_C + E_V) + \frac{k_B T}{2} \ln\left(\frac{N_V}{N_C}\right)$.

[4] E_α is assumed to be the band bending for the *equilibrium* occupation of the trap.

The additional contribution E_α to the electrochemical potential also modifies the equilibrium carrier distribution, Equation (2.35), to

$$\tilde{f} = \frac{1}{1 + \frac{g_0}{g_1} \exp\left(\frac{E_0 - E_F + \tilde{f} E_\alpha}{k_B T}\right)}. \tag{2.43}$$

The interdependence of c_n and e_n however, and therefore the expression for the emission rate given by Equation (2.39) remain unchanged, since also Equation (2.34) is modified towards [Hed95]

$$\tilde{f} = \frac{1}{1 + \frac{e_n}{c_n} \exp\left(\frac{\tilde{f} E_\alpha}{k_B T}\right)}. \tag{2.44}$$

Only the capture rate c_n is hence really changed by the presence of a capture barrier.[5]

The capture behaviour of a deep level system with a capture barrier has been studied experimentally for dislocations and point defects in Si by Omling et al. [Oml85]. A theoretical discussion of many-electron defects with capture barriers can be found in [Hed95].

2.3.5 Temperature Dependence of Emission Rate

Equations (2.39) and (2.40), which were obtained from the detailed balance condition, already indicate the temperature dependence of the emission rates.

For electrons, the root-mean-square (rms) thermal velocity is given by

$$<v_n> = \sqrt{\frac{3 k_B T}{m_e^*}}, \tag{2.45}$$

where m_e^* is the effective mass of the electrons in the conduction band. The conduction band density of states N_C is given by

$$N_C = 2 M_C \left(\frac{2\pi m_e^* k_B T}{h^2}\right)^{\frac{3}{2}}, \tag{2.46}$$

[5]Note, that this conclusion only holds provided that the interaction strength between the charge located at the defect and the carriers in the matrix, and the interaction strength between carriers located on the defect are identical. For a point defect this may be a valid assumption. In the case of a QD however, the intra-QD carrier interaction may be expected to be stronger, due to the finite QD dimensions.

where M_C is the number of conduction band minima, and h is Planck's constant.

Equation (2.39) hence gives

$$e_n(T) = \gamma_n \frac{g_0}{g_1} T^2 \sigma_n \exp\left(-\frac{E_C - E_0}{k_B T}\right), \tag{2.47}$$

where γ_n is a temperature independent constant

$$\gamma_n = \sqrt{12(2\pi)^3}\, \frac{k^2}{h^3} M_C m_e^*. \tag{2.48}$$

Analogously the hole emission rate is

$$e_p(T) = \gamma_p \frac{g_1}{g_0} T^2 \sigma_p \exp\left(-\frac{E_0 - E_V}{k_B T}\right), \tag{2.49}$$

where γ_p is

$$\gamma_p = \sqrt{12(2\pi)^3}\, \frac{k^2}{h^3} M_V m_h^*. \tag{2.50}$$

Equations (2.47) and (2.49) thus describe thermally activated emission processes and it is obvious that a plot of $\ln\left(e_n/T^2\right)$ or $\ln\left(e_p/T^2\right)$ as function of T^{-1} yields a straight line with a slope of $E_C - E_0$ or $E_0 - E_V$, respectively.

Thermally activated capture due to nonradiative processes (e.g. capture by multi-phonon emission) as described in [Bou83], which can lead to a dependence of the capture cross-section on temperature, are not further discussed here.

2.3.6 Influence of the Electric Field

The presence of an electric field F tilts the band structure, which may lead to three mechanisms of emission enhancement [Bou83]: (i) the Poole-Frenkel effect (barrier lowering of a spatially extent potential), (ii) pure tunneling, and (iii) phonon-assisted tunneling, where the carrier absorbs energy from the lattice and then tunnels through the barrier at higher energy. These mechanisms are illustrated in Figure 2.4. Here, only the case of a square potential well is considered, which is a good first approximation for the confining potential in a QD.

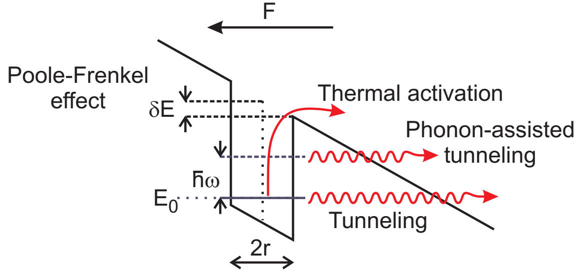

Figure 2.4: *Three mechanisms of field enhanced emission for a confined energy level E_0 in a square potential well: Poole-Frenkel effect (barrier lowering), pure tunneling, and phonon-assisted tunneling (only the one-phonon resonance is indicated).*

Poole-Frenkel Effect

The Poole-Frenkel effect is a classical effect, where the carrier is still emitted by thermal activation over the top of a potential barrier, which is lowered by the presence of an electric field. A one-dimensional model was presented by Frenkel [Fre38], which slightly overestimates the emission enhancement. This is because the Frenkel model regards the emission enhancement only for the direction parallel to the electric field, where it has its maximum. Based on the expression for the emission rate without field e_n one commonly writes

$$e_n^{1d}(F) = e_n \exp\left[\frac{\delta E(F)}{k_B T}\right] = \sigma_n <v_n> \frac{g_0}{g_1} N_C \exp\left[-\frac{E_0 - \delta E(F)}{k_B T}\right], \quad (2.51)$$

where E_0 is the zero-field activation energy and $\delta E(F)$ the effective change in the activation energy of the level, which is for a square potential well with radius r

$$\delta E(F) = eFr. \quad (2.52)$$

From more accurate three-dimensional calculations for a point defect, it follows that Equation (2.51) must be rewritten in the square-well potential case[6] [Har68]

$$\frac{e_n^{3d}}{e_n} = \frac{k_B T}{2\delta E(F)} \left(\exp\left[\frac{\delta E(F)}{k_B T}\right] - 1 \right) + \frac{1}{2}. \quad (2.53)$$

[6] For a Coulomb potential a slightly different relation applies, namely $e_n^{3d}/e_{n0} = (1/\gamma^2)[e^{\gamma}(\gamma - 1) + 1] + 1/2$, where $\gamma = (eF/\pi\varepsilon_0\varepsilon_r)^{1/2} e/k_B T$.

The influence of this kind of field-effect has been studied theoretically for various potential shapes [Mar81]. An example of the influence of the Poole-Frenkel effect on carrier escape is, e.g. electron emission from the deep Ti donor level in InP [Bab92].

Pure Tunneling

If the band structure is tilted due to the presence of an electric field, tunneling through the resulting barrier of finite width becomes possible. Tunneling from a Dirac well with height ΔE into an continuous energy band has been calculated by a Green's function approach [Kor77] and in Oppenheimer approximation. The resulting tunnel rate P_t (or emission probability P) is [Vin79, ME82a][7]

$$P_t(\Delta E) = \frac{eF}{4\sqrt{2m^*\Delta E_0}} \exp\left[-\frac{4}{3}\sqrt{\frac{2m^*}{\hbar^2}}\frac{\Delta E_0^{3/2}}{eF}\right]. \tag{2.54}$$

The exponential factor is the common expression for the transparency of a triangular barrier.

Phonon-Assisted Tunneling

Depending on the temperature, the potential shape and depth, and the electric field, also phonon-assisted tunneling must be taken into consideration. This has been done in a semi-classical approach [Vin79, Mar81] and by a fully quantummechanical model [ME82a, ME82b]. The emission rate is found to be strongly enhanced by the interaction of the initial level with phonon modes available in the lattice, which lead to a set of stationary quasi-levels separated by the phonon energy $\hbar\omega$. Tunneling can then occur from any of theses levels to the conduction band. If the phonons are assumed to be linearly coupled to the level, the coupling strength is described by the "Huang-Rhys" parameter S [Hua50]. The occupation probability is hence a function of $S, \hbar\omega$, and T.

From this approach, the phonon-assisted tunnel rate R can be obtained by summing over the number m of phonons involved [ME82a, ME82b]

$$R = \sum_{m=-\infty}^{+\infty} W_m P_t(E_{a,0} + m\hbar\omega), \tag{2.55}$$

[7] Note the misprints in the prefactor of Equation (9) in [ME82a].

where P_t is given by Equation (2.54) and W_m is the statistic weight commonly applied in multi-phonon calculations [Kei65]

$$W_m = \exp\left[\frac{m\hbar\omega}{2k_BT} - S\coth\left(\frac{\hbar\omega}{2k_BT}\right)\right] I_m\left(\frac{S}{\sinh(\hbar\omega/2k_BT)}\right), \tag{2.56}$$

where I_m is the modified Bessel function of order m. For the W_m holds $\sum_{m=-\infty}^{+\infty} W_m = 1$.

Vincent et al. demonstrated, that for spatially extent potentials as, e.g. the Coulomb potential of deep levels in semiconductors, both the Poole-Frenkel effect and phonon-assisted tunneling are important for typical electric fields ($10^6 \ldots 10^8$ V/m) [Vin79]. The same was found true for other potential shapes [Mar81]. The influence of phonon-assisted tunneling has been studied experimentally for deep levels in various material systems [ME80, Irm83, Qur92, Dad97].

2.3.7 Transient Response

In order to describe the transient behaviour determined by Equation (2.31) of the trap occupation from an arbitrary initial state towards the thermal equilibrium, the notation shall be simplified by introducing a and b as being the sum of the rates of electron gain and loss, respectively. Thus rewriting Equation (2.31) with $a = c_n + e_p$ and $b = e_n + c_p$. yields

$$\frac{df}{dt} = a(1-f) - bf. \tag{2.57}$$

With the boundary condition of the initial occupancy of the traps, given by $f_0 = f(t=0)$, the general solution of Equation (2.57) is

$$f(t) = \frac{a}{a+b} - \left(\frac{a}{a+b} - f_0\right)\exp\left[-(a+b)t\right]. \tag{2.58}$$

The steady state trap occupancy f_∞ is obtained for $t = \infty$ (or from setting Equation (2.31) equal to zero):

$$f_\infty = f(\infty) = \frac{a}{a+b}. \tag{2.59}$$

In general one can hence write

$$f(t) = f_\infty - (f_\infty - f_0)\exp(-t/\tau), \tag{2.60}$$

where τ is the time constant given by

$$\tau^{-1} = a + b = c_n + e_n + c_p + e_p. \tag{2.61}$$

There are two frequently encountered situations for which Equation (2.58) simplifies to a certain extent. First, when the trap state is initially fully occupied one obtains

$$f(t) = \frac{a}{a+b} + \frac{b}{a+b} \exp\left[-(a+b)t\right], \qquad \text{since} \quad f_0 = 1. \tag{2.62}$$

And second, when the trap state is initially empty

$$f(t) = \frac{a}{a+b} \left(1 - \exp\left[-(a+b)t\right]\right), \qquad \text{since} \quad f_0 = 0. \tag{2.63}$$

Initially Filled Majority Carrier Traps

At first sight the dynamics of the trap occupation seems rather complicated, since it generally depends on the four mechanisms of capture and emission of holes and electrons, Equation (2.31). The situation for majority carrier traps in the depletion region however, is considerably simpler, since (i) usually $e_n \gg e_p$ for an electron trap and $e_p \gg e_n$ for a hole trap (cf. Section 2.3.3), and (ii) the free carrier density vanishes in the depletion region leading to $c_n = 0$ or $c_p = 0$ according to Equation (2.29) or (2.30), respectively.[8] Therefore the transient occupation of an *initially completely filled* electron trap, $f_0 = 1$, in the depletion region of an n-type semiconductor is given by

$$\frac{df}{dt} = -e_n f(t) \tag{2.64}$$

and integration thus leads to

$$f(t) \sim \exp(-e_n t). \tag{2.65}$$

For less well-defined initial conditions, the general solution of Equation (2.31), given by Equation (2.58) (or its simplification for initially filled or empty traps, Equation (2.62) or (2.63), respectively), has to be considered.

[8] It is furthermore assumed that the emitted carriers are rapidly swept out of the depletion region by the electric field and therefore no re-capturing can take place.

2.4 Capacitance Transient Spectroscopy

According to Equation (2.26) the depletion width depends on the bias and on the integrated charge in the depletion region. The associated capacitance is hence a sensitive measure for the occupancy of deep levels situated at some position inside the depletion region [Kim74]. The investigation of the transient behaviour of the depletion capacitance after the preparation of a defined initial state therefore allows to draw conclusions on the according carrier dynamics.

Historically, the technique of deriving the trap parameters from the temperature dependence of the transient capacitance has been developed and widely used for studying deep levels due to impurities and defects. In this context it is usually referred to as ”Deep Level Transient Spectroscopy” (DLTS) or ”Capacitance Transient Spectroscopy” [Lan74, Mil77, Lan79b, Rho88, Gri81, Bou83]. Besides the determination of activation energies and capture cross-sections of traps, DLTS also permits to obtain a depth profile of the trap concentration density and the investigation of the influence of the electric field on the emission process, by suitably adjusting the biasing conditions. For the analysis of this technique however, the trap concentration must be assumed to vary only slowly with depth compared to L_D.

2.4.1 Work Cycle

In order to prepare a defined initial state of the traps in the device under investigation, a certain reverse bias V_r is applied, such that a depletion region with a suitable width is formed in which all traps are emptied of carriers. Then a bias pulse of duration t_p and relative height V_h is applied, which reduces the overall bias and conclusively leads to narrower depletion region. The absolute bias during the pulse is given by $V_p = V_r - V_h$. Initially empty traps from inside the depletion region are now situated outside the depletion region, capture free carriers, and are thus filled.

After the pulse, the depletion width is again increased due to the larger reverse bias, and the traps start to re-emit carriers. The situation is thus re-approaching the one before the pulse. The free carriers are considered to follow the change in external bias instantaneously on the time-scale of the experiment. The emission of carriers from the trap states however, depends on the localization energy $E_C - E_0$ and is usually much slower. Its time-dependence can hence be measured by a capacitance meter. This sequence is schematically pictured in Figure 2.5. During the experiment, usually several consecutive capacitance

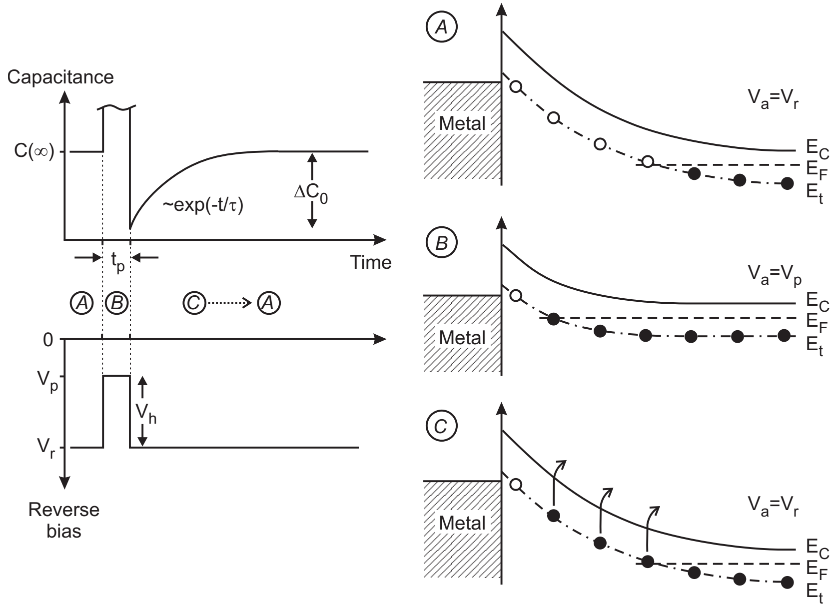

Figure 2.5: *Work cycle during a DLTS measurement. The lower left part of the figure displays the external bias on the device as a function of time, the upper left part the corresponding capacitance (for an exponential emission process with time constant τ). The schematic band structures for the different situations A, B, and C – before, during, and after the pulse, respectively – are displayed on the right-hand side.*

transients are recorded and averaged in order to increase the signal-to-noise ratio.

2.4.2 Capacitance Transients

The general capacitance transient $\Delta C(t)$ with respect to the steady state capacitance $C = C(t = \infty)$ for a small trap concentration ($N_t \ll N_d$) of simple point defects can be derived from the time dependence of the trap occupation [Blo92] as

$$\frac{\Delta C(t)}{C} = \frac{C(t) - C}{C} = -\frac{1}{2}\left(\frac{x_r^2 - x_p^2}{w_r^2}\right)\frac{N_t}{N_d}\left[f(t) - f_\infty\right]. \tag{2.66}$$

Here, w_r is depletion width under reverse bias in equilibrium and the values x_r and x_p reflect the positions for which the trap energy E_0 corresponds to the Fermi level E_F after and during the pulse, respectively. Thus $x_r = w_r - \lambda$ and $x_p = w(V_p) - \lambda$, where the transition distance λ corrects for the difference between the trap energy and the Fermi level, and is given by

$$\lambda = \sqrt{\frac{2\varepsilon\varepsilon_0}{e^2 N_d}\,(E_F - E_0)}. \tag{2.67}$$

It is worth noting, that for the capture dynamics during the pulse the depletion approximation is of crucial importance. It is concluded that capture in the Debye tail of the depletion region may lead to an additional slower filling time constant, which may disturb the measurement of the capture cross-section [Pon84].

From Equation (2.60) one obtains the general result

$$\Delta C(t) = -\Delta C_0 \exp(-t/\tau), \tag{2.68}$$

where ΔC_0 is the initial change in capacitance at $t = 0$. For the emission from an initially filled majority carrier trap $f(t)$ is given by Equation (2.65) and $f_\infty = 0$, hence

$$\Delta C(t) = -\Delta C_0 \exp(-e_n t), \tag{2.69}$$

and

$$\frac{\Delta C_0}{C} = -\frac{1}{2}\left(\frac{x_r^2 - x_p^2}{w_r^2}\right)\frac{N_t}{N_d}. \tag{2.70}$$

The trap concentration N_t can thus be determined from a measurement of ΔC_0 and C.

2.4.3 Evaluation of Transient Data

In order to obtain characteristic trap properties as the activation energy and the capture cross-section from a set of recorded capacitance transients at various temperatures, data evaluation procedures are commonly applied. One basically investigates the contribution to the observed emission process at a chosen reference time constant. From plotting the amplitude of the emission at that reference time constant as function of temperature, or from investigating the strength of the emission at a given temperature for varying reference time constant, relations between temperature and emission rate can be evaluated.

There are several methods for obtaining the emission contribution at a chosen reference time constant, of which only the simple rate window concept and the double-boxcar method shall be described in the following. Then, the two above mentioned evaluation methods are briefly introduced.

Rate Window Concept

The selection of the contribution at a certain reference time constant can be done by a simple rate window technique. The DLTS signal $S(T)$ is then given by the difference of the capacitance at the two times t_1 and t_2 by

$$S(T) = C(T,t_2) - C(T,t_1), \tag{2.71}$$

or with Equation (2.68)

$$S(T) = \Delta C_0 \left[\exp(-t_2/\tau(T)) - \exp(-t_1/\tau(T))\right]. \tag{2.72}$$

A peak in the DLTS signal hence appears for

$$\tau(T) = \tau_{ref} = \frac{t_2 - t_1}{ln(t_2/t_1)} \tag{2.73}$$

as is obtained from differentiating Equation (2.72) with respect to τ. For varying τ_{ref} different peak positions T_{max} will be obtained, a thermally activated emission process provided.

If the capacitance transient is given by an expression like Equation (2.69), i.e. $\tau = e_n^{-1}$, and $e_n(T)$ as in Equation (2.47), the activation energy can be determined from the slope of an Arrhenius plot of $ln(T_{max}^2 \tau_{ref})$ over T^{-1}. From the y-axis intersection of the extrapolated data the capture cross-section σ_n can be obtained.

Double-Boxcar Method

In order to improve the signal-to-noise ratio (SNR), the capacitance transients near t_1 and t_2 can be averaged over an interval of t_{av}, so Equation (2.72) has to be rewritten

$$S = \Delta C_0\, t_{av}^{-1} \left(\int_{t_2}^{t_2+t_{av}} \exp(-t/\tau) dt - \int_{t_1}^{t_1+t_{av}} \exp(-t/\tau) dt \right). \tag{2.74}$$

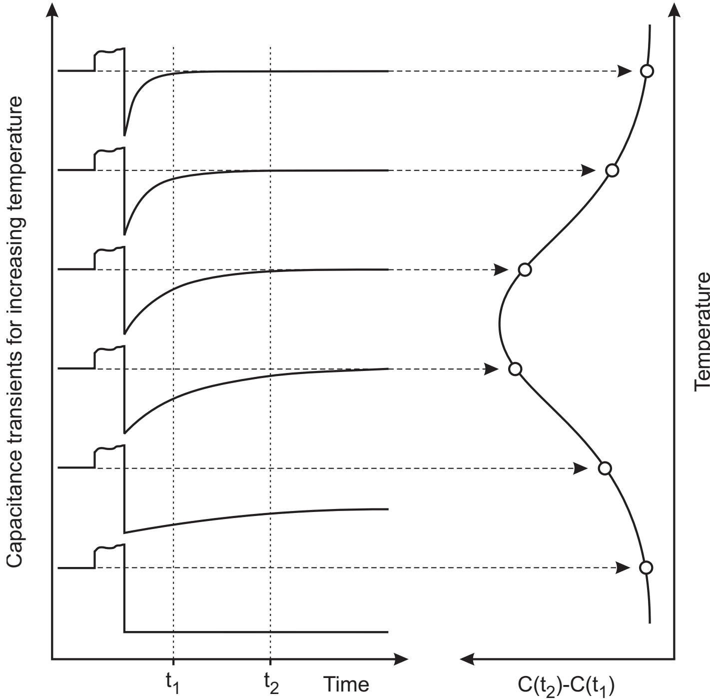

Figure 2.6: *Evaluation of capacitance transients (left side) by a rate window defined by t_1 and t_2 leading to a typical DLTS plot of a thermally activated process (right side).*

The SNR in this case is found to scale as $\sim \sqrt{t_{av}}$ [Mil77]. The reference time constant can only be obtained from a numerical solution of

$$\exp\left[-\frac{t_1-t_2}{\tau_{ref}}\left(1+\frac{t_1}{\tau_{ref}}\right)-\exp\left(-\frac{t_{av}}{\tau_{ref}}\right)\left(1+\frac{t_{av}}{\tau_{ref}}+\frac{t_1}{\tau_{ref}}\right)\right] \\ -\left[1+\frac{t_2}{\tau_{ref}}-\exp\left(-\frac{t_{av}}{\tau_{ref}}\right)\left(1+\frac{t_{av}}{\tau_{ref}}+\frac{t_2}{\tau_{ref}}\right)\right]=0, \tag{2.75}$$

or in good approximation from

$$\tau_{ref}=\frac{t_2-t_1}{ln\left(\frac{t_2+\frac{1}{2}t_{av}}{t_1+\frac{1}{2}t_{av}}\right)}. \tag{2.76}$$

The true τ_{ref} obtained from solving Equation (2.75) is overestimated by this expression by less than 10% [Day79].

Other methods to increase the SNR make use of a lock-in technique or perform a Fourier transform of the original transient data [Kir81].

Deep Level Transient Spectroscopy

This method, due to historical reasons referred to as deep level transient spectroscopy [Lan74, Lan79a], was widely applied in studying the characteristics of defects and traps in semiconductor materials. A so-called DLTS plot is obtained by plotting the contribution to the emission process for a certain reference time constant τ_{ref} as function of the temperature, see Figure 2.6.

Isothermal Capacitance Transient Evaluation

If the temperature is kept fixed and the reference time constant is varied, one can conclusively obtain a plot of the emission contribution as function of the chosen time constant [Oku80]. A maximum in such a plot corresponds to the predominant emission time constant. From such an isothermal capacitance transient (ICT) evaluation, the emission rate at a given temperature can hence directly be determined. The quality of the transient data however, has to be comparatively good to allow for an unambiguous evaluation with this method.

2.5 Quantum Wells

The aforementioned techniques can also be applied to depletion layer devices with hetero-interfaces, quantum wells, and quantum dots embedded, treating such objects as ”giant traps”. The formalism as previously developed for a bulk density of single-level traps however, has to undergo some amendments to account for the abrupt change in carrier density at the interfaces of such structures.

2.5.1 Capacitance-Voltage Characteristic

It is known that in general the C-V profile can only be identified with the free carrier distribution when this distribution varies on a depth scale significantly greater than the Debye length [Blo92]. This is usually not the case for heterostructures and quantum wells. The total amount of charge and the moment of the charge distribution however, are conserved in C-V measurements in these

cases, and this information can be used to determine band discontinuities in heterojunctions, as has been shown by Kroemer et al. [Kro80].

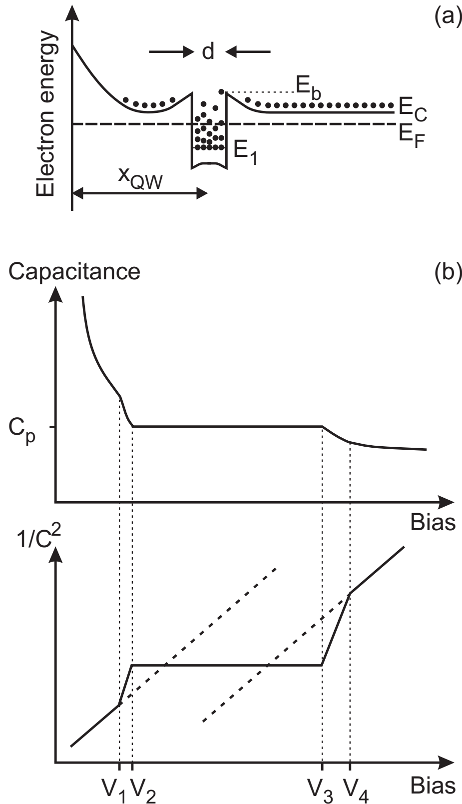

Figure 2.7: *Panel (a) shows the schematic band structure of a quantum well in the vicinity of a Schottky contact (or p-n junction), and panel (b) the ideal C-V and C^{-2}-V characteristics for such a structure exhibiting a plateau due to charge accumulated in the quantum well.*

The capacitance-voltage characteristic of a quantum well in the vicinity of a Schottky contact has been examined by analytically solving Poisson's equation [Let91b, Wan96], or self-consistently solving Schrödinger and Poisson's equation [Lu96, Bro96].

A depletion layer structure with a quantum well embedded is sketched in Figure 2.7 (a). It deviates from the bulk $C^{-2} \sim V$ behaviour by exhibiting a characteristic plateau for the bias region where the depletion edge is pinned to the position of the quantum well, cf. Figure 2.7 (b).

The analytical expressions derived in [Wan96] divide the C-V curve in five different regions, which can be clearly distinguished. Omitting the formulas for simplicity, these regions can easily be distinguished:

- $V < V_1$, where $C(V)^{-2}$ is a straight line with a slope determined by the doping concentration. Here the capacitance resembles the bulk behaviour.
- $V_1 < V < V_2$, where the carriers in the quantum well contribute partially to charge variation of the system and the depletion region above the quantum well adds to the depletion region of the interface. Consequently, a drop in the capacitance is observed.
- $V_2 < V < V_3$, where the capacitance is constant, due to the screening effect of the large amount of carriers in the quantum well.
- $V_3 < V < V_4$, where the quantum well is almost empty and the depletion region underneath the well starts to add to the total depletion region, thus decreasing the capacitance again.
- $V_4 < V$, where $C(V)$ again resembles the bulk behaviour and $C(V)^{-2}$ yields a straight line with a slope determined by the doping concentration.

Provided the width of the plateau is large compared to the transition regions ($V_1 < V < V_2$ and $V_3 < V < V_4$), i.e. $\Delta V = V_3 - V_2 \gg V_1 - V_2, V_3 - V_4$, the amount of charge per area Q_{QW} stored in the quantum well can easily be determined from

$$Q_{QW} \approx C_p \Delta V, \tag{2.77}$$

where C_p is the capacitance of the plateau. Otherwise the transition regions have to be included into an integral over $V_1 < V < V_4$ with suitable weighing functions.

2.5.2 Capacitance Transient Spectroscopy

Soon after the development of capacitance transient techniques it has been recognized that the measurement of the activation energy of carriers from

quantum wells is a powerful tool to determine band offsets [Mar83, Lan87, Deb89, Let91a]. Furthermore, DLTS has been proven to allow the investigation of interfacial defects in structures with quantum wells and thin insertions, cf. e.g. [Wan94, Moo98].

Due to the two-dimensional nature of a quantum well, the density of states per volume is not just given by the density N_t as for a volume concentration of traps, Equation (2.27), but by an energy distribution over the continuous density of states depending on temperature. The resulting emission rate therefore has a different dependence on temperature than in the case of single-carrier traps, Equation (2.47).

As for deep levels, the rate of capture and emission of electrons is considered to be in detailed balance, in order to obtain an expression for the emission rate from a quantum well. Here, the formalism for a quantum well with a single sub-band for electrons is briefly summarized, the analysis of a hole quantum well can be given analogously.[9]

The rate of capture into a quantum well R_c (per unit volume) is given by the product of the density of electrons in the barrier n, the density of unoccupied states in the well p_{QW}, the thermal velocity $<v_n>$, and an effective carrier cross-section σ_{QW}. If the fraction of occupied states in the well is small, the number of unoccupied states per unit volume is hence the density of states per unit energy and unit volume $m_{QW}/\pi\hbar^2 d$ (where m_{QW} is the effective mass of carriers in the quantum well and d the thickness of the quantum well) multiplied by the energy interval $\Delta E_1 = E_b - E_1$ (where E_1 is the energy of the first sub-band of the quantum well and E_b the conduction band edge of the matrix material close to the quantum well)

$$p_{QW} \approx \frac{m_{QW}}{\pi\hbar^2 d}\Delta E_1. \tag{2.78}$$

Further contributions from higher sub-bands can easily be included if necessary. Since $\Delta E_1 \gg k_B T$, the carrier density in the barrier can be described by Boltzmann statistics, Equation (2.16). This gives the capture rate

$$R_c = \sigma_{QW} <v_n> N_C \exp\left(-\frac{E_b - E_F}{k_B T}\right)\frac{m_{QW}}{\pi\hbar^2 d}\Delta E_1. \tag{2.79}$$

Electrons captured into higher states in the quantum well are assumed to rapidly redistribute according to the Boltzmann distribution before being re-

[9] It is worth noting that the depletion approximation can be fulfilled easily for capacitance transient experiments on quantum wells, since the filling pulse bias can be chosen such that the quantum well is situated sufficiently far outside the depletion region and its Debye tail.

emitted. For $\Delta E_1 \gg k_B T$ the carrier density in the quantum well is given by [Blo92]

$$n_{QW} = \frac{m_{QW}}{\pi\hbar^2 d} k_B T \ln\left\{1 + \exp\left(-\frac{E_1 - E_F}{k_B T}\right)\right\}. \tag{2.80}$$

For $E_F < E_1$, the exponential term is less than unity and therefore $\ln(1+x) \approx x$. The rate of emission of electrons per unit volume from the well $R_e = e_{QW} n_{QW}$ is thus

$$R_e = e_{QW} \frac{m_{QW}}{\pi\hbar^2 d} k_B T \exp\left(-\frac{E_1 - E_F}{k_B T}\right). \tag{2.81}$$

From the detailed balance requirement $R_c = R_e$ and using Equation (2.46) for the effective density of states N_C, one obtains

$$e_{QW} = \sigma_{QW} <v_n> 2M_C \left(\frac{2\pi m_e^* k_B T}{h^2}\right)^{\frac{3}{2}} \frac{\Delta E_1}{k_B T} \exp\left(-\frac{\Delta E_1}{k_B T}\right) \tag{2.82}$$

Assuming that σ_{QW} is constant, a plot of $\ln(e_{QW}/T)$ versus T^{-1} should have a slope of $\Delta E_1/k$, since $<v_n> \sim \sqrt{T}$, Equation (2.45).

If $d \ll x_{QW}$, $x_r + x_p \approx 2x_{QW}$, and $x_r - x_p \approx d$ then Equation (2.66) for the capacitance transient becomes

$$\frac{\Delta C(t)}{C} = -\frac{x_{QW} d}{w_r^2} \cdot \frac{n_{w0}}{N_d} \exp(-e_{QW} t), \tag{2.83}$$

where the initial density of electrons in the well n_{w0} is given by Equation (2.80) with E_1 of the steady state, cf. Figure 2.7 (a). It is thus possible to study the temperature dependence of e_{QW} by DLTS. Equation (2.83) indicates that as the reverse bias is varied $\Delta C \sim w_r^{-3}$.

In the above analysis, band bending due to Coulomb repulsion of carriers in the quantum well is not considered explicitly. By referring to E_b instead of E_C in the definition of $\Delta E_1 = E_b - E_1$ however, the possible formation of an effective capture barrier is implicitly taken into account.

Tunneling from Quantum Wells

Tunneling, as previously discussed for deep levels in the context of the influence of the electric field on the emission process, Section 2.3.6, may also play a role for the carrier emission from quantum wells. From its dependence on the external bias, i.e. the electric field, the band offset in quantum wells can be determined [Mar91, Let91a].

Since tunneling through a triangular barrier, Equation (2.54), does not depend on temperature, it may be observed in a DLTS measurement as a plateau at low temperature persisting until thermal activation becomes more efficient and finally dominates the emission. Such a behaviour has been observed by Letartre et al. [Let91c] in a GaInAs quantum well in a GaAs matrix with a conduction band offset of about 145 meV.

2.6 Quantum Dots

Similar to the case of quantum wells, the carrier distribution in semiconductor heterostructures containing QDs is not slowly varying in the vertical direction, but usually changing abruptly in the layer of the QDs. In the horizontal plane of the QDs however, the carrier motion is also quantized and therefore the situation is quite different from the quantum well case. The QD density of states usually consists of several peaks spaced by an energy interval depending on the QD properties. Due to the localization of carriers in three dimensions, the carrier emission process from QDs has certain similarities with the one from deep levels.

A detailed discussion of the carrier dynamics in QDs is presented separately in Chapter 5. In the present section, several aspects of capacitance spectroscopy for the investigation of devices with QDs embedded are described. The features in the C-V characteristic of a depletion layer device with QDs are discussed and explained by numerical simulations of the band structure as function of external bias, and the application of capacitance transient spectroscopy to such samples is demonstrated.

2.6.1 Capacitance-Voltage Characteristic

The dependence of the capacitance of a depletion layer structure with a layer of QDs embedded resembles the case of a quantum well, described in Section 2.5.1, in that a plateau region is formed due to the carrier accumulation in the QD layer. Due to the discrete density of states however, there may be several plateaus related to different energy levels in the QD.

From the width and the position of the plateaus, the associated amount of charge, the energies of the QD levels, and the inhomogeneous broadening due to size fluctuations in the QD ensemble, may be derived by fitting a simulated C-V curve to the experimental data as described below.

A typical C-V characteristic of a p$^+$-n diode with QDs embedded is shown in Figure 2.8. The InAs QDs in the n-doped GaAs matrix are situated at a distance x_{QD} from the p$^+$-n interface. Details of the sample under investigation can be found in Section 3.1. Similar to the C-V curve of a quantum well sample, Figure 2.7, a pronounced deviation from the bulk $C^{-2} \sim V$ behaviour is observed in the bias range where the depletion region is pinned due to localized charge in the QDs. Here, however, two plateaus can be resolved which are interpreted as carrier accumulation in the QD ground and excited states, respectively.

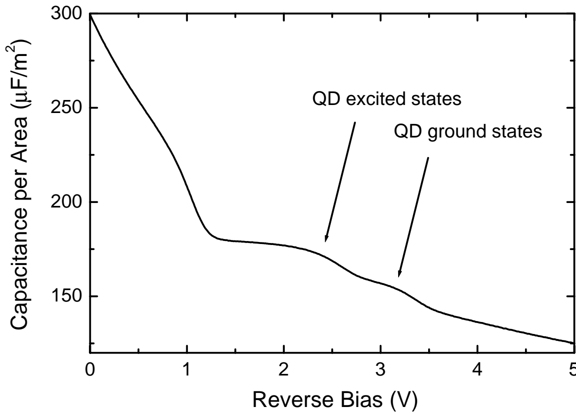

Figure 2.8: *C-V characteristic of a p$^+$-n diode with a layer of QDs embedded at $T = 75$ K and a measurement frequency of $f = 1$ kHz. Two plateaus due to carrier accumulation in the ground and excited states are visible. See also Figure 3.5.*

2.6.2 Modeling the Capacitance-Voltage Characteristic

In this section, a one-dimensional model for the capacitance-voltage characteristic of a p-n diode device with QDs embedded is developed. The model is applied to the C-V curve of the sample studied in detail in Section 3.1. The model presented here is based upon by the work published in [Wet00], from which also the results are taken.

Intra- and Inter-QD Coulomb Interaction

The charge accumulated in the single QDs leads to a rather complicated three-dimensional potential distribution resulting from the Coulomb interaction between the electrons in the QD and the bulk electrons. Furthermore, in the case of high QD sheet densities and low doping concentrations in the matrix material, the carriers in the QDs will also interact with the carriers in other QDs, i.e. *inter-QD* Coulomb interaction will occur.[10] Since the QDs usually do not exhibit a two-dimensional order on their growth surface, the resulting potential landscape can be quite complex. Electrostatic interaction of carriers in the same QD leads to an *intra-QD* Coulomb repulsion energy term, which is, e.g. in the case of InAs/GaAs QDs about 10 to 20 meV.[11] This estimate is in good agreement with experimentally observed values (see, e.g. [Mil97]) and theoretical predictions from QD band structure calculations. In reality however, the Coulomb charging energy is not constant, but depends on the actual configuration of the QD, cf. References [MR97b, Mil97, Sch98, Woj96, Sti99].

The theoretical models for the C-V characteristics of a device with QDs embedded presented in the literature so far [Bru96, Bru98, Bro98, Bru99, Wet00, Wet01], neglect the treatment of intra- and inter-QD Coulomb interaction. They rather include these effects in an averaged way in the underlying distribution of the QD energy levels in order to reduce the problem to a one-dimensional one. This is an oversimplification, because the local band bending in a QD can differ significantly from an two-dimensionally averaged value, and even QDs adjacent to each other may not be in thermodynamic equilibrium, since the localization energy for the carriers in a QD is usually much larger than several $k_B T$.

Assumptions

The position and thickness of the QD layer are referred to as x_{QD} and d, respectively, and the QD sheet density is denoted by N_{QD}. Two discrete QD levels E_i $(i = 0, 1)$ with according inhomogeneous broadening with a full-width at half-maximum (FWHM) of ΔE_i are taken into consideration. The level broadening

[10] In GaAs with a doping concentration of $N_d = 1 \cdot 10^{16}$ cm^{-3}, the Debye length L_D, Equation (2.20), increases from 8 nm to 43 nm for temperatures from 10 K to 300 K. The typical inter-QD distance depends on the material system and the growth conditions and may be small enough to be comparable.

[11] The Coulomb charging energy and its estimation for QDs with the shape of a disk or a sphere, is discussed in more detail in Section 5.2.1. Assuming a disk with $d = 15$ nm in GaAs one obtains a Coulomb charging energy of 23 meV. For a sphere of the same diameter one obtains 15 meV.

due to size fluctuations and Coulomb interaction is taken to be Gaussian with $\sigma_i = \Delta E_i/\sqrt{8\ln 2}$. The degeneracies of the two QD levels are assumed to be 2 and 6.

The energies of the donor and acceptor levels in the structure are E_d and E_a, respectively. Ohmic contacts on top and bottom of the structure are assumed to obtain the appropriate boundary conditions for the integration of the potential and the quasi-Fermi levels.

In order to describe the device under simulation, which consists of layers of different materials (GaAs and InAs) and varying doping concentrations, the following quantities have to be given as a function of the depth x:

- The dielectric constant ε.
- The effective masses of electrons, light-, and heavy-holes, m_e, m_{lh}, and m_{hh}, respectively.
- The respective mobilities μ_e, $\mu_{p,lh}$, and $\mu_{p,hh}$.
- The donor and acceptor density N_d and N_a.

From these given values and the external bias V_a, the following properties can then be derived as function of x, as will be shown below:

- The quasi-Fermi levels for electrons and holes, E_{Fn} and E_{Fp}, respectively.
- The density of ionized donors N_d^+ and acceptors N_a^-.
- The density of free electrons n and holes p.
- The density of electrons in the QDs n_{QD}.
- The total charge density ρ.
- The electron and hole current densities, j_n and j_p, respectively.

Poisson and Drift-Diffusion Equations

With an x-dependent dielectric constant, the one-dimensional Poisson Equation (2.8) has to be rewritten

$$\varepsilon_0 \frac{\partial}{\partial x}\left(\varepsilon(x)\frac{\partial \psi(x)}{\partial x}\right) = -\rho(x). \tag{2.84}$$

The total charge density $\rho(x)$ is given by the sum of the density of free electrons n, the density of light and heavy holes $p = p_{lh} + p_{hh}$, the density of ionized donors N_d^+ and acceptors N_a^-, and the density of electrons in the QDs n_{QD}:

$$\rho(x) = e\left[-n(x) + p(x) + N_d^+(x) - N_a^-(x) - n_{QD}(x)\right]. \tag{2.85}$$

The carrier densities in the conduction and valence band are determined by the Boltzmann approximation for electrons and holes, Equations (2.16) and (2.17) respectively, and the densities of ionized donors and acceptors by the Fermi-Dirac distribution function [Equation (2.35)] as

$$N_d^+(x) = \frac{N_d(x)}{1 + 2\exp\left(\frac{E_d(x) - E_{Fn}(x)}{k_B T}\right)} \tag{2.86}$$

and

$$N_a^-(x) = \frac{N_a(x)}{1 + 4\exp\left(\frac{E_a(x) - E_{Fp}(x)}{k_B T}\right)}, \tag{2.87}$$

respectively (the appropriate degeneracy factors for GaAs were used). The electron and hole current densities in the steady state are given by

$$j_n(z) = \mu_n(x) n(x) \frac{\partial}{\partial x} E_{Fn} \tag{2.88}$$

and

$$j_p(z) = \left[\mu_{p,lh}(x) p_{lh}(x) + \mu_{p,hh}(x) p_{hh}(x)\right] \frac{\partial}{\partial x} E_{Fp}, \tag{2.89}$$

Without generation or recombination taking place in the device, $\frac{\partial}{\partial x} j_n(x) = 0$ and $\frac{\partial}{\partial x} j_p(x) = 0$ must be fulfilled in equilibrium.

The QD electron density per unit volume in the present approximation can be written

$$n_{QD}(x) = \frac{N_{QD}(x)}{d} \sum_i \frac{\alpha_i}{\sigma_i \sqrt{2\pi}} \int \frac{\exp\left(-\frac{\left[E - E_C(x_{QD}) + E_i\right]^2}{2\sigma_i^2}\right)}{1 + \exp\left(\frac{E - E_{Fn}(x_{QD})}{k_B T}\right)} dE \tag{2.90}$$

The total charge per area in the device is given by the maximum electric field in the device [cf. Equation (2.11)] $F_0 = -\frac{\partial \psi}{\partial x}$ at the interface ($x = 0$)

$$Q = \varepsilon(0) \varepsilon_0 |F_0|. \tag{2.91}$$

A self-consistent solution of the drift-diffusion Equations (2.88) and (2.89), and the Poisson Equation (2.84) for a given external bias V_a, yields the potential $\psi(x)$ and hence F_0 and Q. The according C-V characteristic can thus easily be obtained from $C(V) = dQ/dV_a$. Leaving the QD energy levels E_i and the respective broadenings ΔE_i as free parameters, appropriate values can be obtained from a fit of the described model to the experimental data.

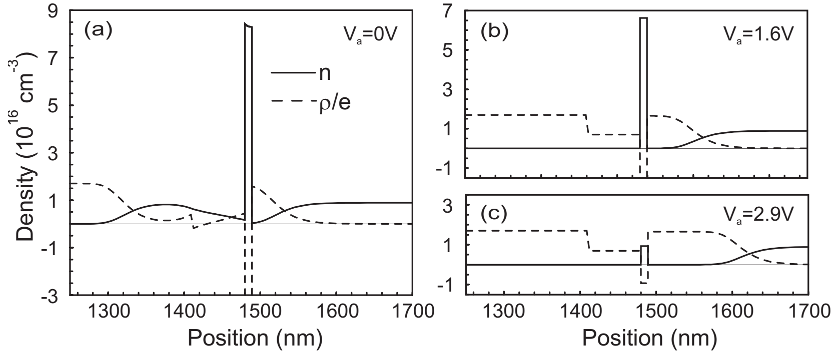

Figure 2.9: *The free electron density $n(x)$ and the total charge density $\rho(x)/e$ at three different reverse biases. In panel (a), $V_a = 0.0$ V, the QDs are completely filled and correspondingly $n \approx 8$. In (b), $V_a = 1.6$ V, some electrons are already removed and $n \approx 6.5$. At $V_a = 1.6$ V, panel (c), $n \approx 1$ and the QDs are almost emptied of carriers (after [Wet00]).*

Results

After adjusting the bulk doping concentration by fitting the C-V characteristic for $V_a < 0.8$ V and $V_a > 3.6$ V, the whole C-V curve is fitted by altering the QD energy levels and the according inhomogeneous broadenings. The resulting free electron density n and the total charge density ρ/e for different applied voltages are displayed in Figure 2.9. They confirm the suspected correspondence of the smaller plateau at about 3.0 V with the depletion of the QD ground state and the larger plateau with the depletion of the excited states.

From the fitted C-V characteristic, solid line in Figure 2.8, one obtains the energy levels as summarized in Table 2.1. In order to compensate for a slight systematic deviation in the voltage range around 1.0 V of the model from the particular experimental curve, a weak local electric field in the QD layer of 2.5×10^5 V/m had to be assumed. This apparent field in the simulation might

Variable	Fit Value [meV]
E_0	211 ± 20
E_1	100 ± 20
ΔE_0	141 ± 30
ΔE_1	95 ± 30

Table 2.1: *Results of fitting the simulated C-V curve to the experimental data for the case with a local electric field [Wet00].*

be due to, e.g. a local decrease in doping concentration or diffusion of In atoms from the QDs into the GaAs layer above. The accuracy of the fitting procedure is estimated to be about a few 10 meV, see inset of Figure 2.10.

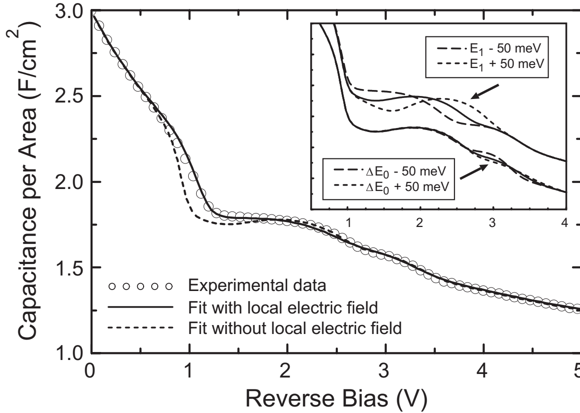

Figure 2.10: *Comparison of simulated C-V curves (solid and dashed line) with experimental data (open circles) showing good agreement. The inset shows the influence of a variation of* ± 50 *meV in two of the four parameters,* E_1 *and* ΔE_0*, on the simulation (after [Wet00]).*

Discussion

The energy levels obtained are in good agreement with the results of the DLTS investigation of this sample presented in Chapter 3 and the numerical calculations of the QD band structure in Section 3.1.4.

The values obtained for the level broadening however, can not directly be compared to physical properties of the QDs, since they do represent several different contributing effects as the inhomogeneous broadening due to size fluctuations in the QD ensemble, intra-, and inter-QD Coulomb interaction. Especially for the excited states, additional influences as due to deviations from perfect degeneracy and a partial delocalization into states of the wetting layer system, may lead to a modified dependence on QD size fluctuations. The accuracy of the results could be enhanced by employing a numerical fitting routine.

As previously mentioned, the inaccuracies due to the averaged treatment of the intra- and inter-QD Coulomb interaction of bound carriers leads to uncertainties which strongly depend on the experimental conditions and are difficult to predict. A fully three-dimensional description of the potential landscape is hence of great interest.

2.6.3 Capacitance Transient Spectroscopy

Here, a single layer of QDs with density N_{QD} per area in n-doped material (with doping concentration N_d) shall be considered. As in the case of capacitance transient experiments on quantum wells, the depletion approximation can easily be made valid by choosing a sufficiently large filling pulse height to put the QDs well outside the depletion region and render capture in the Debye tail hence negligible. The work cycle of an DLTS experiment of a structure with QDs embedded is depicted in Figure 2.11.

The reverse bias V_r is chosen such that before the bias pulse the depletion region extends well over the position of the QDs, which are hence emptied of carriers. During the pulse, the depletion region is shorter than the distance of the QD layer from the interface and the QDs are consequently filled with carriers. After switching back to the reverse bias situation, the QDs are again situated inside the depletion region and start to emit the trapped carriers. While the QDs contain carriers, the depletion width is larger than in the initial situation, where the QDs are empty. As a consequence, the capacitance after the bias pulse is smaller and increases as carriers are emitted from the QDs, finally re-approaching the initial situation. By recording the capacitance transients, it is hence possible to monitor the carrier emission process from the QDs.

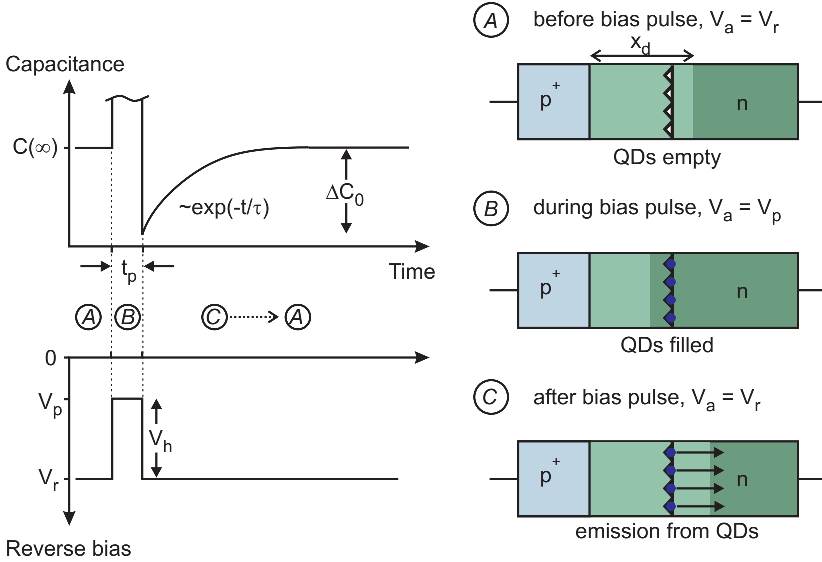

Figure 2.11: *DLTS work cycle of a p$^+$-n diode with QDs embedded. On the left hand side the applied voltage (bottom) and the capacitance (top) as function of time are displayed. The right hand side shows the depletion region in the device and the charging state of the QDs for the three bias situations A, B, and C (i.e. before, during, and after the bias pulse, respectively).*

As first approximation, the carrier emission from the QDs can be considered equivalently to carrier emission from traps. Equation (2.66) is thus applied

$$\frac{\Delta C(t)}{C} = \frac{C(t) - C}{C} = -\frac{1}{2}\left(\frac{x_r^2 - x_p^2}{w_r^2}\right)\frac{n_{QD}}{N_d d}\left[f(t) - f_\infty\right], \tag{2.92}$$

where d is the thickness of the QD layer and n_{QD} the charge density in the QD layer. In the case of QDs initially filled with electrons one obtains

$$\Delta C(t) = -\Delta C_0 \exp(-e_{QD} t), \tag{2.93}$$

where e_{QD} is usually given by thermal activation, Equation (2.47), and

$$\frac{\Delta C_0}{C} = -\frac{1}{2}\left(\frac{x_r^2 - x_p^2}{w_r^2}\right)\frac{n_{QD}}{N_d d}. \tag{2.94}$$

With $d \ll x_{QD}$, $x_r + x_p \approx 2x_{QD}$, and $x_r - x_p \approx d$ as already used in the quantum well case, Section 2.5.2, one obtains

$$\frac{\Delta C(t)}{C} = -\frac{x_{QD}}{w_r^2} \cdot \frac{n_{QD}}{N_d} \exp(-e_{QD}t). \tag{2.95}$$

It is thus expected that the amplitude of the capacitance change depends on the depletion width or the applied bias as

$$\Delta C \sim w_r^{-3}, \text{ or } \sim (V_b + V_a)^{-3/2}, \tag{2.96}$$

respectively.

The charge density n_{QD} can easily be estimated by Equation (2.95) from the initial capacitance amplitude ΔC_0 and the steady-state capacitance C, since for $t = 0$

$$n_{QD} = -\frac{\Delta C_0}{C} \cdot \frac{w_r^2 N_d}{x_{QD}}. \tag{2.97}$$

Chapter 3

Carrier Escape Mechanisms in InAs/GaAs Quantum Dots

In this chapter the experimental results of the first transient capacitance experiments on InAs QDs in a GaAs matrix are reported. In Section 3.1 the emission of *electrons* from QDs is investigated and the contributing emission mechanisms, thermally activated emission and pure tunneling, are identified. Then, in Section 3.2, *hole* and *electron* emission of QDs grown under very similar conditions are compared and important differences are revealed. The experimental results indicate that tunneling is significantly suppressed in the case of holes, which may be understood in terms of the larger effective mass of the electrons in the tunnel barrier and the smaller quantization energy in QDs. Information on the experimental setup can be found in Appendix A.

3.1 Electron Emission

In order to identify and study the emission of electrons from QDs, the DLTS responses from a set of three GaAs p^+-n diode samples were compared; the first with a triple layer of InAs QDs, the second with only a triple InAs quantum well, and the third without any InAs. While the DLTS signal in the first sample is unambiguously shown to originate from the QDs, the other two

samples do not give rise to any DLTS signal below room temperature. The QD DLTS signal clearly exhibits contributions from tunneling and thermally activated tunneling probably involving excited states.

From the experimental observations, conclusions regarding the QD energy level scheme are deduced and compared with the results of numerical calculations of the electronic states based on eight-band $\mathbf{k}\cdot\mathbf{p}$ theory including strain and piezoelectricity. The good agreement between experimental results and calculations confirms the interpretation of the experimental results and the quality of the theoretical predictions.

Furthermore, the dependence of the DLTS signal on reverse and pulse bias was studied; the results are explained by a partial emptying and filling of the QD levels. From these measurements, a depth-profile of the DLTS signal is derived, which supplies additional evidence for the QD layer being the source of the observed DLTS signal.

After a general characterization of the samples in Section 3.1.1, the results of the capacitance-voltage and DLTS measurements are presented in Section 3.1.2 and Section 3.1.3, respectively. Having provided the results of the numerical calculations of the QD energy levels in Section 3.1.4, the outcome of the investigations is summarized and discussed in Section 3.1.5.

3.1.1 Samples

Three samples with a suitable layer sequence for p^+-n diode preparation were grown by metal-organic chemical vapor deposition (MOCVD) in the "Institut für Festkörperphysik", TU-Berlin, on (100)-oriented n^+GaAs substrates. First, a 1.6 μm thick Si-doped GaAs buffer with a doping density of $N_d = 1.7 \times 10^{16}\text{cm}^{-3}$ was deposited. Then the InAs QD (or reference) layers were grown. In the case of the QD sample an insertion of three separate layers of nominally 1.7 ML InAs with caps of 2.8 nm undoped GaAs on top of the InAs layers were deposited. The amount of InAs corresponding to a smooth layer thickness of 1.7 ML is just above the critical thickness for QD formation in the Stranski-Krastanow growth mode [Hei96b, Hei98a, Str38b, Eag90, Leo94, Muk98]. Because of the thin GaAs spacer layers, the QDs grow vertically aligned and are electronically strongly coupled [Led96]. Such closely stacked islands act as a single localizing potential for carriers.[1] For the wetting layer (WL) sample somewhat less InAs (nominally 1.2 ML) was deposited, so that no

[1]The triple QD layer was used in order to provide large localization energies in combination with high material quality. The latter is of importance for DLTS measurements, since signals from electrically active defects may disturb the investigation of the carrier emission from the QDs.

transition from two-dimensional to zero-dimensional growth took place. For the reference sample the InAs layers were omitted completely. The rest of the growth sequence and all other growth parameters however, were kept identical.

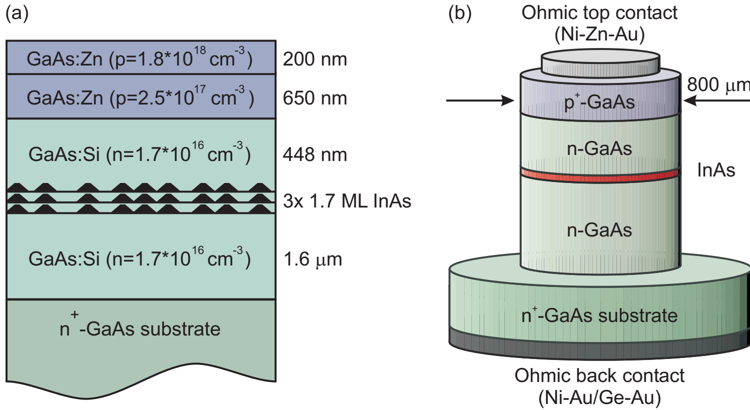

Figure 3.1: *(a) Layer sequence of the samples after the MOCVD growth, here the one containing the QDs. (b) Schematic drawing of a processed diode mesa with ohmic contacts.*

Following this insertion, for all samples a 448 nm n-GaAs spacer layer ($N_d = 1.7 \times 10^{16}\text{cm}^{-3}$) and 650 nm of Zn-doped GaAs ($N_a = 2.5 \times 10^{17}\text{cm}^{-3}$) were deposited, in order to to form an p^+-n junction. Finally, a 200 nm thick, highly Zn-doped GaAs ($N_a = 1.8 \times 10^{18}\text{cm}^{-3}$) top-layer was added. The schematic layer structure of the samples is depicted in Figure 3.1(a). The thickness and doping concentration of the spacer layer are crucial parameters for proper operation of the samples. They are chosen, such that at zero bias the insertion is situated outside the depletion region; but for a few volts reverse bias the depletion region can be extended well over the layer under investigation. The dependence of the depletion width on these two parameters is given by Equation (2.15).

Using standard optical lithography and lift-off techniques ohmic contacts were formed to the top and the back of the structure. Eventually mesas with a diameter of 800 μm were defined by chemical wet-etching, see Figure 3.1(b). For details of the sample processing see Appendix A.2.

From cross-section transmission electron microscopy (TEM) of a piece of the wafer containing the QDs, Figure 3.2, a base width of about 12 nm and a

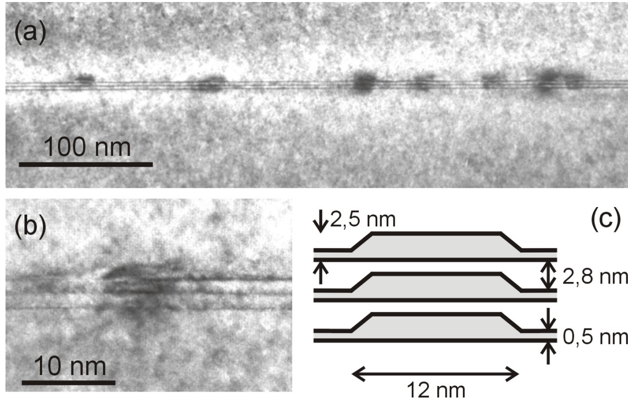

Figure 3.2: *Cross-section TEM image of the QD layer (a), close-up of a single QD stack (b), and approximate average geometry (c).*

height of 2.5 nm for each of the three QDs in a stack was obtained. The whole stack has a height of about 9 nm and the spacing in between the QDs is only about 0.8 nm. The wetting layer has a thickness of about 0.5 nm, corresponding to approximately 1 ML of InAs. It is assumed that the shape of the single QDs resembles a truncated pyramid with $\{101\}$ facets. From plan-view TEM images, Figure 3.3, a QD sheet density of $N_{QD} = 100\ \mu\text{m}^{-2}$ was determined. Very few defects were observed in the TEM images.

A standard photoluminescence (PL) measurement at low temperature, $T =$ 8.5 K, using the 514.5 nm line of a 0.5 W Ar^{+}-laser as excitation source, attenuated to give a power density of about 50 W/cm^2 on the sample surface, was used to measure the spectra displayed in Figure 3.4. In all three samples the peak of the GaAs bulk exciton with a phonon replica appears at about 1.5 eV. Furthermore a weak signal at about 1.17 eV is present in all data, which is correlated to the highly doped substrates used. Its origin is not yet clarified. The reference sample does not show any further luminescence.

In the wetting layer sample, a strong peak at 1.4 eV is due to two-dimensionally confined excitons in the triple InAs quantum well. The high signal intensity of this peak is an indication of the excellent material quality, since non-radiative recombination is apparently weak.

In the QD sample, a similar but weaker peak due to two-dimensionally confined excitons is present at 1.36 eV. Furthermore a rather broad but pronounced signal from excitonic recombination of carriers in the QDs appears

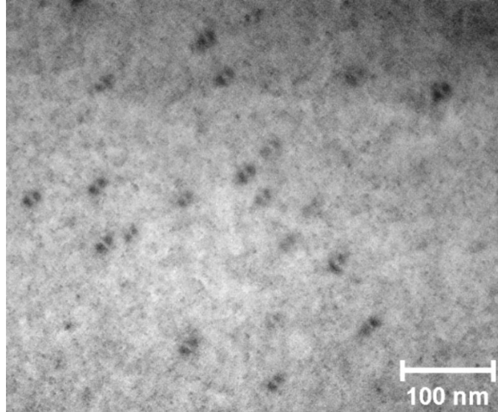

Figure 3.3: *Plan-view TEM image of the QD sample. The QDs with a sheet density of* $N_{QD} \approx 100\ \mu m^{-2}$ *are clearly visible as dark spots.*

at 1.12 eV. The full width at half maximum of this peak, about 150 meV, reflects the ensemble fluctuations of the QD energy levels due to slightly varying material composition, shape and size of individual QDs [Hei98b, Hei98c]. The integrated intensity between 0.95 eV and 1.45 eV is 10% larger than the integrated intensity of the wetting layer sample in the same energy range. The material quality of the QD sample is therefore concluded to be not deteriorated by the formation of the QDs. This is in good agreement with the TEM observations, which revealed only a very small dislocation density.

3.1.2 Capacitance-Voltage Characteristics

The current-voltage (I-V) dependence of the processed diodes were measured first to check for proper device operation. The break-through reverse bias was typically $10-20$ V, and built-in voltages V_b between 1.2 V and 1.4 V were obtained in good agreement with the expected value of about 1.35 V for the given doping concentrations [Sze81].

Thereafter static C-V measurements at varying temperatures (between 15 K and 300 K) and measurement frequencies (between 200 Hz and 1 MHz) of the three samples were made. The AC signal amplitude of the capacitance meter was usually kept at 100 mV for acceptable signal to noise ratios (SNR) and measurement integration times. It was checked that smaller amplitudes (down

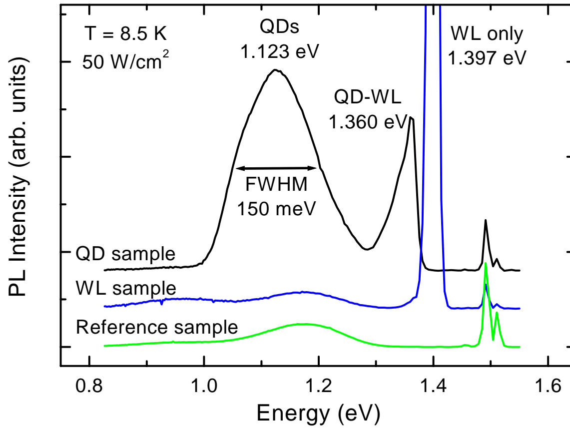

Figure 3.4: *Low-temperature photoluminescence spectra with an excitation density of 50 W/cm^2 of QD, wetting layer (WL), and reference sample (data displayed offset).*

to 10 mV) did not reveal any further structure in the data. Mainly the QD C-V curve showed a significant dependence on these two parameters, since at high frequencies and low temperatures the localized electrons in the QDs can not follow the AC measurement frequency. As a result, the plateau structure visible in the data can not be resolved anymore. For temperatures above about 100 K, the two plateaus tend to ”smear out”. The optimum conditions in order to resolve the full structure were determined to be a frequency of 1 kHz or less and a temperature of about 75 K for the given sample.

The measurement results of the three different samples are displayed in Figure 3.5. As discussed in Section 2.5.1 and Section 2.6.1, the quantum well and QD samples exhibit plateaus due to carrier accumulation in the InAs layer. From the C-V measurements the appropriate biasing conditions for capacitance transient measurements can be derived. It is to be expected, that a reverse bias of 3.5 V or more is required to completely empty the QDs, and that a filling pulse bias of about 3.0 V or 1.5 V must be applied to fill the QD ground or excited states, respectively.

From the approximate width of the two plateaus of the QD sample, $\Delta V_g \approx 0.25$ V and $\Delta V_e \approx 0.75$ V, and the according capacitances, $C_g = 152\ \mu\text{F/m}^2$ and $C_e = 173\ \mu\text{F/m}^2$, the amount of charge stored in the ground and excited states

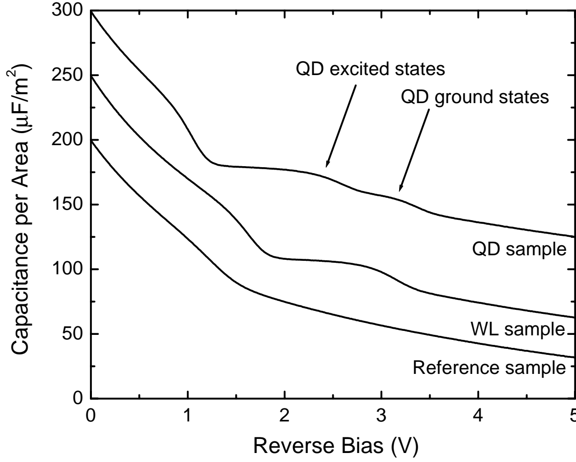

Figure 3.5: *C-V characteristics at $T = 75$ K and a measurement frequency of $f = 1$ kHz of the sample with InAs QDs (top curve) and the two reference devices with triple InAs quantum well (middle curve) and without any InAs (bottom curve). The data for the quantum well and the reference device are displayed offset by $-50\ \mu F/m^2$ and $-100\ \mu F/m^2$, respectively.*

can be estimated as for quantum wells[2], Equation (2.77). Relating the result to the QD sheet density of $N_{QD} = 100\ \mu\mathrm{m}^{-2}$, yields about $n_0^{cv} \approx 2$ electrons per QD in the ground state and about $n_1^{cv} \approx 8$ electrons in the excited states. The total amount of charge is hence approximately 10 electrons per QD. A discussion of the capacitance-voltage dependence of a depletion layer sample with QDs embedded, and a numerical simulation of the C-V data of the sample investigated here, have been presented in Section 2.6.

The width of the plateau in the C-V characteristic of the quantum well sample, Figure 3.5, $\Delta V_e \approx 0.74$ V and the capacitance $C_e = 151\ \mu\mathrm{F/m}^2$ yield a sheet charge density of about $7 \times 10^{10}\ \mathrm{cm}^{-2}$. This value is by about 30% less than the amount of charge in the QDs, which is reasonable taking into account that the localization in the wetting layer system is significantly weaker than in the QDs. Also the reference device without InAs exhibits a slight deviation from the $C^{-2} \sim V$ behaviour at about 1.5 V, due to small variations of the

[2]Note however, that due to the small width of the plateaus compared to the transition regions towards the bulk $C^{-2} \sim V_r$ behaviour, the accuracy of such an estimate is relatively poor in the present case.

doping concentration caused by the thin undoped GaAs layer and the growth interruption.

3.1.3 DLTS Measurements

In this section, the capacitance transient measurements of the three samples are summarized. After clearly identifying the DLTS signal, due to the QDs from comparison with the reference samples, its features and its dependence on the biasing conditions are studied. Typically transients of 210 ms duration were sampled with a resolution of 2000 points at temperature steps of about 1 K. The data was subsequently evaluated by the double-boxcar method, Section 2.4.3.

Identification of Electron Emission from Quantum Dots

In Figure 3.6 DLTS spectra for a reference time constant of $\tau_{ref} = 21$ ms of the three samples for a detection reverse bias of $V_r = 3.5$ V and a pulse voltage of $V_p = 0.2$ V are displayed. The pulse duration was 10 ms in all measurements.

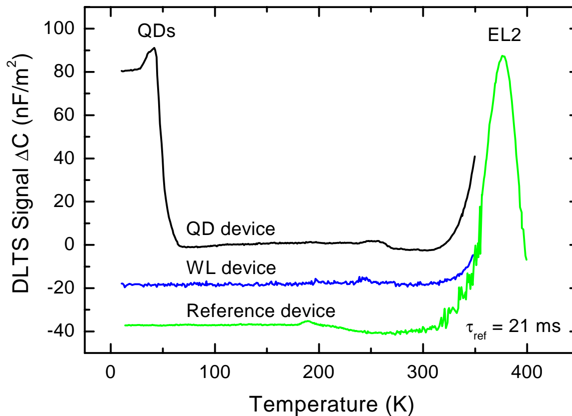

Figure 3.6: *DLTS signal of the three samples for a reference time constant of 21 ms ($V_r = 3.5$ V and $V_p = 0.2$ V). The data of the InAs WL device and the reference device without InAs are displayed offset by -20 nF/m^2 and -40 nF/m^2, respectively.*

Only the QD sample exhibits a DLTS signal at low temperature up to about 70 K. The positive sign of the DLTS signal indicates emission of majority

carriers, hence due to electrons in the given sample structure. At elevated temperatures, around about 370 K, a peak appears in the DLTS data for all samples. The common EL2 arsenic-antisite defect of GaAs [Dab89] is identified as the origin of this signal. EL2 is always present MOCVD-growth of GaAs at the low temperatures necessary for QD formation.[3] The positive sign of the DLTS signal indicates the emission of majority carriers; hence electrons in the given case.

The low-temperature DLTS signal in the QD sample, displayed in magnification in Figure 3.7(a), is attributed to emission from the QDs. Up to a temperature of about 25 K the DLTS signal is constant. Then a peak at about 40 K appears, after which the signal disappears completely at about 70 K. The QD DLTS signal does not show any dependence on the pulse width, which was checked for pulse widths of down to 500 μs.

From a standard Arrhenius plot of the peak position for different reference time constants, Figure 3.7(b), an activation energy of $E_a = (94 \pm 10)$ meV and a capture cross-section $\sigma_n \approx 1 \times 10^{-12}$ cm^2 were obtained. Assuming a normal distribution of the QD energy levels due to ensemble fluctuations, fitting simulated DLTS peak, dashed line Figure 3.7(a), yields a broadening with a FWHM of $b_{fwhm} = 40$ meV.

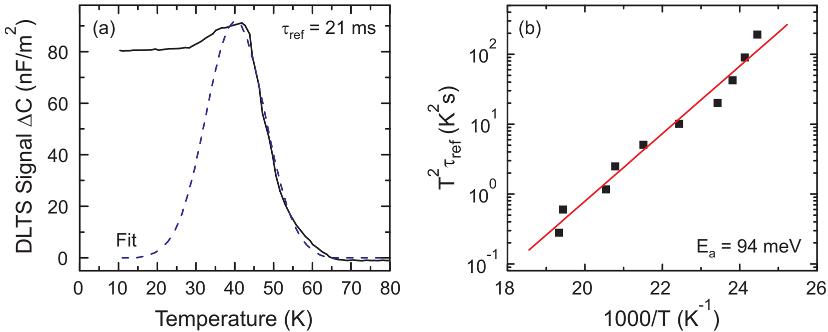

Figure 3.7: *(a) Close-up of the QD DLTS signal from Figure 3.6. The dashed line is a fit, see main text for details. (b) Arrhenius plot of the peak and a linear fit with* $E_a = 94$ *meV and* $\sigma_n = 1 \times 10^{-12}$ *cm*^{2}.

The temperature independent contribution to the DLTS signal of the QD sample below 30 K is interpreted in terms of pure tunnel emission, see

[3] The presence of electrically active defects, may severely hamper or even prevent the observation and interpretation of carrier emission from QDs, see e.g. [Kri98, Wal00].

Section 2.3.6. From an ICT evaluation, Section 2.4.3, of the transient data at low temperatures for increasing reverse bias, a few emission time constants in the range of 5 ms for $V_r = 3.3$ V down to 0.8 ms for $V_r = 4.1$ V were determined. From this data the barrier height is estimated according to Equation (2.54). A value of $\Delta E_t = 165$ meV is obtained. The accuracy of this value however, is probably not very good, since the dependence of the emission rate on the reverse bias, and hence the electric field, is too strong to allow for a fit of the model to experimental data in a sufficiently large field range. An other, rather fundamental problem arises here; the value of the electric field at the position of the QDs in the presence of charge can only roughly be estimated from the external bias. For a more accurate prediction of the electric field, a self-consistent calculation according to the model discussed in Section 2.6.2 is necessary.

As the electric field is increased by increasing the reverse bias V_r, the tunnel contribution is strongly enhanced and quickly dominates, as can be seen from the DLTS signal, see below, Figure 3.8(b). The thermally activated peak looses intensity and quickly vanishes. An additional contribution due to field-induced phonon-assisted tunneling can also not be ruled out.

Due to the comparatively large height of the QD stacks the influence of barrier lowering induced by the electric field (Poole-Frenkel effect) must be taken into consideration, cf. Section 2.3.6. Its influence can be estimated by Equation (2.52). For the reverse bias $V_r = 3.5$ V, the electric field at the position of the QDs is about 4.5×10^6 V/m, as can be obtained from Equation (2.12). One thus obtains a barrier lowering as strong as $\Delta E_{BL} = 20$ meV.

Partial Emptying by Variation of Reverse Bias

If the filling pulse bias is kept fixed at $V_p = 2.0$ V and the reverse bias V_r is varied in the range between 2.6 V and 4.3 V in steps of 100 mV, it is expected to observe significant changes in the DLTS signal shape and amplitude, since for the smaller biases the QDs are not entirely emptied of electrons, cf. Figure 3.5 and the according discussion of the C-V data in Section 3.1.2. The DLTS results for this bias range are displayed in two sets for clarity, Figure 3.8.

For reverse biases below about 3.5 V, not all QD energy levels are lifted above the Fermi level and only the higher levels can be emptied. As a consequence, the DLTS signal is expected to be weaker than in the case of entirely emptied QDs, and the high temperature part of the DLTS spectrum, which roughly corresponds to larger activation energies, should be suppressed for decreasing V_r. These expectations are met by the experiment, see Figure 3.8(a).

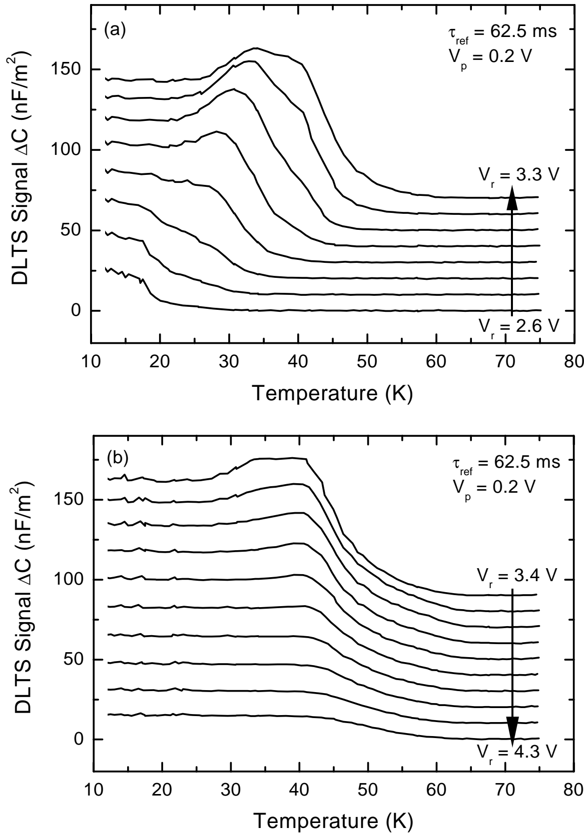

Figure 3.8: *DLTS data for fixed filling pulse bias $V_p = 2.0$ V and increasing reverse bias $V_r = 2.6$ V, 2.5 V, …, 3.3 V [panel (a), from bottom to top], and $V_r = 3.4$ V… 4.3 V [panel (b), from top to bottom], with a pulse length of 1 ms for a reference time constant of 62.5 ms. The curves are displayed offset for clarity.*

For reverse biases V_r above the value for which the DLTS signal shape is fully developed, around 3.4 V to 3.5 V, a decreasing overall amplitude of the DLTS signal without strongly changing features is observed, see Figure 3.8(b).

In addition to the general dependence of the DLTS signal on the reverse bias, as described by Equation (2.96), the tunnel emission contribution becomes stronger for increasing reverse bias, then dominates, and finally sup-

presses the DLTS signal. Accordingly the peak at about 40 K disappears for $V_r = 4.0$ V and the DLTS signal shape becomes flat. This behavior indicates for an increasing relative strength of the tunneling contribution. The effect of the thermally activated process however, is still clearly visible in the measurements. It manifests itself in the remaining high-temperature flank, where the thermally activated process begins to empty the QDs faster than the tunnel emission.

A field effect, which would lead to a detectable shift of the peak positions as function of the reverse bias, can not be observed after the QD DLTS signal is fully developed, cf. Figure 3.8(b). Due to the suppression of the peak by direct tunneling however, its position can only be observed in a small bias range ($V_r = 3.4$ V, $\ldots 3.9$ V).

Partial Filling by Variation of Filling Pulse Bias

Keeping the reverse bias fixed $V_r = 3.5$ V and decreasing the filling pulse bias $V_p = 3.4$ V, 3.3 V, ..., 2.5 V, 2.0 V, 1.5 V, and 0.2 V, yields a different picture, see Figure 3.9. For the lowest filling pulse bias of 3.4 V almost no DLTS signal is visible. With decreasing pulse bias, the peak at about 40 K increases until it reaches its saturated value for about 2.9 V. The low-temperature shoulder still rises until a pulse bias of about 2.6 V. For smaller pulse biases the DLTS signal does not change anymore.

The observed behaviour for large filling pulse biases shows, that for small pulse heights the QD energy levels in the ensemble are only partly filled. The signal strength is hence weak corresponding to the fraction of the QDs previously occupied during the bias pulse. For bias pulses at which all QDs are filled, the DLTS signal saturates. This behaviour is observed for a pulse bias of about 2.9 V.

Bias Profile

The results from the previous two sections concerning partial emptying and partial filling in the DLTS experiments are summarized in Figure 3.10. In this diagram, the DLTS signal strength at the position of the thermally activated peak at 40 K as a function of the bias parameters is plotted. Since a certain bias roughly corresponds to a depletion width (neglecting the influence of the QD layer), such a plot can hence be considered a depth profile of the DLTS signal. A real conversion however, of the applied bias into a certain depth in the case of a semiconductor heterostructure as investigated here, would require

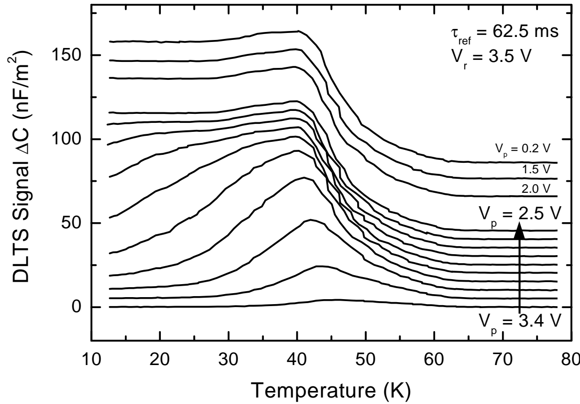

Figure 3.9: *DLTS data for fixed reverse bias* $V_r = 3.5$ *V and decreasing filling pulse bias* $V_p = 3.4$ *V, 3.3 V, ..., 2.5 V, 2.0 V, 1.5 V, and 0.2 V (from bottom to top) with a pulse length of 10 ms for a reference time constant of 62.5 ms. The curves are displayed offset for clarity.*

a numerical simulation of the band structure for each applied bias, taking into account the QD properties as discussed in Section 2.6.2. Due to the uncertainties concerning the QD level scheme this is not always a feasible approach. In correlation with the insight gained from the C-V characteristics, Figure 3.5, one nevertheless obtains important information on the origin of the DLTS signal.

In the case of a fixed reverse bias $V_r = 3.5$ V, the DLTS signal is very weak for $V_p = 3.4$ V, then rises for decreasing pulse bias, and soon saturates at about $V_p = 2.9$ V. This behaviour is interpreted with help of the static C-V characteristic, Figure 3.5. The emission from the QD ground states can only be observed if they are previously filled, which hence happens for bias pulses of less than 2.9 V. Similarly, the DLTS signal appears in the case of fixed filling pulse bias $V_p = 2.0$ V only for reverse biases below about 2.8 V and a maximum amplitude is reached for about 3.4 V. (The decreasing DLTS signal for greater reverse biases has already been discussed above.)

The consistency of these observations with the bias range in which the QD ground states are emptied in the static C-V characteristic, Figure 3.5, supports the attribution of the QD DLTS signal to these levels.

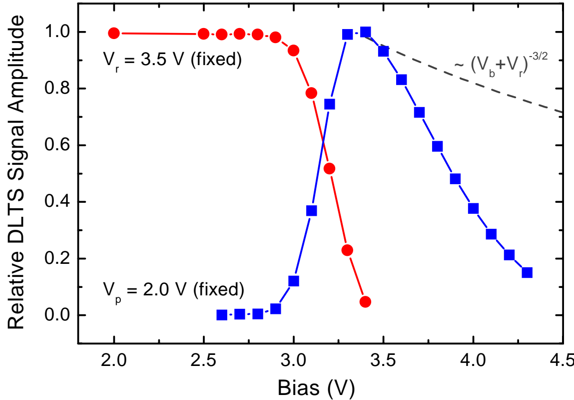

Figure 3.10: *DLTS bias profile obtained from the peak amplitudes at 40 K of the data presented in Figures 3.8 and 3.9. The amplitude for fixed reverse bias $V_r = 3.5$ V and increasing pulse bias V_p (circles), remains constant until for a pulse bias of more than $V_p = 2.8$ V the QD states can only partly be filled and the DLTS signal disappears. The DLTS signal in the measurements with fixed pulse bias $V_p = 2.0$ V (squares) rises for reverse biases above $V_r = 2.8$ V, has a maximum for about 3.5 V, and then decreases again. The theoretical $\sim (V_b + V_r)^{-3/2}$ dependence of the DLTS signal strength without tunnel emission, Equation (2.96), is indicated by the dashed line.*

3.1.4 Numerical Calculations of QD Energy Levels

Using the software package developed by Stier et al. [Sti99, Sti01a] based on eight-band **k**·**p** theory including strain and piezoelectricity, numerical calculations of the wave functions of localized electrons and the according energy level scheme have been performed for the present QD geometry. By this method, a ground state energy of $E_0 = 195$ meV relative to the GaAs conduction band edge, and a set of three almost degenerate excited states at $E_{1,2} = 115$ meV and $E_3 = 111$ meV were obtained.[4]

The almost three-fold degeneracy of the excited state is not surprising, keeping in mind that the given QD geometry is relatively close to that of a box. That means, that the dimensions in all three spatial directions are almost identical, which leads to a degeneracy factor of three. Including spin dege-

[4] A few more bound excited states with considerably smaller localization energies are predicted by the calculations. These are omitted here for simplicity, since they influence neither the interpretation of the experimental data nor the following discussion.

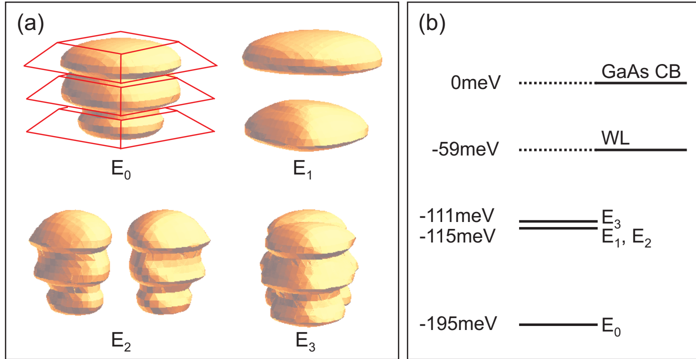

Figure 3.11: *(a) Isosurface plots for 65% of the total probability density of the lowest four electron states calculated by eight-band* **k·p** *theory including strain and piezoelectricity. For the ground state E_0 the assumed QD geometry is indicated. (b) Corresponding energy level scheme.*

neracy, eight-band **k·p** theory hence predicts a two-fold degenerate ground state, a roughly six-fold degenerate excited state, and a quantization energy of about 80 meV. The total probability densities of these states are depicted in Figure 3.11(a).

The similarities of E_0 with an s-orbital are obvious, since no nodal planes are visible in the probability density. The excited states resemble p-orbitals, for they each have a nodal plane, where they exhibit an almost vanishing probability density. For E_1 this is the horizontal (001) plane, and for E_2 and E_3 the nodal planes are the (110) and $(1\bar{1}0)$ plane, respectively. The degeneracy between E_2 and E_3 is lifted due to piezo-electricity. The degeneracy between E_1 and E_2 is purely coincidental. It is lifted for slightly different QD dimensions and aspect ratios, which was confirmed by a separate set of calculations (not shown here).

The energy of the first sub-band of the triple quantum well (the three wetting layers) is determined by a one-dimensional self-consistent calculation of the solution of the Schrödinger equation including strain [Hei98a]. The energy level scheme of the QD system is displayed graphically in Figure 3.11(b).

3.1.5 Discussion

The main observations can be summarized:

- A DLTS signal at low temperatures is observed *only in the QD sample*, the samples with wetting layers and without InAs do not exhibit any DLTS signal.
- The DLTS signal is due to *electron* emission from the QDs and consists of a *temperature independent tunneling* contribution and a *thermally activated emission* mechanism.
- From variations of the filling pulse and reverse biases the *QD ground states* were identified as the source of the QD DLTS signal. By this method partial emptying and filling was studied.
- No DLTS signal could be attributed to excited QD states or the wetting layer.

The results obtained from experiments and the numerical calculations are summarized in Table 3.1.

Quantity	Description	Value
n_0^{cv}	number of carriers in QD ground state from CV	2
n_1^{cv}	number of carriers in QD excited states from CV	8
E_a	thermal activation energy	94 meV
b_{fwhm}	QD ground state level broadening	40 meV
ΔE_t	tunnel barrier	165 meV
ΔE_{BL}	estimated barrier lowering	20 meV
E_0	QD electron ground state energy from calculations	195 meV
ΔE_{01}	QD electron quantization energy from calculations	80 meV

Table 3.1: *Summary of the results from the investigation of electronic states in InAs QDs.*

The interpretation of the temperature independent DLTS signal from the QD sample at low temperatures being due to tunnel emission is confirmed by several further observations. The escape rate for tunneling through a triangular barrier, Equation (2.54), does not vary with temperature; a behaviour which is exactly observed in the experiment and obvious from the constant DLTS signal below 30 K, see the data presented in Figure 3.7. Moreover the increasing

relative strength of the tunnel contribution to the DLTS signal for increasing reverse bias, as apparent from Figure 3.8(b), and the quickly decreasing DLTS signal amplitude, Figure 3.10, support the presented model. A similar effect of tunnel emission has previously been reported for DLTS studies of quantum wells [Let91c].

The significant difference between the activation energy E_a and the tunnel barrier ΔE_t is explained by the co-existence of two different emission paths. First, there is direct tunnel emission from the QD ground states into the GaAs conduction band through the triangular barrier resulting from the ban bending due to the electric field. And second, thermally activated emission probably involving excited QD states. Here, electrons from the QD ground states are assumed to be thermally activated into excited states and subsequently emitted (by thermal and tunnel emission). This interpretation is summarized in Figure 3.12.

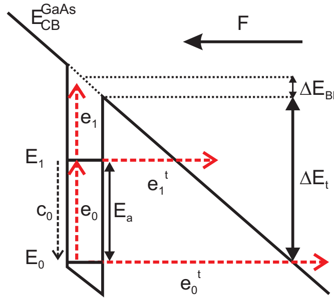

Figure 3.12: *Schematic conduction band of the QD structure in the presence of an electric field with thermal and tunnel emission indicated.*

The total emission rate in the present situation is given by $\eta \simeq e_0 + e_0^t$, Equation (5.9), where e_0^t is the tunneling rate from the QD ground state into the GaAs conduction band and e_0 the rate of thermal activation from the QD ground state to the excited state. The results of a detailed analysis of the carrier dynamics in such a two-levels system, cf. Section 5.1, indicate that due to the phonon-mediated nature of the relaxation process, the temperature dependence of the relaxation rate, and hence of the pre-factor of the resulting emission rate, depend on the efficiency of the relaxation process. This is of relevance for the choice of a suitable Arrhenius plot for determining the thermal activation energy. The temperature dependence of the relaxation rate resulting from multi-phonon processes, can be estimated to lie somewhere in the range

of T^x, $x \in [0,2]$, cf. Section 5.1.3. The standard Arrhenius plot, $\ln\left(T^2\tau\right)$ over T^{-1}, used so far for the evaluation, Figure 3.7(b), hence implicitly assumes a T^2-dependence leading to an expression, which resembles the temperature dependence of deep levels, Equation (2.29). For the other limiting case however (i.e. a temperature independent relaxation rate) a $\ln(\tau)$-over-T^{-1} Arrhenius plot would be required. For the given data, a linear fit in such a graph yields an activation energy decreased by less than 10%. Without knowing the exact dependence of the temperature dependence of the pre-factor of the carrier emission rate, the results in the present case can hence still be assumed to be correct with an accuracy of about 10%. The uncertainties concerning the form of the temperature dependence of the emission rate also hamper a straightforward interpretation of the experimentally determined capture cross-section σ_n.

The experimentally obtained value for the thermal activation energy $E_a =$ 94 meV (or $E_a = 85$ meV assuming temperature independent carrier relaxation, $\hbar\omega \gg k_BT$) corresponds satisfactorily (or rather well) with the numerically calculated value for the quantization energy between QD ground and excited state $\Delta E_{01} = 80$ meV. Furthermore the tunnel barrier determined from the experiment $\Delta E_t = 165$ meV agrees well with the calculated QD ground state energy $E_0 = 195$ meV minus the barrier lowering due to the electric field $\Delta E_{BL} = 20$ meV. The good agreement between the numerically calculated QD level scheme and the experimental results supports the above described model and illustrates the predictive powers of the numerical calculations for providing realistic QD level schemes for a given geometry.

It is furthermore concluded, that in the experiment discussed here only emission from the QD ground states is observed, since the emission of electrons from excited states would be several orders of magnitude faster. A time-constant in the order of ns is to be expected as can be estimated for tunneling with a barrier height of ≤ 100 meV and not even taking further thermally activated emission mechanisms into account.

Since the number of particles in the QDs is small, many-particle effects only play a subordinate role and a rate equation description as commonly used for deep levels in semiconductors, Section 2.3, is approximately sufficient. The "conventional" DLTS evaluation of the transient data as performed in Section 3.1.3 is hence justified.

Due to the small number of carriers (≤ 2) relevant in the present experiment, the effect of Coulomb charging could not be resolved. In experiments on InP QDs in GaInP, a shift of the DLTS peak and the according activation energy was attributed to the influence of Coulomb charging [Ana95, Ana98]. In admittance spectroscopy and DLTS experiments on Ge QDs in Si, Cou-

lomb charging manifests itself in a modified many-carrier activation energy, [Mie00a] (see also Chapter 4).

Also the much smaller value of $b_{fwhm} = 40$ meV of the DLTS signal as compared to the PL FWHM of 150 meV is perfectly understandable. Since the thermally activated process leads from the QD electron ground state to the excited states, the size fluctuations shift both electron levels into the same direction. For a smaller QDs, both levels are shifted slightly towards the matrix conduction band. The influence of the size fluctuations of the ensemble is hence only reflected in changes of the *quantization* energy of the QDs, rather than a modified electron-hole *transition* energy. This is a major difference compared to optical inter-band transitions, since here in a smaller QD the electron and hole levels are shifted towards conduction band and valence band, respectively.[5] As a consequence, the changes of the energy levels of holes and electrons due to size fluctuations accumulate, leading to a stronger broadening in the transition energy than in the quantization energy.

A very similar conclusion on the emission process of electrons in the presence of an electric field was recently drawn from photocurrent experiments on p-i-n structures containing InAs/GaAs QDs with a very similar PL ground state transition energy [Fry00b, Fry00c, Fry01]. From direct measurements of the electric field dependence, an electron ground state energy of 190 meV was deduced [Fry00a] from a one-dimensional tunneling model [Kuo99, Kuo00] in good agreement with the above discussed results of this work and the theoretical predictions.

[5] This behaviour is also clearly apparent from theoretical predictions of QD level schemes, cf. e.g. Figure 4 in [Sti99].

3.2 Comparison of Electron and Hole Emission

In order to compare the emission mechanisms of electrons and holes from InAs QDs in GaAs, two different samples were investigated, both containing a single layer of very similar QDs in a depletion layer diode structure. For electron escape, the strong influence of tunneling on the emission process as reported in the first half of the present chapter was confirmed. For the emission of holes however, a significantly different behaviour was observed; namely, escape by direct thermal activation from the QD hole ground states into the GaAs valence band. The difference is explained by the significantly larger effective mass of holes in the barrier material, which leads to a considerably reduced tunneling probability. Furthermore, a good agreement of the derived QD level scheme with theoretical predictions is found.

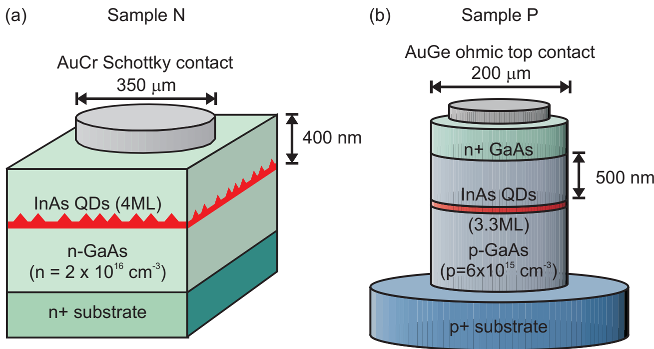

Figure 3.13: *Schematic layer structure of (a) sample N and (b) sample P.*

3.2.1 Samples

Two types of samples, both grown at the "A. F. Ioffe Physico-Technical Institute", St. Petersburg, were studied, differing only in the type of doping of the matrix material in which the InAs QDs are embedded; one is n-type GaAs and the other p-type GaAs. The QDs in both samples have been grown under identical conditions by molecular beam epitaxy (MBE) and can therefore be assumed to have very similar physical properties. In both samples, the QD layer is situated well outside the depletion region at zero external bias. The

two samples, schematically displayed in Figure 3.13, are in the following referred to as ”sample N” and ”sample P”.

Sample N was grown on a n^+GaAs (001) substrate. After a 1 μm uniformly doped n-type GaAs buffer ($n = 2 \times 10^{16}$ cm^{-3}), the QDs were sandwiched between two undoped 10 nm GaAs layers. A nominal thickness of 4 ML InAs at a temperature of 485°C was deposited. During the growth interruption of 20 seconds, the formation of QDs was monitored by reflection high-energy electron diffraction (RHEED) patterns. Finally a 400 nm thick uniformly doped n-type GaAs spacer ($n = 2 \times 10^{16}$ cm^{-3}) was grown. To form diodes, Au-Cr Schottky contacts were evaporated through a shadow mask with circular holes of 350 μm diameter.

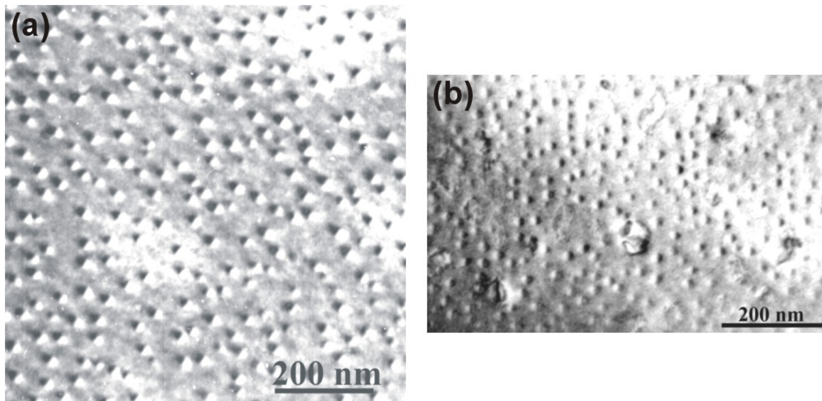

Figure 3.14: *Plan-view TEM images of the QD layer in sample N (a) and sample P (b).*

The second sample (P) has been realized as a n^+-p diode. The reason for this different approach is that proper Schottky barriers are difficult to obtain on p-type GaAs, since barrier heights are typically much smaller than on n-type GaAs [Sze81]. The basic principle of the tunable depletion region however, is of course the same. On top of a p^+GaAs (001) substrate, a 1μm thick uniformly doped p-type GaAs buffer ($p = 6 \times 10^{15}$ cm^{-3}) was created. Then the QDs were grown at a temperature of 480°C, again sandwiched between two undoped GaAs layers of 10 nm thickness each. Nominally 3.3 ML InAs was deposited for QD formation during the growth interruption. On top of the QD structure, a spacer of 500 nm uniformly doped p-type GaAs ($p = 6 \times 10^{15}$ cm^{-3}), and a 500 nm n^+-GaAs layer ($n = 2 \times 10^{18}$ cm^{-3}) to form the p-n junction were grown. Circular mesas of 200 μm diameter were

defined by optical lithography and wet chemical etching. Ohmic top and back contacts were established by respectively evaporating and alloying Au-Ge and Au-Zn.

From plan-view TEM images of the QDs, Figure 3.14, a sheet density of about $N_{QD} \approx 350\ \mu\text{m}^{-2}$ was derived. The lateral dimensions are difficult to obtain from such an image, since the strain contrast leads to a systematic overestimation of the dimensions of the QDs [Ruv95]. From the given image a typical diameter of the QDs of about 20 nm was derived. The true value however, is estimated to be probably more in the order of about 16 nm.

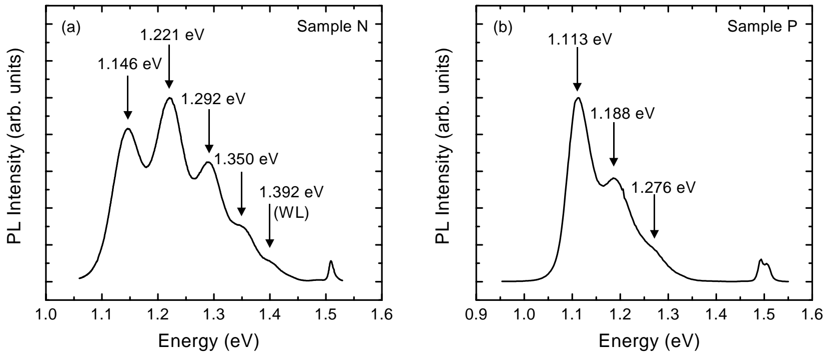

Figure 3.15: *Photoluminescence of sample N (a) and sample P (b) at a temperature of 10 K with an excitation density of about 500 W/cm^2. Several peaks due to excitonic transitions in the QDs are visible in both cases.*

To reveal excitonic transitions in the QDs, standard photoluminescence (PL) measurements were performed at low temperature, $T = 10$ K, using the 514.5 nm line of a 0.5 W Ar^+-laser as excitation source with a power density of about 500 W/cm^2 on the sample, Figure 3.15. QD ground state luminescence is observed at 1.146 eV in sample N and at 1.113 eV in sample P. The FWHM of the PL signal was 55 meV in both samples. Further peaks in the spectrum, due to transitions involving excited states, appear at higher energies, shifted by 75 meV and 88 meV in the case of sample P, and by 75 meV, 71 meV and 58 meV in sample N. The overall PL signal amplitude and the visibility of excited state transitions in sample P appear reduced compared to sample N. This is due to the highly doped and relatively thick additional top layer necessary for the n^+-p diode formation. The almost identical features in the PL spectra demonstrate the structural similarities of both sets of QDs.

Luminescence from the wetting layer is only weakly observed for sample N, where the peak at 1.392 eV is attributed to recombination of bound electrons and holes. The fact that the wetting layer luminescence is quite weak compared to the relatively strong signal visible in Figure 3.4, can be explained by the comparatively high QD density in the present case.

3.2.2 Capacitance-Voltage Characteristics

In order to determine the appropriate biasing conditions for the capacitance transient experiments, the static C-V characteristics of both samples were measured at different temperatures and measurement frequencies. Two representative curves are displayed in Figure 3.16.

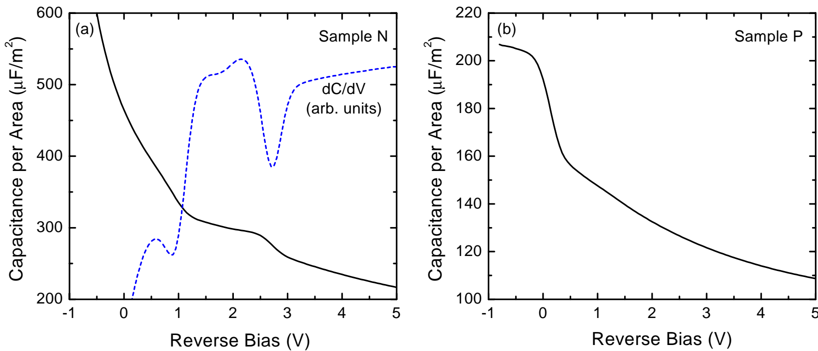

Figure 3.16: *C-V characteristics at $T = 160$ K and a measurement frequency of $f = 1$ MHz. (a) The two-fold plateau structure due to carrier accumulation in QD ground and excited states in the capacitance curve of sample N is only weakly visible. The derivative dC/dV of the data (dotted line) however, exhibits a small dip at about 1.3 V. The plateau in the C-V curve of sample P, panel (b), ends at about 0.5 V reverse bias. Its beginning is not visible for the bias range applicable.*

The C-V characteristic of sample N, Figure 3.16(a), shows the typical plateau structure due to carrier accumulation in the QDs, cf. Section 2.6.1. The two plateaus corresponding to electrons in the ground and excited states however, are almost indistinguishable. This may be due to the smaller energy splitting resulting from the somewhat larger QD dimensions compared to the

previously studied case, cf. Section 3.1.[6] In the derivative of the C-V data [dotted line in Figure 3.16(a)] however, a dip at 1.7 V is clearly visible. From the total width of the plateau (about 1.0 V) and its capacitance (300 μF/m^2), an amount of charge corresponding to about $n^{cv} \approx 5.3$ electrons per QD is derived with help of Equation (2.77). For a reverse bias of about 2.8 V, the QDs are emptied of carriers and the capacitance resembles the typical $C^{-2} \sim V_r$ dependence of the space charge capacitance in a uniformly doped material.[7]

The plateau in the C-V characteristics of sample P, Figure 3.16(b), can not be completely resolved, since the depletion layer is apparently already pinned to the InAs insertion for zero bias.[8] For a reverse bias of about 0.5 V however, the QDs are completely emptied of carriers. This situation is required for the DLTS measurements.

Since the QDs remain always at the edge of the depletion region even for a weak forward bias, the QDs can not be filled with the maximum number of carriers they could theoretically accommodate. This does not necessarily disturb the DLTS measurements, so long as the QDs can be filled with at least a few carriers, which is the case in the present situation.

3.2.3 DLTS Measurements

First, the general features of the DLTS spectra of both samples are discussed, before the dependence of the DLTS signal strengths on pulse and reverse bias is presented. With these experiments the QD layer is verified as the origin of the emitted charge and the electric field dependence of the DLTS signal is studied. Furthermore, the method for controllably charging and emptying the QDs with suitable bias conditions is demonstrated.

---

[6] The dependence of the energy level spectrum of a QD as a function of the dimensions is, e.g. studied theoretically with help of numerical calculations [Sti99].

[7] More information on the C-V characteristics of sample N can be found in a study employing also admittance spectroscopy in [Bru99].

[8] The fact that the depletion region extends into the InAs layer at zero bias could be avoided by either increasing the doping concentration, or the distance between the QD layer and the n-p interface for the given case, cf. Equation (2.15). The adjustment of low doping concentrations in the 10^{16} cm^{-3} range with an accuracy in the order of 10% as necessary for capacitance experiments as presented here, turns out to be relatively difficult. This holds true especially in MOCVD growth, where the background doping concentration is typically in the order of a few 10^{15} cm^{-3} anyway. Significantly higher doping concentrations ($\geq 5 \times 10^{16}$ cm^{-3}) however, lead to considerably shorter depletion layers and higher electric fields, which may cause other experimental problems.

General Observations

The DLTS signal at low temperatures from both samples is presented in Figure 3.17. The data of sample N resembles the behaviour previously studied in Section 3.1; a peak due to thermal activation at about 40 K and a roughly constant contribution due to temperature independent tunneling towards lower temperatures. From a conventional Arrhenius plot, Figure 3.18, an activation energy of $E_a^N = (82 \pm 10)$ meV and a capture cross-section of $\sigma^N \approx 3 \times 10^{-12}$ cm^2 are obtained.

With Equation (2.52) a barrier lowering in the order of $\Delta E_{BL}^N \approx 6$ meV is estimated for sample N assuming a QD height of 3 nm. For a reverse bias of 2.8 V as used in the DLTS experiment the electric field is estimated to be about 4.1×10^6 V/m at the position of the QDs. The barrier lowering here is significantly lower than in the previously discussed case of the triple QD stacks (≈ 20 meV), because of the considerably smaller height of the QD system.

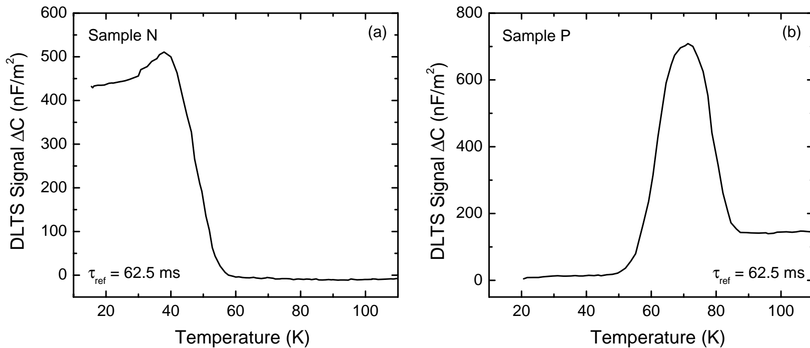

Figure 3.17: *DLTS signal for a reference time constant of 62.5 ms of (a) electron emission from the QDs in sample N ($V_r = 2.8$ V and $V_p = 0.2$ V) and (b) hole emission from the QDs in sample P ($V_r = 2.0$ V and $V_p = -0.4$ V). In both cases bias pulses with a duration of 10 ms were applied.*

There is a significant difference in the DLTS signal from sample P compared to the DLTS signal of sample N. No contribution from tunneling at low temperatures can be observed, and a peak due to thermally activated emission of holes appears at about 70 K. A weak DLTS signal towards higher temperatures is the onset of a DLTS peak related to defects in the p-type GaAs. An Arrhenius plot of the peak maxima for varying reference time constant,

Figure 3.18, yields $E_a^P = (164 \pm 10)$ meV and a capture cross-section of $\sigma^P \approx 5 \times 10^{-12}$ cm^2.

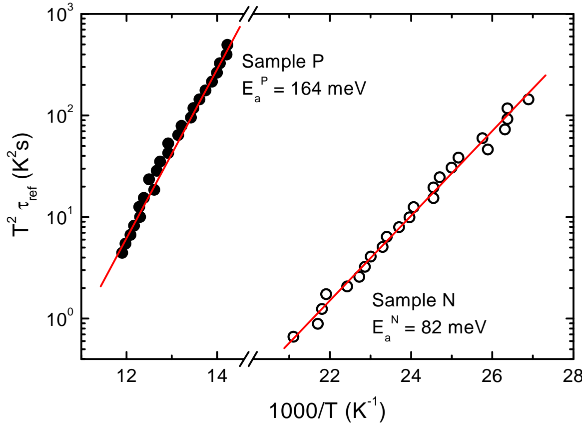

Figure 3.18: *Standard Arrhenius evaluation of the peaks in the DLTS spectra of sample N (open circles) and sample P (solid circles), see Figure 3.17.*

Dependence of DLTS Signal on Bias Conditions

Varying the reverse and pulse bias conditions in the DLTS measurements of sample N, Figure 3.19, leads to very similar behaviour of the shape and strength of the DLTS signal as previously observed in Section 3.1.

The relative DLTS signal amplitude of this set of measurements is displayed in Figure 3.20. The similarity of the behaviour observed here with the data of the triple-stack QDs presented in Figure 3.10 is obvious, although the QD structure in the present experiment is rather different. As expected, the DLTS signal amplitude for the single layer of QDs exhibits the same bias dependence as the closely coupled triple layer in the previous case. The good agreement hence supports the interpretation of the underlying emission mechanisms of direct tunneling and thermally activated tunneling.

The DLTS signal amplitude remains practically constant for fixed reverse bias $V_r = 2.8$ V and increasing filling pulse bias V_p, until for $V_p \geq 2.2$ V the signal is strongly suppressed, reflecting the fact that the QDs can not be completely charged. For fixed filling pulse bias $V_p = 1.0$ V, it appears that the QD DLTS signal only is observable for reverse biases $V_r \geq 2.2$ V. A maximum

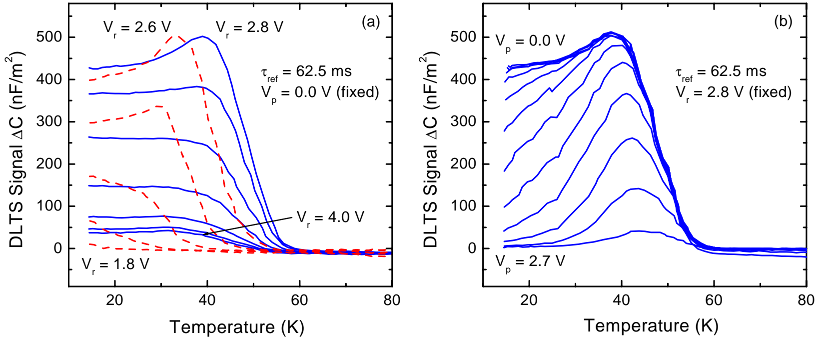

Figure 3.19: *DLTS signal of sample N for a reference time constant of 62.5 ms for varying bias conditions. (a) DLTS signal for fixed pulse bias $V_p = 0.0$ V and increasing reverse bias $V_r = 1.8$ V, 2.0 V, ..., 2.6 V (dashed lines, bottom to top), 2.8 V, ..., 4.0 V (solid lines, top to bottom). (b) DLTS signal of the measurements with fixed reverse bias $V_r = 2.8$ V and increasing pulse bias $V_p = 0.0$ V, 1.0 V, 1.8 V, 1.9 V, ..., 2.7 V (top to bottom).*

is reached for $V_r = 2.8$ V and then the overall amplitude decreases again purely due to geometric reasons, Equation (2.96), and the increasing tunnel rate.

Again, the bias range for which the DLTS signal can be generated, from 2.2 V to 2.8 V, coincides with the bias range in the C-V characteristic, Figure 3.16(a), where the QD ground states are emptied. This confirms the attribution of the DLTS signal in sample N to the QD ground states.

From measurements with varying reverse and pulse bias of sample P, Figures 3.21 and 3.22, a DLTS amplitude profile is generated for the DLTS peak at about 70 K, Figure 3.23. The onset of the DLTS signal for low reverse or pulse biases can not be resolved as a result of the situation discussed previously for the C-V characteristic. The major difference is the decrease of the DLTS signal for increasing reverse biases, which takes place on a much larger bias range and nicely resembles the theoretically expected $\sim (V_b + V_r)^{-3/2}$ dependence, Equation (2.96).

From this behaviour two conclusions can be drawn. Firstly, the DLTS signal originates from a single layer in the sample, which in conjunction with the C-V data, Figure 3.16(a), is identified as the QD layer. Secondly, the $\sim (V_b + V_r)^{-3/2}$ decrease of the DLTS signal presents further evidence for the

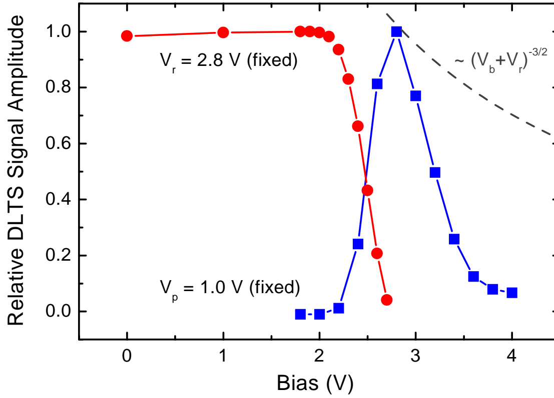

Figure 3.20: *DLTS bias profile of the peak at about 40 K of sample N obtained for varying bias conditions. The DLTS signal for fixed reverse bias $V_r = 2.8$ V and increasing pulse bias V_p (circles) remains constant until for a pulse bias of more than $V_p = 2.2$ V the QD states can only partly be filled and the DLTS signal disappears. The DLTS signal in the measurements with fixed pulse bias $V_p = 1.0$ V (squares) rises for reverse biases above $V_r = 2.2$ V, has a maximum for about 2.8 V, and then decreases quickly again. The theoretical $\sim (V_b + V_r)^{-3/2}$ dependence of the DLTS signal strength without tunnel emission, Equation (2.96), is indicated by the dashed line.*

absence of tunnel emission of holes, which would lead to a faster decreasing signal with reverse bias as observed in the case of electron emission.

The activation energy of the QD peak in sample P is found to decrease with increasing reverse bias applied as displayed in Figure 3.24. A standard $\ln\left(T^2\tau\right)$ over T^{-1} Arrhenius plot was used to obtain the activation energies. The straight line is a linear fit to the data yielding an extrapolated zero bias activation energy of $E^P_{a,0} = 194$ meV and a slope of -9 meV/V. The extrapolated zero-bias activation energy $E^P_{a,0}$ is considered to be the more relevant figure than the previously obtained activation energy for a finite reverse bias, which is modified by the effects of the electric field. The zero-bias activation energy is therefore considered in the following discussion.

The field-dependence of the activation energy of hole emission in sample P is too strong to be explained only by the Poole-Frenkel effect, which is estimated to be less than -3 meV/V [Equation (2.52), assuming $r \approx 2.5$ nm]. Assuming the Poole-Frenkel effect to be the origin of the field-enhancement of the

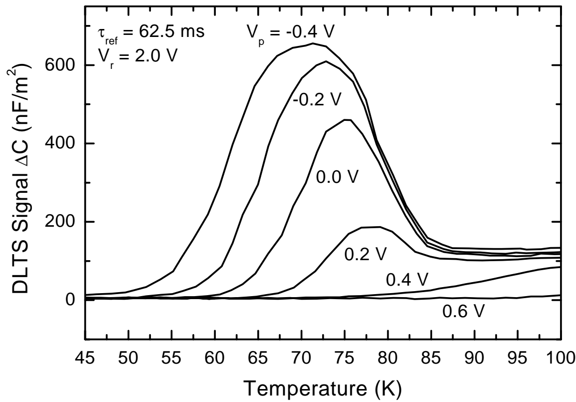

Figure 3.21: *DLTS signal of sample P for fixed reverse bias $V_r = 2.0$ V and increasing filling pulse bias $V_p = -0.4$ V, -0.2 V, ..., 0.6 V (from top to bottom) with a pulse length of 10 ms for a reference time constant of 62.5 ms.*

emission, would yield $r = 7$ nm and hence a QD height of about 14 nm, which is much to big.

The stronger dependence of the activation energy and hence the emission rate on the external bias is hence probably an indication of *electric-field-induced phonon-assisted tunneling*, see Section 2.3.6. It was carefully attempted to fit a model to the data, taking thermal activation with additional Poole-Frenkel barrier lowering, and phonon-assisted tunneling into account. The numerical fitting procedure based on evolutionary strategies [Rec72, Hei96a] always yielded reasonable values for the activation energy and the capture cross-section (similar to those obtained from the DLTS evaluation), but the values for the Huang-Rhys parameter and the phonon energy varied in a rather wide range ($S = 14 \dots 22$ and $\hbar\omega = 11 \dots 20$ meV). Even with dedicated measurements the reproducibility of the fitting results could not be enhanced.

3.2.4 Discussion

The results of the measurements and the derived or estimated values presented in the previous sections are summarized in Table 3.2.

The hole escape process turns out to be significantly different from the electron escape process, the latter of which has already been discussed in detail

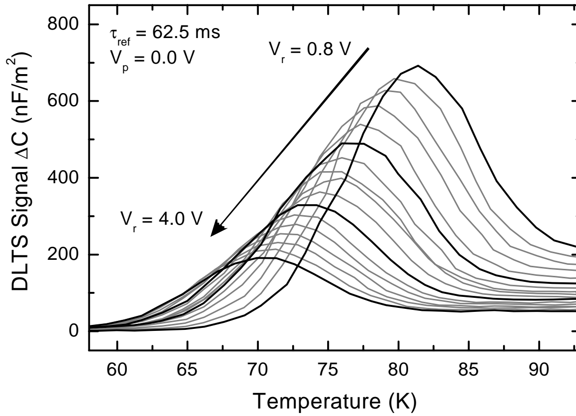

Figure 3.22: *DLTS signal of sample P for fixed filling pulse bias* $V_p = 0.0$ *V and increasing reverse bias* $V_r = 0.8$ *V, 1.0 V, ..., 4.0 V (from top to bottom) with a pulse length of 10 ms for a reference time constant of 62.5 ms. The bias range corresponds to an electric field range at the position of the QDs of about* $1.7 \times 10^6 \dots 5.2 \times 10^6$ *V/m. The data show a pronounced field-effect shifting the peak position towards lower temperatures as the reverse bias increases.*

in Section 3.1. For holes, no tunneling contribution at low temperatures was observed and the activation energy of the thermally activated process is significantly larger. This is attributed to thermal activation from the QD hole ground state to the GaAs valence band.

Using the PL ground state transition energy as a measure for the QD dimensions, with help of [Sti99] (taking the exciton binding energy, ≈ 20 meV, and the temperature shift into account) a QD base length of about 15 nm is estimated in good agreemente with the corrected TEM observations. This base length is then used to determine the calculated electron and hole energy levels with help of Figure 4 of [Sti99].

The observed hole activation energy ($E_a^P = 194$ meV) agrees well with the theoretically predicted hole ground state energy (185 meV). For the electrons, there is satisfying agreement of the experimentally determined activation energy for electrons ($E_a^N = 82$ meV) with the theoretically predicted value for the ground/excited state energy splitting (70 meV), and the PL peak splitting ($\Delta E_{0,1} = 75$ meV). An energy splitting of 80 meV, in good agreement with

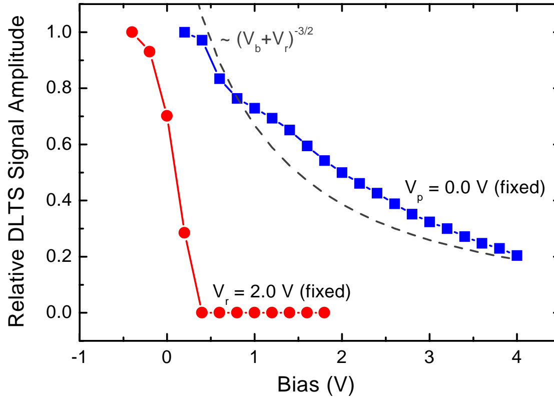

Figure 3.23: *DLTS bias profile of the peak at about 70 K of sample P. The DLTS signal for fixed reverse bias* $V_r = 2.0$ *V and increasing pulse bias* V_p *(circles) quickly vanishes until for* $V_p = 0.4$ *V the QD states not be filled anymore and the DLTS signal disappears. The DLTS signal in the measurements with fixed pulse bias* $V_p = 0.0$ *V (squares) decreases as the reverse bias increases. The decrease in DLTS signal amplitude is in rather good agreement with the* $\sim (V_b + V_r)^{-3/2}$ *dependence predicted by Equation (2.96), a fit of which is indicated by the dashed line (using* $V_b = 1.28$ *V).*

the results from the DLTS measurements, was also obtained from admittance spectroscopy measurements and the C-V characteristic [Bru99].

The apparent difference in the emission mechanisms for electrons and holes is attributed to the different effective masses of electrons and holes, since the effective mass influences the tunneling probability, see Equation (2.54). For InAs and GaAs the heavy hole effective mass typically by a factor of 10 larger than the electron effective mass. Since diffusion of In from the QDs into the matrix material is commonly observed [Wu97, Fry00b, Liu00], the exact value of the effective mass for holes in the barrier is difficult to predict. The emission mechanisms of electrons and holes are sketched in Figure 3.25.

The weaker dependence of the DLTS signal amplitude of hole emission on reverse bias furthermore indicates that pure tunneling does not play a major role for the time constants investigated. From the dependence of the activation energy on reverse bias however, it is concluded that phonon-assisted tunneling may contribute to the hole emission process.

The major difference between pure thermal activation and phonon-assisted tunneling manifests itself in the electric-field dependence of the emission rate

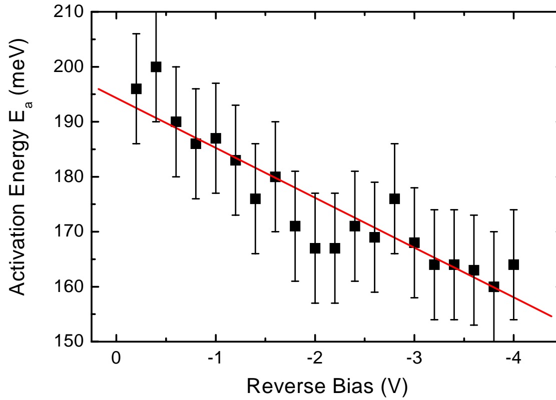

Figure 3.24: *Dependence of the activation energy of the QD DLTS peak in sample P on reverse bias V_r. The error bars correspond to the estimated accuracy of the activation energies as determined from Arrhenius plots, about ±10 meV. The straight line is a linear fit of the data (y-axis intersection $E^P_{a,0} = 194$ meV and slope -9 meV/V).*

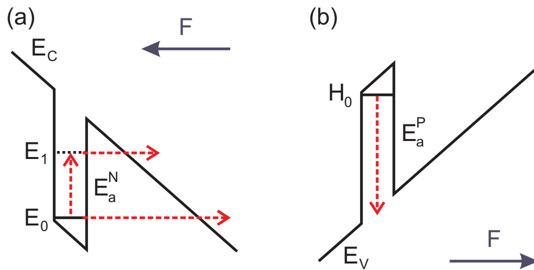

Figure 3.25: *Emission mechanisms of electron and hole escape in the presence of an electric field. Electrons from the QD ground state are emitted by direct tunneling and thermally activated tunneling probably involving excited QD states (a), whereas holes are emitted by pure thermal activation from the ground state into the matrix materials valence band (b).*

as discussed in Section 2.3.6. This mechanism could not be studied in detail in the present sample, since only a rather limited field range is accessible in the given sample structure. An investigation of phonon-assisted tunneling of holes from InAs/GaAs QDs remains hence subject to future work.

Quantity	Description	Value
E_a^N	thermal activation energy for sample N	(82 ± 10) meV
σ^N	capture cross-section for sample N	3×10^{-12} cm^2
$E_{a,0}^P$	thermal activation energy for sample P	(194 ± 10) meV
σ^P	capture cross-section for sample P	5×10^{-12} cm^2
n_{QD}^{cv}	number of carriers per QD from CV	5.3
ΔE_{BL}	estimated barrier lowering	5 meV
E_{PL}	PL ground state transition energy (10 K)	1.130 eV
$\Delta E_{0,1}$	PL ground/excited state energy splitting	75 meV
E_0	QD electron ground state from calculations	255 meV
ΔE_{01}	QD electron quantization energy from calculations	70 meV
H_0	QD hole ground state from calculations	185 meV

Table 3.2: *Summary of the results from the investigation of hole and electron emission from InAs QDs in GaAs. The calculated values were taken from [Sti99].*

Chapter 4

Hole Emission from Many-Particle States in Ge/Si Quantum Dots

In this chapter carrier emission from Ge QDs embedded in a Si matrix is studied by capacitance transient spectroscopy. Hole emission from QD states and the Ge wetting layer is observed. The amount of charge stored on the QDs is controlled by the filling pulse bias and can be directly monitored by DLTS measurements. For the hole ground state energy an activation energy of 350 meV is obtained in good agreement with optical data and results from admittance spectroscopy.

Due to their comparatively large dimensions, the QDs can be charged with a maximum of more than 50 carriers. Emission from such many-particle states is discussed in terms of a simple model assuming independent emission, which allows the reproduction of the experimentally observed dependence of the DLTS signal and the apparent activation energy on filling pulse bias. Finally, the shortcomings of the present model are discussed. A more sophisticated microstate description is presented in Section 5.2.

4.1 Samples

The samples of this study were grown at the ”Walter Schottky Institut”, TU-München, by solid-source MBE at a temperature of $T = 550$ °C on highly p-doped (100) Si substrates. On top of a 120 nm Si buffer layer, weakly doped with boron ($p = 1.0 \times 10^{16}$ cm^{-3}) and 8.5 ML Ge in the Stranski-Krastanow growth mode leading to QD formation [Eag90, Mo90, Sch95, Sun96, Abs96, Sch99] were deposited. In the reference sample the Ge was substituted by the same amount of Si. The QD layer was covered by 480 nm of boron-doped Si ($p = 1.0 \times 10^{16}$ cm^{-3}). On top of these layers, Schottky diodes with an area of 0.14 mm^2 were defined by standard optical lithography, mesa etching, evaporation of Ti/Au (barrier height about 0.6 V), and lift-off. Further details of the samples and the QD growth process can be found in [Asp00, Mie01].

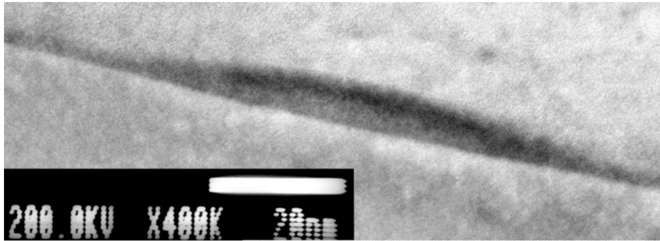

Figure 4.1: *Cross-section TEM image of a single Ge QD in Si [Mie01].*

The properties of the QDs in the Ge layer were characterized by atomic-force microscopy (AFM), high-resolution cross-section transmission electron microscopy (HRTEM), and photoluminescence (PL) [Mie00c]. From AFM measurements of uncapped reference samples with QDs, a sheet density of $N_{QD} = 45\ \mu$m^{-2} is determined. The HRTEM investigation, Figure 4.1, yields typical QD diameters of about 70 nm and island heights of about 6.5 nm. The Ge wetting layer was found to have a thickness of about 4 ML.

PL spectroscopy at 6 K, Figure 4.2, exhibits emission from the Ge QDs at 820 meV with a full-width at half-maximum (FWHM) of 70 meV. The broadening is due to TO-phonon replica [Abs96] and QD ensemble inhomogeneities; the latter is estimated to lead to a FWHM broadening of about 50 meV or less in the present case. Since the Ge/Si band discontinuity is known to be of type II, the PL emission is attributed to recombination of electrons from the Si conduction band with confined holes in the Ge QDs. A hole ground state energy of $E_{h0,PL} = 350$ meV is therefore deduced, which is in good agreement

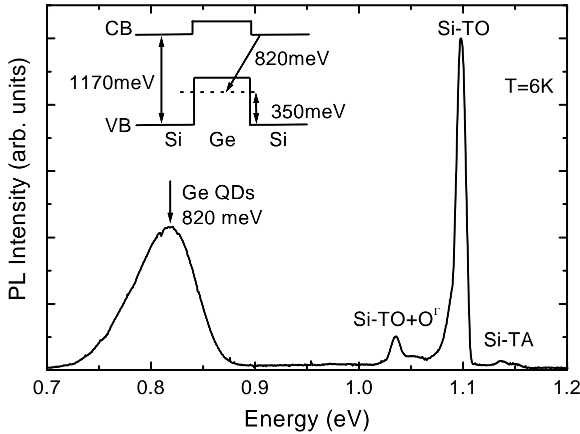

Figure 4.2: *Photoluminescence data of the QD structure at $T = 6$ K [Mie01]. The inset shows the schematic band line-up and the spatially indirect optical transition attributed to recombination of holes in the Ge QDs with electrons from the Si.*

with an activation energy of 355 meV obtained from admittance spectroscopy investigations [Mie00a, Asp01] and results from photo-current spectroscopy [Mie00b].

In Figure 4.3, the layer structure of the QD sample is displayed together with schematic band diagrams for different external bias situations. For zero bias the depletion region does not yet extend towards the Ge layer, which is hence filled with holes. The maximum amount of charge on the QDs is limited by quantization and the resulting band bending, which also leads to depletion regions on either side of the Ge, Figure 4.3(b). The band bending at the position of a QD is naturally equivalent to the Coulomb repulsion between the confined carriers.

For increasing reverse bias, the amount of charge localized in the QDs decreases, Figure 4.3(c), until for sufficiently high bias the QDs are empty, Figure 4.3(d). This behaviour is also reflected by the capacitance-voltage characteristic (C-V) of the QD sample, Figure 4.4, which exhibits a pronounced plateau between about 1.5 V and 4.0 V. This is due to charge accumulation in the QDs, cf. Sections 2.5.1 and 2.6.1. The extension of the plateau exhibits a clear dependence on the measurement frequency. At 200 K the plateau can only fully be resolved at a measurement frequency of 1 kHz or less, because

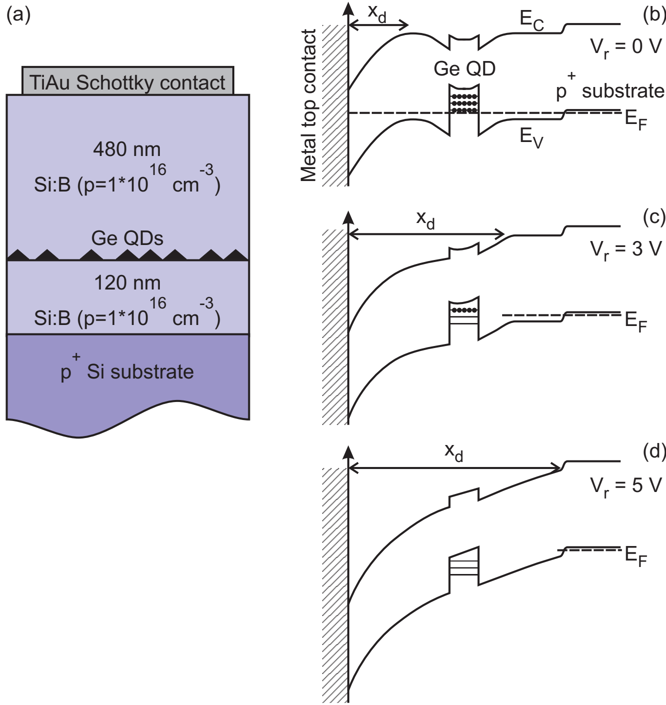

Figure 4.3: *Sample layers (a) and schematic band structure for different external biasing conditions. For zero external bias $V_r = 0.0$ V the QDs are filled (b), for a medium reverse bias $V_r = 3.0$ V part of the charge is removed (c), and for $V_r = 5.0$ V the QDs are completely emptied (d).*

the carriers confined in the QDs can not follow the AC voltage if the frequency is larger than the emission rate. In the following only the case for sufficiently low frequencies is considered.

Above 4.0 V the QDs are completely emptied and the depletion region underneath the QD layer adds to the total depletion width. This results in a drop in capacitance. For higher reverse biases the depletion region extends towards the highly doped substrate, which results in a fixed depletion width and hence a constant capacity. From the width of the plateau, about 2.5 V, and the capacitance, about 157 μF/m^2, one estimates a charge density in the QD layer corresponding to about $n_0^{CV} \approx 55$ holes per QD employing Equation (2.77).

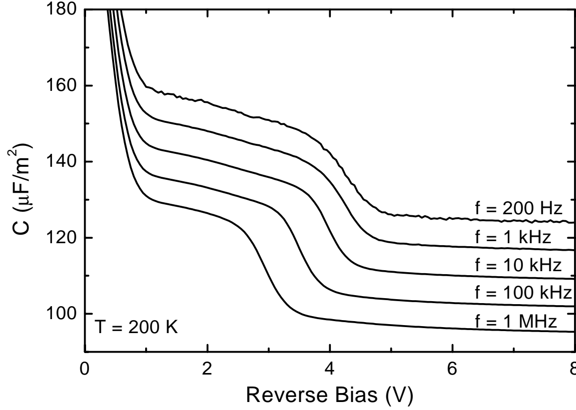

Figure 4.4: *C-V characteristic of the QD sample at $T = 200$ K for increasing frequency $f = 200$ Hz, 1 kHz, 10 kHz, 100 kHz, and 1 MHz. Except for $f = 200$ Hz, the data is displayed vertically offset.*

Additional features in the plateau, due to quantization in the QDs, can not be resolved, since the quantization energy is very small as a consequence of the rather large dimensions of the given QD system. This has been verified for a large range of temperatures (10 K – 350 K) and frequencies (100 Hz – 1 MHz).

To estimate the quantization energy ΔE_q, we follow the basic assumptions outlined in Section 5.2.1 and apply a simple two-dimensional harmonic oscillator model with a potential depth of 350 meV and a radius of 35 nm. This approach yields $\Delta E_q = 12$ meV. The Coulomb energy $\Delta E_C = 5$ meV is estimated according to Equation (5.19) assuming a disk-like geometry of the QDs.

4.2 DLTS Experiments and Discussion

A series of DLTS measurements for varying reverse and pulse bias conditions were performed. The filling pulse length was set to 10 μs during all the experiments. In the QD sample, a pronounced signal due to hole emission is visible at temperatures below 180 K (see, e.g. Figure 4.5). No further DLTS signal can be observed up to 350 K. The absence of a DLTS signal in measurements on the reference sample without QDs, for the whole temperature range of 20 K to 350 K, leads to the attribution of the observed DLTS structure to the Ge QDs.

This interpretation is further supported by the dependence of the data on the bias conditions.

4.2.1 Partial Filling by Variation of Pulse Bias

Applying a fixed reverse bias $V_r = 5.0$ V and decreasing the filling pulse bias V_p leads to an increasing DLTS signal consisting of a peak at about 140 K and a broad contribution towards lower temperatures, Figure 4.5.

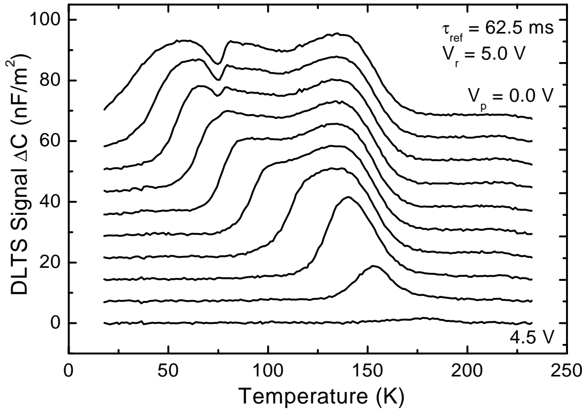

Figure 4.5: *DLTS signal of the QD sample for a reference time constant of 62.5 ms, fixed reverse bias $V_r = 5.0$ V, and decreasing filling pulse bias $V_p = 4.5$ V, 4.0 V, ..., 0.5 V, and 0.0 V (from bottom to top). The curves are displayed offset for clarity.*

For a pulse bias of $V_p = 4.5$ V, no DLTS signal is visible. As the pulse bias is decreased the peak at about 140 K develops and soon saturates in height for $V_p \leq 3.5$ V. For further decreasing pulse bias, a broad DLTS signal towards lower temperatures arises. Finally, for pulse biases under 1.5 V, a small minimum at about 75 K and a second broad peak at about 60 K appear. Applying standard Arrhenius plot data evaluation of the DLTS signal, Figure 4.6(a), yields the dependence of the apparent activation energy on pulse bias as displayed in Figure 4.6(b). The accuracy of the obtained activation energies is estimated to be about ±20 meV. The hole capture cross-sections σ_p determined by the Arrhenius evaluation were in the order of 10^{-15} cm^2 up to 10^{-14} cm^2.

The activation energy of the 140 K peak decreases with decreasing filling pulse bias from about 350 meV for $V_p = 3.5$ V to about 300 meV for $V_p = 3.0$ V.

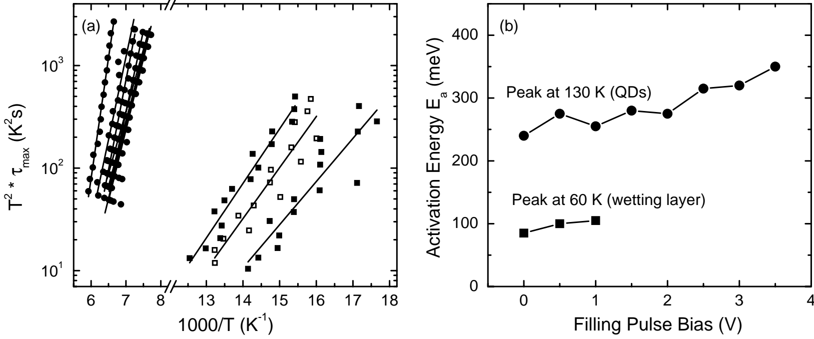

Figure 4.6: *(a) Standard Arrhenius plot evaluation of the QD DLTS peak at 140 K (circles) and the peak attributed to hole emisson from the wetting layer at 60 K (squares) for the DLTS data of Figure 4.5. (b) Activation energies as function of filling pulse bias.*

For further decreasing pulse bias, the activation energy only decreases slowly towards about 250 meV at $V_p = 0.0$ V. The 60 K peak has a roughly constant activation energy (about 100 meV) for the bias range ($V_p = 1.0$ V...0.0 V) it is visible.

This behaviour is explained by partial filling of the hole energy levels in the Ge QDs. For high filling pulse biases the depletion region during the pulse is only weakly decreased and only the lowest energy levels of the larger QDs in the ensemble are situated below the Fermi energy. Only few carriers can hence enter the QDs occupying only the lowest states, which leads to a large apparent activation energy of 350 meV resembling the Ge/Si band discontinuity.

For decreasing pulse biases, an increasing number of holes can be filled into the QDs leading to an increasing contribution of multi-particle interaction to the total energy. These contributions result from the quantization and the limited degeneracy of each quantum level and the Coulomb charging energy. The energy necessary to remove a hole from the highest states of such a well-filled QD is hence significantly smaller than in the case of a QD filled with only a few carriers. This effect may hence explain the observed activation energies. It is worth noting, that the emission from many-particle states in the present experiment is measured and interpreted in an averaged way. As a second consequence of the many-carrier occupation of QDs for smaller pulse biases, an additional DLTS signal appears at lower temperatures corresponding roughly to smaller activation energies. If the QD states are filled up to their

highest levels, also states in the wetting layer are occupied during the filling pulse. The peak at about 60 K is hence attributed to hole emission from wetting layer states. Somewhat puzzling is the dip at about 70 K in the DLTS spectrum, which could be related to an enhanced multi-step emission process for holes of energies close to that of the wetting layer.

4.2.2 Partial Emptying by Variation of Reverse Bias

A rather different picture arises from keeping the filling pulse bias fixed at $V_p = 0.5$ V and varying the reverse bias $V_r = 1.0$ V, 1.5 V, ..., 5.5 V, and 6.0 V, Figure 4.7. For reverse biases larger than about 4.5 V, the DLTS signal resembles the structure as previously discussed, decreasing somewhat in overall amplitude for increasing reverse bias as expected from Equation (2.96). Decreasing the reverse bias below 4.5 V leads to a suppression of the high-temperature part of the DLTS signal. This is in perfect accordance with the picture sketched out in the previous paragraphs. Here however, the QDs are always completely filled. For reverse biases of less than 4.5 V, the lowest QD levels are no longer lifted above the Fermi level, cf. Figure 4.3 and Figure 4.4. As a consequence, the DLTS signal at higher temperatures, corresponding to larger activation energies, disappears.

The strong enhancement of the DLTS signal at the ”edge”-temperature above which no DLTS signal is visible, is not yet understood and may be due to a enhanced emission process for the QD energy levels just above the Fermi level after the pulse. Furthermore, the additional peak appearing at higher temperatures for pulse biases below 2.5 V, which quickly shifts towards lower temperatures for decreasing pulse bias, is rather strange. No activation energy can be obtained from standard Arrhenius plot evaluation for this peak. These observations are possibly an indication of a strongly modified emission process of multiply charged QDs being lifted only partly above the Fermi energy.

The dependence of the DLTS signal amplitude of the peaks attributed to the QDs and the wetting layer on reverse bias is presented in Figure 4.8. Both signals approximately exhibit the $\sim (V_b + V_r)^{-3/2}$ dependence expected for a two-dimensional emission source in the depletion layer, Equation (2.96).

The activation energies of the peaks in Figure 4.7 were obtained by standard Arrhenius plot evaluation Figure 4.9(a). The resulting activation energies as function of reverse bias are displayed in Figure 4.9(b). For a reverse bias of 4.0 V or larger, the activation energy of the QD peak remains roughly constant at about (260 ± 20) meV and quickly decreases with decreasing reverse bias until it approaches the apparent activation energy of the wetting layer emission

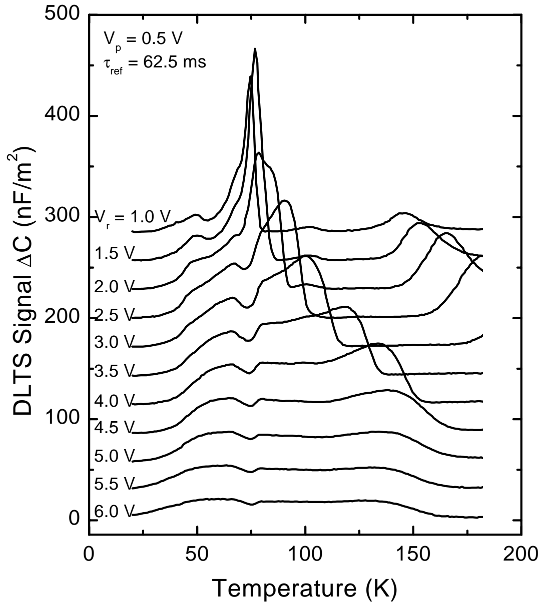

Figure 4.7: *DLTS signal of the QD sample for a reference time constant of 62.5 ms, fixed pulse bias $V_p = 0.5$ V, and decreasing reverse bias $V_r = 6.0$ V, 5.5 V, …, 1.5 V, and 1.0 V (from bottom to top). The curves are displayed offset for clarity.*

(100 meV … 150 meV, depending on the reverse bias). This behaviour is attributed to the fact, that it is impossible to empty the lowest QD states for reverse biases below about 4.5 V, cf. Figure 4.4. Emission from higher states only may hence explain the observed decreased activation energy. This is, because only the *averaged* activation energy is observed in the present experiment.

The activation energy of the emission from the wetting layer is found to slightly increase from 100 meV for $V_r \geq 4.5$ to about 150 meV for $V_r \leq 2.5$ V. For reverse biases of 3.0 V or less however, a clear attribution of the observed DLTS peak to emission from QDs or wetting layer can no longer be given. Due to the wetting layer states being energetically closer to the Si valence band, it seems nevertheless reasonable to ascribe the observed signal to hole emission from these states.

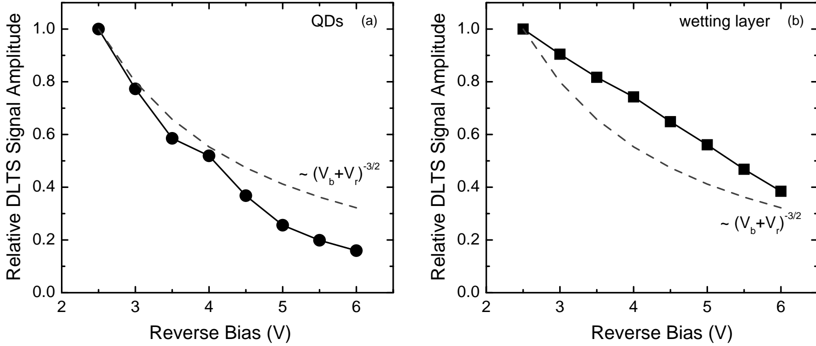

Figure 4.8: *Relative DLTS signal amplitude for increasing reverse bias (from Figure 4.7) for the peaks attributed to hole emission from the QDs (a) and the wetting layer (b). The dashed lines are the theoretically expected dependence given by Equation (2.96).*

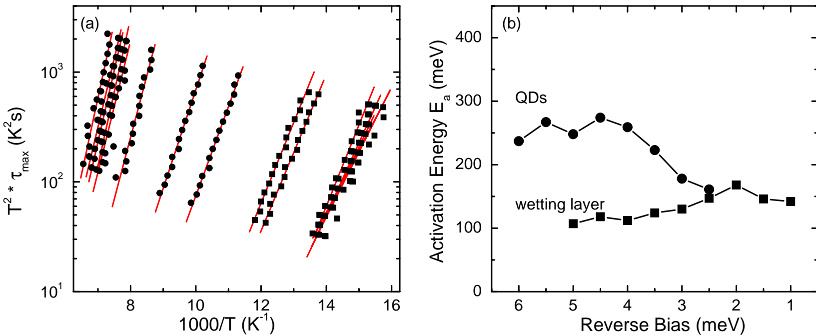

Figure 4.9: *(a) Standard Arrhenius plot evaluation of the peaks in the DLTS data of Figure 4.7. (b) Resulting activation energies of the QD peak (circles) and the peak attributed to emission from the wetting layer (squares) as function of reverse bias.*

4.2.3 Simulations

In order to obtain a qualitative confirmation of the above discussed interpretation of the DLTS signal, a simple harmonic oscillator model is applied, assuming an energy spectrum determined by Coulomb charging and quantization. For this model, a potential depth of 350 meV is assumed. Cou-

lomb charging and quantization are taken to be given by the above derived values, $\Delta E_C = 5$ meV and $\Delta E_q = 12$ meV respectively. Furthermore, ensemble broadening of the QD levels is taken into account with an equal FWHM of 50 meV. These assumptions lead to a quasi-continuous energy spectrum, see Figure 4.10. For the capture cross-section, the experimentally determined value of 10^{-15} cm^2 was used. DLTS spectra were generated by summing over the emission rates of all occupied energy levels.

A two-dimensional harmonic oscillator model as used here, allows the qualitative prediction of the energy level structure of large QDs with big aspect ratios of base width to height. In the case of highly-strained smaller QDs however, e.g. InAs/GaAs QDs, three-dimensional calculations of the bound states are necessary to obtain realistic predictions for the QD energy levels. Also many-particle effects due to Coulomb charging depend sensitively on the actual wave functions and can hence only be estimated in the presented way for comparatively large QDs.

In order to account for partial filling, a limit energy E_{fill} relative to the bottom of the confinement potential is introduced, which corresponds to the Fermi energy during the filling pulse and up to which the QDs states are assumed to be charged with holes by the filling pulse. Then DLTS spectra are simulated as function of E_{fill}, see Figure 4.11.

It is worth noting, that the present model implicitly assumes independent single-particle emission from many-particle states. A QD occupied by n carriers however, has n possibilities to change into a $n-1$ carrier state by emission of one of the carries with a probability depending on which particle is emitted. If carriers from lower quantum states are emitted, relaxation of carriers in higher states may occur. Such a trickle-down effect is not accounted for in the simple rate equation model used here.

The supposition of holes from the highest levels being emitted first, is nevertheless qualitatively somehow acceptable, since the thermal activation energy for the higher levels is smaller than the energy necessary to activate carriers occupying the lower levels. Carriers from the higher quantum states are hence emitted with a higher probability than carriers from lower states.[1]

The simulated DLTS curves, Figure 4.11, agree qualitatively well with the measured DLTS data of Figure 4.5 in that for increasing E_{fill} a weak initial peak at about 140 K appears, which soon saturates and develops a broad shoulder towards lower temperatures. The activation energies of this signal are determined applying standard Arrhenius plot evaluation as for the experi-

[1] See also the more detailed discussion presented in Chapter 5.

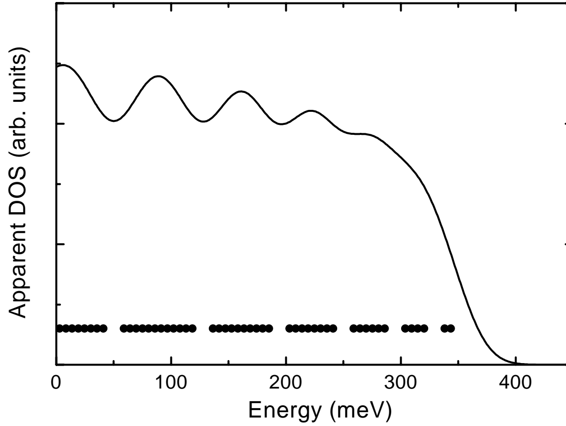

Figure 4.10: *Quasi-continuous energy spectrum used for the simulations (continuous line) assuming an energy level broadening with a FWHM of 50 meV due to ensemble fluctuations. The dots indicate the positions of the sharp energy levels determined from quantization and Coulomb charging.*

mental data, Figure 4.12(a). By this procedure, the dependence of the apparent activation energy on the limit energy E_{fill} is obtained, see Figure 4.12(b). The behaviour of the activation energy for in creasing filling (i.e. decreasing limit energy E_{fill}) resembles the experimentally observed behaviour quite well. The activation energy first decreases from about 350 meV for $E_{fill} = 10$ meV (corresponding to only the lowest QD levels being filled) before saturating at an activation energy of about 280 meV for $E_{fill} \geq 90$ meV [Figure 4.12(b)].[2]

The qualitative agreement between the simulated DLTS spectra with the experimental observations are taken as further evidence for the given interpretation of the observed DLTS signal as being due to hole emission from multiply-charged Ge QDs.

4.3 Summary of the Results

The emission process of holes from Ge QDs embedded in Si was observed by capacitance transient spectroscopy. In a reference sample without QDs no

[2]Note that the x-axis of Figure 4.12(b) and Figure 4.6(b) can not readily be related.

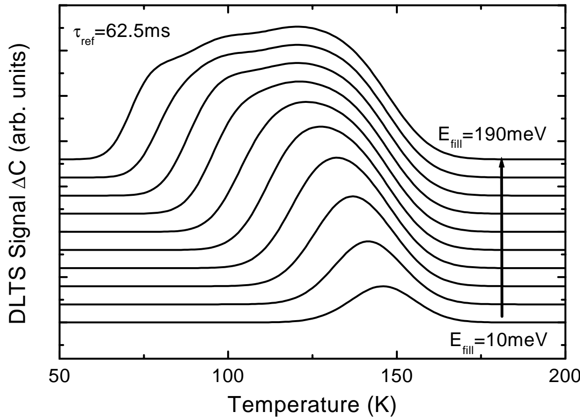

Figure 4.11: *Simulated DLTS curves according to the model described in the text for increasing limit energy E_{fill} (bottom to top) for a reference time constant of 62.5 ms. The curves are displayed offset for clarity. Note the good qualitative agreement with the measured DLTS data in Figure 4.5. The peak due to the wetting layer, which was not taken into consideration for the simulations.*

DLTS signal could be obtained. The DLTS signal in the QD sample was found to be strongly dependent on reverse and pulse bias conditions. An investigation of the dependence of the DLTS signal shape on bias conditions lead to the attribution of the DLTS signal to emission from multiply-charged QDs with a dense energy spectrum. This interpretation was supported by the dependence of the activation energy on filling pulse bias obtained from standard Arrhenius plot evaluations. If only the lowest QD levels are filled, the activation energy of 350 meV resembles the Ge/Si band discontinuity. It is worth noting, that these apparent activation energies are not a direct measure for the energy spectrum of the QDs, since emission from such many-particle states depends on which carrier from a given configuration is emitted. In the present treatment however, the emission process is observed and evaluated in an averaged manner.

A second peak at lower temperatures, which appears only if the QDs are completely filled during the bias pulse, is attributed to hole emission from the Ge wetting layer. The results of the experiments are summarized in Table 4.1.

The attribution of the observed DLTS signal is supported by studying the emission for varying reverse and pulse bias conditions. Adjusting the pulse bias, allows for only partly filling the QDs, which suppresses the peak due to

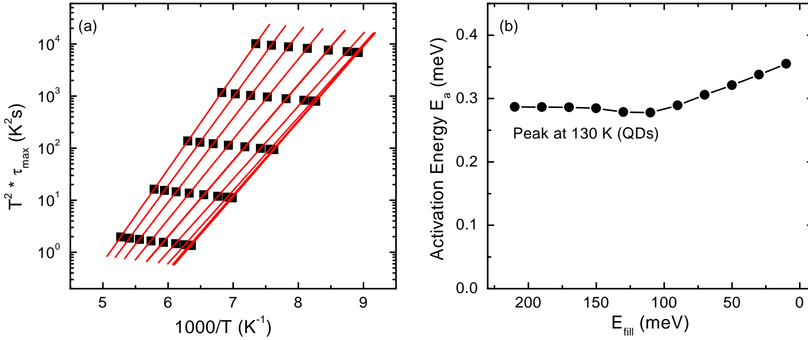

Figure 4.12: *(a) Standard Arrhenius plot evaluation of the peak at about 130 K in the simulated DLTS signal presented in Figure 4.11, and (b) resulting activation energies. Note, that the x-axis of panel (b) was reversed in order to show the similarity with the experimental results displayed in Figure 4.6(b).*

Quantity	Description	Value
n_{QD}^{cv}	number of carriers per QD from CV	55
E_{140K}	act. energy of 140K peak (QD ground states)	250 ... 350 meV
E_{60K}	act. energy of 60K peak (Ge wetting layer)	100 meV
σ_p	hole capture cross-section	$10^{-15} \ldots 10^{-14}$ cm^2
ΔE_q	estimated quantization energy	12 meV
ΔE_C	estimated Coulomb energy per hole	5 meV

Table 4.1: *Summary of the results from the investigation of hole emission from Ge QDs in Si.*

hole emission from the wetting layer and the DLTS signal at lower temperatures. For decreasing the reverse bias, only the higher QD states contribute to the emission process and consequently the DLTS signal at higher temperatures is suppressed.

A simple two-dimensional harmonic oscillator model with a constant Coulomb-charging term was applied to simulate the DLTS signal, allows the reproduction of the experimentally observed features for the investigations with varying filling pulse bias. The good agreement between the model and the experimental observations supports the previously given interpretation. A more appropriate description of the emission process needs to take into consideration

the dependence of the activation energy on the number of carriers in the QDs and the quantization energy of the particle emitted. The model hence needs to distinguish between the possible configurations of charged QDs, leading to a typical microstate approach as, e.g. described in [Gru97]. An according model for emission from many-particle states of QDs is presented in Section 5.2.

In the present experiments, the influence of Coulomb charging could be observed by the decreasing average activation energy with increasing degree of filling of the QDs. For smaller QDs however, a step-like increase of the activation energy obtained from admittance spectroscopy was observed [Asp01]. A direct observation of Coulomb charging by admittance spectroscopy was also recently claimed [Zha98, Zha99].

Very recently, a few other DLTS investigations of carrier emission from QDs in various material systems were reported; for GaSb/GaAs QDs the investigations turned out to be difficult due to growth-related defects [Mag00], for InAs/InP QDs similar observations [Pet00] were made as previously for GaInP/InP QDs [Ana95, Ana98], and the DLTS investigation of 40 nm Ge/Si QDs yielded activation energies between 320 meV and 295 meV depending on the degree of filling [Zha00], which agrees well with the results presented here.

Chapter 5

Carrier Dynamics in Quantum Dots

In the previous chapters several experimental studies of carrier emission from different QD systems were presented. It is the aim of this chapter, to develop an appropriate approach for the description of the carrier dynamics in QDs in general.

If a QD has only a single confined state, the emission dynamics is comparable to that of a deep level as discussed in a rate equation model in Section 2.3. Taking into account a second level in a conventional rate equation description, already leads to significant complications, which will be briefly discussed in Section 5.1. For certain cases (e.g. electron emission from InAs/GaAs QDs), such a model suffices to explain the observed carrier dynamic.

Many real QD systems however, require a more general description, since they usually have several levels due to quantization and can be occupied by many carriers. *Many-particle effects* are hence not negligible in such situations. In a conventional rate equation approach many-particle effects can not be accounted for. Also the thermal equilibrium among the QDs in an ensemble, which is implicitly assumed in a rate equation model, may not be justified. A more suitable description can be provided by a microstate approach, which is outlined in Section 5.2. In such a model, which may take into account the actual configuration of a set of carriers in a particular QD, many-particle effects can hence easily be included. Furthermore, the extension of the microstate model towards experiments with optical generation of carriers is indicated in Section 5.2.4.

Based on the microstate model, simulated DLTS spectra are presented in Section 5.3 and evaluated by the standard procedure involving Arrhenius plots. The obtained activation energies are compared with the underlying QD level scheme. Furthermore, the shortcomings of a conventional rate equation model are pointed out.

5.1 Two-Level System

Carrier dynamics in multi-level systems is a difficult topic due to the various contributing inter-level excitation and relaxation processes. Their number is rapidly increasing with the number of levels taken into consideration. For a single-level system, the emission rate is usually derived from a detailed balance argument.

Already a general description of a two-level system becomes considerably more difficult and has to rely on certain assumptions [Gib77, Ree80]. The resulting expressions for the emission transient case are summarized in Section 5.1.1. It is concluded, that depending on the efficiency of the carrier relaxation from the excited to the ground state, the temperature dependence of the emission transient is determined by either the inter-level spacing or the ground state energy depending on the efficiency of the relaxation process.

If the presence of a moderate electric field leads to non-negligible tunnel emission, these solutions can still be considered approximately valid as discussed in Section 5.1.2. Such a situation is relevant, e.g. for the case of electron emission from InAs/GaAs QDs as studied in Chapter 3.

5.1.1 Emission Transients in a Two-Level System

A single-carrier two-level system as depicted in Figure 5.1(a) shall be discussed here. The ground state of energy E_0, occupation f_g, and degeneracy g_g (relative to the degeneracy when empty, i.e. $g_g = g_{g,1}/g_{g,0}$) may exchange electrons with the excited state of energy E_1, degeneracy g_x, and occupation f_x, by relaxation and activation of carriers at rates c_0 and e_0, respectively. The excited state captures electrons from the band at a rate $c_1 = \sigma_n <v_n> n$, Equation (2.29), and re-emits electrons at a rate e_1. The level spacing shall be referred to by $\Delta = E_1 - E_0$. Ignoring direct traffic between the ground state and the conduc-

tion band, the emission rates are determined by the common direct balance argument as [Ree80]

$$e_0 = \frac{g_x}{g_g} c_0 \exp\left(-\frac{\Delta}{k_B T}\right) \tag{5.1}$$

$$e_1 = \frac{1}{g_x} \sigma_n <v_n> N_C \exp\left(-\frac{E_C - E_1}{k_B T}\right). \tag{5.2}$$

Provided Δ is larger than a few $k_B T$ the total occupation transient for the emission case is (omitting a fast, but very weak additional term)

$$f(t) = f_g(t) + f_x(t) \simeq f_g^0 \exp(-\eta\, t), \tag{5.3}$$

where f_g^0 is the initial occupation of the ground state and the decay constant is

$$\eta = \frac{e_0\, e_1}{c_0 + e_1}. \tag{5.4}$$

The initial occupation of the excited state can safely be assumed to vanish, since in thermal equilibrium the probability to find a carrier in the excited state is very small. Equation (5.4) can be simplified if c_0 and e_1 differ, as is shown in the following paragraphs.

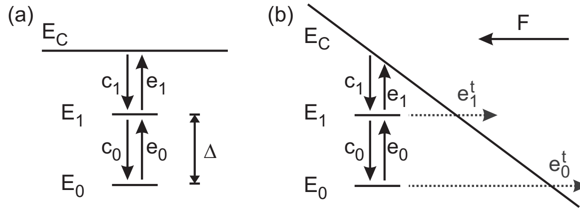

Figure 5.1: *Energy level structure and terminology for a two-level system without, panel (a), and with an electric field leading to additional tunnel emission from the QD states, panel (b).*

Fast Relaxation into the Ground State

If carrier relaxation from the excited state towards the ground state is more efficient than the emission from the excited state into the conduction band, i.e. $c_0 \gg e_1$, using Equations (5.1) and (5.2) the decay constant becomes

$$\eta \simeq \frac{1}{g_g} \sigma_n <v_n> N_C \exp\left(-\frac{E_C - E_0}{k_B T}\right). \tag{5.5}$$

The emission hence resembles thermal activation from a single deep level with an energy of $E_C - E_0$ relative to the conduction band edge, cf. Equation (2.39). In a capacitance transient experiment E_0 can hence be determined with help of a common Arrhenius plot of the type $\ln\left(\eta/T^2\right)$ over T^{-1}.

Fast Emission from the Excited State

If the emission from the excited state is much faster than the relaxation to the ground state, $e_1 \gg c_0$, the total decay constant is

$$\eta \simeq e_0 = \frac{g_x}{g_g} c_0 \exp\left(-\frac{\Delta}{k_B T}\right). \tag{5.6}$$

With the temperature dependence of the carrier relaxation rate $c_0 \sim T^2$, cf. Section 5.1.3, the activation energy Δ can now be determined from experimental data with help of an Arrhenius plot of $\ln\left(\eta/T^2\right)$ over T^{-1}.

5.1.2 Two-Level System with Electric Field

The presence of an electric field leads to a tilted band structure and hence a finite tunneling probability for carriers situated on the two levels. If tunnel emission from the ground and excited states with rates e_0^t and e_1^t has to be considered, cf. Figure 5.1(b), the above given expression for the decay constants must be modified. The tunnel rates may be more or less temperature dependent, see Section 2.3.6. In the following however, only temperature independent direct tunneling through a triangular barrier, Equation (2.54), is considered. As long as e_0^t is much smaller than e_0, the thermal equilibrium in the two-level system will not be significantly disturbed and the above provided detailed balance argument remains valid.

The escape rates can now be rewritten in order to account for the tunneling contribution. The emission from the excited state is given by $\tilde{e_1} = e_1 + e_1^t$ and the total decay constant η, Equation (5.4), is increased by e_0^t and has to be written

$$\tilde{\eta} = \frac{e_0\,\tilde{e_1}}{c_0 + \tilde{e_1}} + e_0^t. \tag{5.7}$$

As in the case without tunneling discussed above, analogous simplifications for situations with fast or slow relaxation into the ground state, $c_0 \gg \tilde{e_1}$ or $\tilde{e_1} \gg c_0$, respectively, can be made. The latter case is of major importance here, since the tunneling significantly enhances the total emission from the excited state.

In analogy to Equation (5.5) one obtains hence for $c_0 \gg \tilde{e}_1$

$$\begin{aligned}\eta &\simeq \frac{g_x}{g_g}\exp\left(-\frac{\Delta}{k_BT}\right)(e_1+e_1^t)+e_0^t \\ &= \frac{1}{g_g}\sigma_n <v_n> N_C \exp\left(-\frac{E_C-E_0}{k_BT}\right)+\frac{g_x}{g_g}\exp\left(-\frac{\Delta}{k_BT}\right)e_1^t+e_0^t\end{aligned} \tag{5.8}$$

For $\tilde{e}_1 \gg c_0$ Equation (5.7) turns into [cf. Equation (5.6)]

$$\eta \simeq e_0+e_0^t = \frac{g_x}{g_g}c_0\exp\left(-\frac{\Delta}{k_BT}\right)+e_0^t. \tag{5.9}$$

Compensating for the constant tunnel rate e_0^t, provided it is known, one can hence still determine Δ from a common Arrhenius plot of the type $\ln\left(\eta/T^2\right)$ over T^{-1}. This holds true, provided $c_0 \sim T^2$, as discussed in the following section.

5.1.3 Carrier Relaxation Processes in Quantum Dots

In order to determine the emission rate from a detailed balance argument for a two-level system as discussed above, the rate c_0 of carrier relaxation from the excited to the ground state, and especially its temperature-dependence, must be known.

Although relaxation in QDs was predicted to be rather slow [Ben91], no experimental evidence for a particularly weak relaxation probability has been found so far. A number of processes have been proposed to account for the absence of the suppression in relaxation probability, including Auger scattering [Boc92, Fer99], multi-phonon processes [Ino92], and defect-assisted relaxation [Sch96b].

The predominant mechanisms however, by which a carrier in bulk material can loose energy and relax into a lower state, is the emission of phonons or photons. The latter, namely relaxation due to the spontaneous emission of a photon, has an emission probability which is proportional to the third power of the phonon frequency ω_k [DiB68]. Radiative inter-band recombination is hence usually rather effective in QDs due to the typically large transition energies involved, which are in the order of about 1 eV. Sublevel relaxation in QDs due to spontaneous emission of photons however, is hence comparatively slow, since the typical QD quantization energies are in the order of only several 10 meV. The situation is somewhat more complicated for phonon emission as will be discussed in more detail in the following paragraphs.

Phonon Emission

The confinement in all three spatial directions in the QD giving rise to a δ-function-like density of states, was predicted to lead to a ”phonon-bottleneck” [Ben91]. As a consequence, a suppressed photon-emission efficiency from the ground state was expected. In higher-dimensional systems, e.g. quantum wells, the dominant relaxation process is longitudinal-optical (LO) phonon emission via Fröhlich interaction with subpicosecond relaxation times. In a QD however, this process is suppressed due to the discrete nature of the energy levels, unless the level separation equals the LO phonon energy $\hbar\omega_{LO}$ (the energy of the LO phonon for $q = 0$).

The deformation potential interaction with longitudinal-acoustic (LA) phonons, which is already weak in the bulk compared to the Fröhlich interaction, becomes even weaker with decreasing QD size, due to the decreasing form factor. The reason for this behaviour is that the form factor decreases rapidly with q and therefore with the energy of the emitted LA phonon. Relaxation via LA phonon emission in QDs is hence slower than in the bulk by many orders of magnitude [Boc90].

The suppression of relaxation due to LA phonon emission should be even stronger for electrons than for holes, since the effective mass of electrons is typically much smaller than the effective mass of holes, and hence the level spacing is correspondingly larger for electrons (see, e.g. the results from numerical predictions of QD level schemes [Sti99]).

The probability c_q for emission of one (LO or LA) phonon of energy $\hbar\omega_q$ is given by (see e.g. [Yu96])

$$c_q = \tau^{-1} = \frac{2\pi}{\hbar}|M_q|^2(n_q+1)\delta(\Delta - \hbar\omega_q), \tag{5.10}$$

where M_q is the according matrix element and n_q the Bose-Einstein distribution function

$$n_q = \frac{1}{\exp\left(\hbar\omega_q/k_B T\right) - 1}. \tag{5.11}$$

The term $(n_q + 1)$ in Equation (5.10) reflects the fact that the emission probability is the sum of stimulated and spontaneous emission. The former depends on the presence of n_q available phonons, whereas the latter is independent of the population of phonons and has hence a fixed weight of 1.

Besides single-phonon emission, more complex multi-phonon processes may occur. Relaxation processes, e.g. involving the emission of two phonons

with wave vectors **q** and **k**, exhibit an even stronger dependence on the availability of phonons [Jia98]

$$c_{q,k} \sim (n_q+1)(n_k+1)\delta(\Delta-\hbar\omega_q-\hbar\omega_k), \tag{5.12}$$

which is described by the term $(n_q+1)(n_k+1)$. Such multi-phonon processes however, are usually much weaker in amplitude due to a smaller matrix element. LO±LA phonon processes [i.e. one LO phonon is emitted and one LA phonon is either emitted (+) or absorbed (-)] were nevertheless shown to open up ”energy windows” for efficient relaxation around the LO phonon energy with a probability [Ino92]

$$c_{q,k} = \tau^{-1} \sim (n_q+1)(n_k+1/2\pm1/2)\delta(\Delta-\hbar\omega_q\mp\hbar\omega_k) \tag{5.13}$$

The relevance of multi-phonon processes involving several different phonons of the bulk material, the wetting layer, and the QDs, is also indicated by photoluminescence excitation spectroscopy (PLE) of InAs/GaAs QDs [Ste96, Hei96c]. In such experiments relatively broad (30-130 meV) resonances above the detection energy are observed, which are attributed to either electronic transitions reflecting the excited spectrum [Faf94, Hei96d], or multi-phonon resonances [Hei97, Ign01]. Similar signatures of phonon processes are also observed in PL investigations with near-resonance excitation [Faf95, Ray95, Sch96a, Bog01]. In time-resolved bolometric experiments, a strong contribution to the emission from acoustic phonons was concluded [Haw99]. In near-field PLE experiments, efficient carrier relaxation was also observed [Tod99].

For an accurate prediction of the total relaxation rate due to multi-phonon interaction in a given QD system, all possible processes would have to be summed up after calculating the according matrix elements. Due to the variety of uncertainties concerning material parameters, the QD geometry, available phonon modes, and the shape of the bound particle wave-functions, which are prerequisites to calculate the matrix elements, this is as yet infeasible.

Temperature Dependence of Phonon Emission

Of particular interest for the interpretation of the experiments dealt with in this work is the temperature dependence of the relaxation rate. Taking into account only first order phonon processes, according to Equation (5.10) a

$$c_0 \sim (n_q+1) = \frac{1}{\exp(\hbar\omega_q/k_BT)-1}+1 \tag{5.14}$$

dependence on temperature and phonon energy is expected. From this expression two cases of asymptotic behaviour can be derived. Provided the phonon energy is much greater than the thermal energy, $\hbar\omega_q \gg k_B T$, Equation (5.14) turns into $c_0 \sim 1$ indicating temperature independent carrier relaxation due to purely spontaneous phonon emission. If $\hbar\omega_q \ll k_B T$, one obtains $c_0 \sim T$.

Two-phonon emission exhibits, according to Equation (5.12), a $c_0 \sim (n_q + 1)(n_k + 1)$ dependence with the two asymptotic cases of $c_0 \sim 1$ and $c_0 \sim T^2$. In principle, the high-temperature behaviour should hence resemble a T^x behaviour, where x is the number of phonons emitted. Higher order phonon emission processes will on the other hand have significantly smaller matrix elements leading to negligible contributions.

As a upper limit may serve the T^2 temperature dependence of the capture rate of free carriers into a deep level, Equation (2.29). This seems a reasonable assumption, since for free carriers in a band the resonance requirement with suitable phonon energies is lifted and hence a wealth of single- and multi-phonon processes may contribute to the relaxation process. Since multi-phonon processes are widely observed in photoluminescence experiments on QDs (see previous paragraph), one may thus safely assume $c_0 \sim T^2$. Note however, that this may depend on the material system under investigation.

5.2 Microstate Model

A sheet of QDs may be regarded – in most general terms – as a many-level many-particle system. It can be described by a more or less ordered array of localizing potentials in a plane with, depending on size and material fluctuations, more or less similar bound states. In addition to carrier exchange mechanisms between the QDs, the wetting layer, and the matrix material, the number of possibly relevant intra- and inter-QD carrier exchange and interaction mechanisms is rather large. Analytical solutions in such a case can commonly not be obtained.

A model for the carrier dynamics in a QD ensemble can not generally assume a *thermal* distribution of the occupancies among the QDs, since inter-QD carrier exchange is not necessarily fast enough for all temperatures. A conventional rate equation approach based on an averaged energy level occupancy of the QDs may hence lead to erroneous results, as has been recently discussed for photoluminescence experiments [Gru97].

5.2.1 Basic Assumptions

Standard capacitance transient experiments employ filling of the QDs with bias pulses, the QDs will hence usually contain majority carriers only. Such a situation where the QDs are occupied with a single carrier type is considered in this section.

The most general idea of a microstate model for the carrier dynamics in an ensemble of QDs during a capacitance transient experiment would be to take explicitly into account every possible configuration of k carriers in a QD, all possible transition mechanisms due to reconfiguration inside a QD, carrier exchange with other QDs, the wetting layer, and the matrix material. A full description of all contributing exchange and interaction processes would lead to a problem of tremendous complexity. It is obvious that significant simplifications are necessary.

A basic formalism for the description of QDs is established here. In doing so, pragmatic reasons were given priority over conceptual scrupulousness. It was intended to characterize such a system by parameters with practical relevance.[1]

It is furthermore intended to keep the discussion of the assumptions as general as possible, since such a microstate description may be applied to all kinds of problems related to carrier dynamics in QDs, not only transient capacitance experiments.

No Inter-QD Coupling

Although inter-QD coupling due to Coulomb interaction may not always be completely negligible, cf. Section 2.6.2, this effect is ignored here for simplicity. As a consequence, the carrier dynamics of a particular QD can be treated independently from the occupancies of all other QDs in the ensemble.

Energy Levels

Because of the absence of inter-QD coupling, a common set of L energy levels E_i, $0 \leq i < L$, with degeneracy g_i is sufficient to characterize the QDs. In the simplest approximation, the levels and their degeneracies may be obtained

[1] This leads to a slight formal inconsistency in the case of the electrostatic interaction of carriers in a QD with the barrier and with other carriers in a QD. For the former case the capture barrier for a filled QD is chosen as significant parameter, whereas in the latter case the Coulomb charging energy for each additional charge is preferred (because it is readily observable in experiments). From a theoretical point of view, both effects have the same origin.

from a simple two-dimensional harmonic oscillator model with a quantization energy of $\Delta E_q = \hbar\omega$, where

$$\omega = \sqrt{\frac{2V_0}{er^2 m^*_{QD}}}, \quad (5.15)$$

V_0 is the depth of the potential well relative to the valence band of the matrix material, r its radius, and m^*_{QD} the effective carrier mass in the QD. The energy levels in this model are hence given by $E_i = V_0 - i \cdot \Delta E_q$, with the degeneracies $g_i = 2(i+1)$. Such a model can only provide a qualitative prediction for QD level schemes. Particularly small QDs (as e.g. in the case of typical InAs/GaAs QDs), exhibit significant deviations from this simple description due to the strong influence of strain and piezoelectricity effects. More sophisticated models calculate the QD band structure numerically taking the actual geometry, chemical composition, strain effects, and piezoelectricity into account [Gru95, Woj98, Jia98, Sti99, Wan99, Sti01a]. It is concluded that the structural (i.e. geometrical and chemical) properties of the QD have a strong influence on the carrier-carrier interaction in the QDs [Sti01b].

Level Distribution due to Ensemble Fluctuations

Fluctuations in the composition and dimensions of QD in a large ensemble can lead to an effective distribution in the energy levels. This effect may be taken into account by a Gaussian distribution for each level around E_i with a standard deviation $\tilde{\sigma}_i$. Expressions f dependent on E_i must then be rewritten

$$f(E_i) \longrightarrow \frac{1}{\sqrt{2\pi}\tilde{\sigma}_i} \int f(E - E_i) \exp\left(-\frac{(E-E_i)^2}{2\tilde{\sigma}_i^2}\right) dE. \quad (5.16)$$

The standard deviation $\tilde{\sigma}_i$ is easily converted into a value for the full-width at half-maximum (FWHM) ΔE_i by

$$\Delta E_i = \tilde{\sigma}_i \cdot \sqrt{8 \ln 2}. \quad (5.17)$$

Coulomb Charging

So far, the electrostatic interaction of the carriers in a particular QD has not been taken into account. Its influence however, on the total energy of the many-particle system, may be quite significant. This is revealed, e.g. for InAs/GaAs QDs by experiments directly detecting the addition energy of carriers [Mil97, Luy99]. For each additional charge the total energy of the carriers in a QD is

increased by an amount ΔE_C. In the simplest approximation this effect may be accounted for by a constant Coulomb charging energy for every additional charge after the first. The energy levels have then to be modified depending on the number of carriers k to

$$E_i^k = E_i + (k-1)\Delta E_C \qquad \text{for} \quad 1 \leq k \leq M, \tag{5.18}$$

where M is the maximum number of carriers per QD. The Coulomb charging energy ΔE_C must be either measured, calculated or estimated.

An estimate of the Coulomb charging energy can be obtained from the capacitance of a QD C_{QD} by

$$\Delta E_C = \frac{e^2}{C_{QD}}. \tag{5.19}$$

The capacitance of a QD may be approximated by the capacitance of a disk or a sphere. Assuming a disk with radius r in a matrix with relative permittivity ε_{matrix}, the capacitance is given by

$$C_{QD}^{disk} = 8\varepsilon_0\varepsilon_{matrix}\, r, \tag{5.20}$$

and for a sphere with the same radius by

$$C_{QD}^{sphere} = 4\pi\varepsilon_0\varepsilon_{matrix}\, r. \tag{5.21}$$

More realistic values for Coulomb charging energies may be determined from self-consistent numerical calculations of many-particle QD states [Woj96, Sti99].

Local Thermal Equilibrium

Carrier relaxation times in QDs are typically many orders of magnitude faster (in the order of $\leq$ ns) [Sau98, Hei99, Fry00a] than the time scale of the carrier exchange processes with the matrix material, which are investigated experimentally by capacitance spectroscopy (time constants are typically in the order of ms). The carriers in a QD can therefore be assumed to be always in a local thermal equilibrium and explicit treatment of inter-level scattering can be omitted.

As a consequence, the average occupation f_i^k of the ith energy level (assumed to be of single degeneracy when empty and of degeneracy g_i when

occupied) of a QD occupied by k carriers at a given temperature T may be described by a local Fermi distribution

$$\tilde{f}_i^k = \frac{1}{1 + \frac{1}{g_i} \exp\left(\frac{E_i^k - \mu^k}{k_B T}\right)}. \tag{5.22}$$

Here μ^k is the local chemical potential in a QD with k carriers, which is easily determined by demanding

$$\sum_{i=0}^{L-1} g_i \tilde{f}_i^k = m. \tag{5.23}$$

The assumption of a thermal distribution in every *particular* QD represents a severe simplification, since now one can describe all QDs occupied by the same number of carriers k commonly. In the following, the fraction of the QDs in the ensemble with k carriers shall be denoted by F_k. It is clear that $\sum_{m=0}^{k} F_k = 1$.

Restriction to Single-Carrier Processes

Combined several-particle emission and capture processes are neglected. The microstate description can hence be further simplified, since only transitions connecting the $(k-1)$- and $(k+1)$-carrier states with the k-carrier state must be taken into consideration for the time-dependence of F_k.

Capture Probability

The capture probability c_{QD} per carrier in the matrix material with carrier density n for capture into an empty QD state shall be given (as in the case of a deep level, Section 2.3.1) by $c_{QD} = \sigma_{QD} < v_n > n$, where σ_{QD} is the capture cross-section of this process, $< v_n >$ is the rms thermal velocity, Equation (2.45), and n is the density of carriers in the matrix, Equation (2.16). Provided the capture probability into all energy levels is equal, the total capture probability is given by $c_{QD}(M-k)$. A QD filled with M carriers hence cannot capture any further carriers.

The above definition does not yet take into account the presence of a capture barrier. In the case of multiply-charged QDs however, a capture barrier of relevant strength may be likely to be formed. In this case c_{QD} becomes

a function of k (see Section 2.3.4). If the capture barrier energy is E_α for a completely filled QD, the capture rate is given by

$$c_{QD}^k = \sigma_{QD} <v_n> n \exp\left(\frac{-\frac{k}{M}E_\alpha}{k_B T}\right), \tag{5.24}$$

and the total capture probability must be rewritten

$$C_k = \sigma_{QD} <v_n> n \exp\left(\frac{-\frac{k}{M}E_\alpha}{k_B T}\right)(M-k). \tag{5.25}$$

The contribution from the capture barrier to the total energy must also be taken into account for the Fermi distribution in the QDs, Equation (5.22).

In the case of a point defect, the effect of the electrostatic interaction of carriers inside the QD, represented by the Coulomb charging energy, and the effect on the carriers in the matrix material as described by the capture barrier E_α would be of approximately equal strength [$E_\alpha \approx (k-1)\Delta E_C$, in the given notation]. For a QD however, the interaction of carriers inside a QD with the carriers in the matrix can be assumed to be weaker than the electrostatic intra-QD interaction, because of the decreased spatial overlap of the quantummechanical wave-function of a localized carrier with the matrix material volume in the former case.

Emission Probability

In order to derive an expression for the thermally activated emission rates, the same approach as in the case of a simple deep level, Section 2.3.2, is applied. With help of the detailed balance argument one can write – in analogy to Equation (2.34) – for the equilibrium case

$$\tilde{f}_i^k = \frac{c_{QD}^k}{c_{QD}^k + e_i^k}, \tag{5.26}$$

where e_i^k is the emission probability per carrier from the ith level of a QD filled with k carriers. Since the equilibrium is also described by the Fermi distribution Equation (5.22), one obtains

$$e_i^k = c_{QD}^k \frac{1}{g_i} \exp\left(\frac{E_i^k - E_F - \frac{k}{M}E_\alpha}{k_B T}\right), \tag{5.27}$$

where E_F is the equilibrium Fermi energy. With Equations (5.24), (2.45), and (2.46) this yields – analogous to Equation (2.47) –

$$e_i^k(T) = \gamma_n \frac{1}{g_i} T^2 \sigma_{QD} \exp\left(-\frac{E_C - \left[E_i + (k-1)\Delta E_C - \frac{k}{M} E_\alpha\right]}{k_B T}\right), \quad (5.28)$$

where $\gamma_n = \sqrt{12(2\pi)^3}\,\frac{k^2}{h^3} M_C m_e^*$, Equation (2.48). It is worth noting, that m_e^* is the effective electron mass of the matrix material. If barrier lowering effects and/or tunnel emission as discussed in Section 2.3.6 were to be included, the e_i^k would have to be accordingly modified.

For the microstate description the total emission rate R_k for a QD with k carriers is required, which is easily obtained by summing over all levels weighed with the appropriate degeneracy and the Fermi distribution, Equation (5.22),

$$R_k = \sum_{i=0}^{L-1} g_i \tilde{f}_i^k e_i^k. \quad (5.29)$$

If ensemble fluctuations were to be taken into account, the substitution rule, Equation (5.16), would have to be applied to this expression, since both $\tilde{f}_i^k$ and e_i^k, depend on the energy levels E_i.

5.2.2 Master Equation

With the assumptions discussed above a very simple model as depicted in Figure 5.2 results, which is characterized by the following master equation (with special cases for $k = 0$ and $k = M$)

$$\begin{aligned}
\frac{dF_k}{dt} &= C_{k-1}F_{k-1} + R_{k+1}F_{k+1} - (R_k + C_k)F_k \quad \text{for} \quad 0 < k < M, \quad (5.30)\\
\frac{dF_0}{dt} &= -C_0F_0 + R_1F_1,\\
\frac{dF_M}{dt} &= C_{k-1}F_{k-1} - R_MF_M.
\end{aligned}$$

For a given initial condition $\mathbf{F^0} = (F_0^0, F_1^0, \ldots, F_M^0)$ the state of the system at any time t can be predicted by a solution of this master equation.

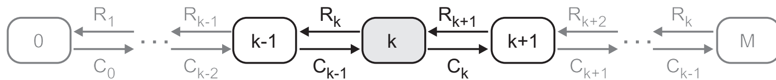

Figure 5.2: *Transition chain of the microstate model for an ensemble with a maximum number of M carriers per QD. The fraction of the QDs with k carriers is reduced by capture of a carrier with a rate C_k and emission of a carrier with rate R_k. It is increased by carrier emission from one of the QDs in the $(k+1)$-state with rate R_{k+1} and capture into a QD with $(k-1)$ carriers with rate C_{k-1}.*

Parameters

It is worth summarizing the underlying parameters of the microstate model. In order to describe a particular QD system, the following values have to be known (or estimated):

- The energy levels E_i, their fluctuation distribution characterized by $\tilde{\sigma}_i$, and their degeneracies g_i.
- The Coulomb charging energy ΔE_C.
- The capture barrier E_α.
- The capture cross-section σ_{QD}.
- The temperature T.

The maximum number of carriers M per QD can usually be derived from the E_i, g_i, and ΔE_C.

5.2.3 Pure Emission

Of major relevance for DLTS experiments is the case of the emission during the transient after the filling pulse. In the case of QDs, they can be assumed to be situated inside the depletion region. The presence of a depletion region at the position of the QDs has two major consequences: Firstly, practically no free carriers exist in the vicinity of the QDs ($n = 0$), therefore no capture processes from the matrix into the QD have to be considered. And secondly, as a result of the electric field, carriers emitted from the QDs into the matrix material can

be assumed to be removed immediately and hence re-capturing does not occur either.

As a conclusion all capture rates C_k equal 0, simplifying Equation (5.30) [in a certain analogy to Equation (2.64)] to

$$\begin{aligned} \frac{dF_k}{dt} &= R_{k+1}F_{k+1} - R_kF_k \qquad \text{for} \quad 0 < k < M, \\ \frac{dF_0}{dt} &= R_1F_1, \\ \frac{dF_M}{dt} &= -R_MF_M \end{aligned} \tag{5.31}$$

In a conventional rate equation model, the carrier emission from a system containing several carriers in multiple levels would be described by independent emission from each separate level. In order to obtain a total occupation transient, these ”independent” emission processes would be summed. This is of course wrong, since a trickle-down effect of carriers is completely neglected. Such a process may occur, if a carrier from a lower level is emitted before the higher levels are completely emptied and subsequently carrier relaxation in the QD takes place. Although the carriers in higher states usually have a higher probability to be emitted, the trickle-down effect has to be taken into account to avoid erroneous interpretation of experiments, which is discussed in Section 5.3.

5.2.4 Microstate Model for Optical Carrier Excitation

In capacitance transient experiments with optical pulses, QDs can be occupied by electrons *and* holes due to capture of electron-hole pairs. The QDs have hence to be described by their configuration depending on the number of bound electrons *and* holes, k and l, respectively. In addition to single-carrier capture and emission processes, now electron-hole pair capture and recombination processes must also be taken into account. Emission of electron-hole pairs from a QD may usually be omitted, since recombination takes place on a much shorter time-scale.

Here, only the simple case of the energy of the exciting optical radiation being larger than the band-gap energy of the matrix material is considered. This means that electron-hole pairs are generated somewhere in the bulk of the matrix and subsequently captured into the QDs. In this case, the capture rates for all empty excitonic states of a QD can be assumed to be equal.

The more special case of the energy of the illumination being adjusted, such that electron-hole pairs are generated resonantly in the QDs, causes significantly more complications. This is because the fluctuations in the QD ensemble may lead to the charging of only a sub-set of all QDs having a suitable electron-hole energy level separation allowing for resonant carrier generation. Though very interesting from an experimental point of view – energy- and thereby size-selective charging experiments may be conducted by this method –, a formalism capable to account for such effect would boost the complexity of the present model and is therefore beyond the scope of this work.

In QDs it is reasonable to assume radiative recombination to prevail over non-radiative recombination. It is furthermore supposed that the radiative lifetime τ_r is the same for all bound electron-hole pairs in a QD. The excitonic recombination rates $R^{exc}_{k,l}$ are therefore all given by τ_r^{-1}. The maximum number of carriers M is taken to be the same for electrons and holes.

Master Equation

As mentioned, there are now six processes modifying the fraction of QDs with k electrons and l holes, $F_{k,l}$; capture and emission of electrons or holes separately, and capture and recombination of electron-hole pairs. The according model is depicted in Figure 5.3.

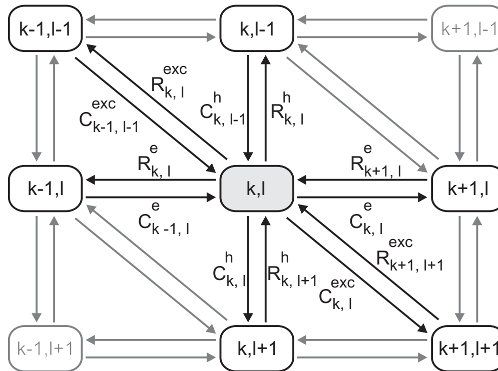

Figure 5.3: *Microstate model allowing for occupation of QDs by electrons and holes. All processes changing the number of electrons k and holes l are indicated. Horizontal and vertical arrows represent processes increasing or decreasing the number of one sort of carriers, whereas diagonal arrows represent electron-hole pair capture and emission.*

The time dependence of the $F_{k,l}$ is hence determined by the following master equation for $0 < k,l < M$

$$\begin{aligned}\frac{dF_{k,l}}{dt} &= C^{exc}_{k-1,l-1}F_{k-1,l-1} + R^{exc}_{k+1,l+1}F_{k+1,l+1} \\ &+ C^{e}_{k-1,l}F_{k-1,l} + R^{e}_{k+1,l}F_{k+1,l} \\ &+ C^{h}_{k,l-1}F_{k,l-1} + R^{h}_{k,l+1}F_{k,l+1} \\ &- \left(R^{exc}_{k,l} + C^{exc}_{k,l} + R^{e}_{k,l} + C^{e}_{k,l} + R^{h}_{k,l} + C^{h}_{k,l}\right)F_{k,l}, \qquad (5.32)\end{aligned}$$

and simplified equations for $k = 0$ and/or $l = 0$, which can be derived in analogy to Equation (5.30) with the appropriate terms disappearing.

Emission Case

After the illumination has been switched off, the electron-hole pair capture rates can be assumed to vanish, since the excitonic life-time is much shorter than the time-scale relevant for the capacitance experiments. Furthermore, all remaining electron-hole pairs in a QD can be taken to have recombined leaving only a net-occupation of electrons or holes in the QDs. Which sort of carriers remains, depends on the ratio of their individual emission rates. If electron emission is generally faster, a net-hole occupation is expected to result and vice-versa.

The system for pure emission after the filling procedure, is hence described in the same way as the emission in the case of electrical filling experiments in analogy to Equation (5.31) by the master equation for $0 < k,l < M$

$$\begin{aligned}\frac{dF_{k,l}}{dt} &= R^{exc}_{k+1,l+1}F_{k+1,l+1} + R^{e}_{k+1,l}F_{k+1,l} + R^{h}_{k,l+1}F_{k,l+1} \\ &- \left(R^{exc}_{k,l} + R^{e}_{k,l} + R^{h}_{k,l}\right)F_{k,l}, \qquad (5.33)\end{aligned}$$

and simplified equations for $k = 0$ and/or $l = 0$.

The initial conditions however, may in the present case depend more sensitively on the model parameters determining the carrier dynamics during the illumination.

5.3 DLTS Simulations

Based on the microstate model introduced in Section 5.2, simulated DLTS spectra are studied here. Qualitative results for a simplified QD level structure

are investigated. The QD levels are modeled by a two-dimensional harmonic oscillator model taking Coulomb charging into account. As example, hole emission from Ge/Si QDs is studied, since QDs in this material system can be fabricated in a wide size range and many-particle effects can easily be observed experimentally, cf. Section 4. After investigating the DLTS signal as function of the QD size and the degree of filling of the QDs in Section 5.3.1, the results are compared with the outcome of a conventional rate equation approach in Section 5.3.2. The results are summarized and discussed in Section 5.3.3. It is shown, that DLTS may serve as a very sensitive tool to investigate the electronic structure of QDs.

5.3.1 QD Dimensions and Filling

DLTS spectra were calculated for varying QD diameter and number of carriers in order to study the dependence of the DLTS signal on the QD dimensions and the degree of filling. Since the case of pure (thermal) emission is studied here, the simplified master equation presented in Section 5.2.2 was solved. After simulating emission transients for varying temperature, DLTS spectra were obtained by using a standard rate window concept as described in Section 2.4.3.

The QDs are assumed to be approximately lens-shaped with a large aspect ratio of diameter to height, which is commonly observed in overgrown QD structures [Abs96, Mie00c]. The Coulomb energy is therefore estimated according to Equations (5.19) and (5.20). For the depth of the potential V_0, a value of 350 meV was used corresponding to experimental results, Chapter 4, and the Ge/Si valence band offset. Broadening of the DLTS data due to ensemble fluctuations resulting from variations in size and composition was not taken into account, since it was intended to study the general features of the simulated DLTS spectra. As initial condition, all QDs in the ensemble were assumed to be charged with N_{fill} holes.

In Figures 5.4 and 5.5, the results of the simulations for several different QD diameters d and varying initial filling are summarized. For an increasing number of carriers, the increasing influence of many-particle effects becomes clearly visible in the DLTS data.

For small QDs with a diameter of $d = 10$ nm, a quantization energy of $\Delta E_q^{10nm} = 87$ meV and a Coulomb energy of $\Delta E_C^{10nm} = 38$ meV were estimated and used to determine the energy of the N-carrier states. As a result of these rather large values, emission from the different QD levels and N-carrier states is resolved by separate peaks in the DLTS plot, see Figure 5.4(a). It is worth noting, that although the microstate description takes intra-QD carrier

relaxation into account, a DLTS signal from each N-carrier state is observed separately. This is a result of the significantly different temperatures, for which the carriers are emitted with a time constant comparable to the reference time constant of the DLTS experiment. In other words, a trickle-down effect is not expected to be visible in the data as long as the energy spacing between the different N-carrier states is larger than the thermal energy k_BT.

If the QD diameter is increased towards $d = 20$ nm, Figure 5.4(b), the QDs can be charged with up to 12 holes. This is due to the significantly smaller quantization and Coulomb energies, $\Delta E_q^{20nm} = 44$ meV and $\Delta E_C^{20nm} = 19$ meV, respectively. In the simulated DLTS data, the separate peaks for states with differing carrier number N can only be resolved for low temperatures. The peak at about 170 K is due to hole emission from the $N = 1$ and $N = 2$ states. The individual peaks can not be distinguished anymore and form a common peak with a shoulder. The quantization energy however, is still large enough to lead to clearly separated groups of peaks for different quantization energies E_i. For the DLTS signal related to hole emission for $N > 6$, the individual peaks become visible again, due to the smaller k_BT. At more elevated temperature an other effect becomes apparent; the peak height of the individual peaks increases for an increasing number of holes, since trickle-down of holes becomes relevant. This is because ΔE_C^{20nm} is comparable to the thermal energy in the experiment, at least in the higher temperature range. An influence of this effect is hence visible in the data for about $T \geq 100$ K (corresponding to $k_BT \geq 9$ meV).

For further increasing QD diameter $d = 70$ nm, the separate peaks can not be distinguished anymore, and even the broad peaks for different quantization energies start to ”melt” together, Figure 5.5(a). These observations reflect the significantly decreased quantization and Coulomb charging energies, $E_q^{70nm} = 12$ meV and $\Delta E_C^{70nm} = 5$ meV, respectively.

In the case of $d = 150$ nm, the characteristic energies become very small ($E_q^{150nm} = 6$ meV and $\Delta E_C^{150nm} = 3$ meV) and the density of states in the QDs hence approaches the one of a quantum well. This is reflected in a broad quasi-continuous DLTS signal, Figure 5.5(b).

5.3.2 Microstate Model vs. Conventional Rate Equations

Here, the simulated DLTS signal for different QD diameters generated by a conventional rate equation approach is compared to the results from the micro-

state description.[2] For the comparison, identical activation energies for the thermal emission processes were considered. The results of both methods are presented in Figure 5.6.

Significant differences in the simulated DLTS spectra become apparent. The conventional rate equation model leads to a somewhat different peak form in the case of large quantization and Coulomb energy, Figure 5.6(a) and (b). If the QD dimensions increase and conclusively quantization and Coulomb charging decrease, the rate equation model predicts peaks related to the different quantization energies, which are too sharp, and furthermore yields wrong peak positions and heights. These deviations result from describing the occupation of the QD ensemble as an averaged value, neglecting inter-QD relaxation processes and the different number of carriers individual QDs may contain.

5.3.3 Discussion

From the above described observations it is clear that the DLTS signal due to carrier emission from QDs exhibits a very sensitive dependence on the electronic structure of the QDs. The influences of quantization and Coulomb charging are clearly reflected in the DLTS spectra. For large quantization and Coulomb energies (i.e. small QD dimensions), several peaks may be observed, which are directly related to carrier emission from certain QD levels. These DLTS peaks may hence be used to determine energy differences between the QD levels and the band edge of the matrix material via the activation energy.

It is furthermore concluded, that the influence of many-particle effects on carrier emission from charged QDs by DLTS is rather strong. A straightforward interpretation of the measured data is therefore not generally possible for characteristic QD energies smaller than, or comparable to, the thermal energies $k_B T$ in the experiment. From comparison with simulations however, conclusions on the QD level structure may be drawn from the DLTS signal. It is furthermore demonstrated that a microstate model must be applied for the description of the carrier dynamics of QDs, since a conventional rate equation approach neglects particularities of the QD ensemble and leads to erroneous results.

The ideal evaluation method for capacitance transient experiments would be to numerically fit a microstate model to the recorded transients or the DLTS

[2]Note, that the microstate model must be considered the benchmark, since it takes intra-QD carrier relaxation into account, which a conventional rate equation approach does not. The microstate description is therefore the more realistic model.

spectra. Due to the rather high computational expenses in evaluating the micro-state model, this is not (as yet) a feasible approach.

The simulated DLTS spectra exhibit a strongly size- and filling-dependence. Time-resolved capacitance spectroscopy may therefore be used as a very sensitive tool for the electrical characterization of QDs.

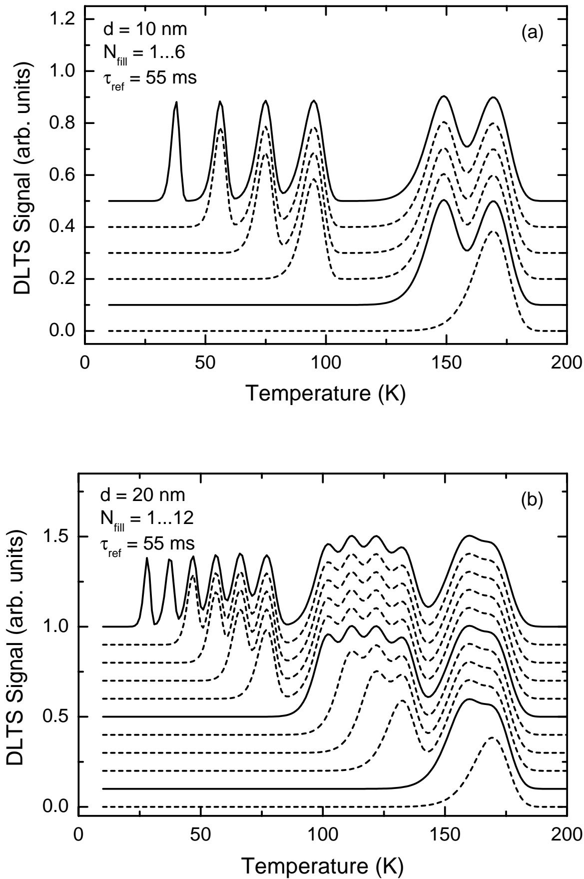

Figure 5.4: *Simulated DLTS spectra for Ge/Si QDs with different diameter and varying degree of filling from the microstate model described in Section 5.2. The reference time constant is $\tau_{ref} = 55$ ms. (a) QD diameter $d = 10$ nm, DLTS curves for filling with up to 6 holes; (b) QD diameter $d = 20$ nm, DLTS curves for up to 12 holes. Solid lines were used to indicate first three "closed states", i.e. for N_{fill} =2, 6, and 12 holes.*

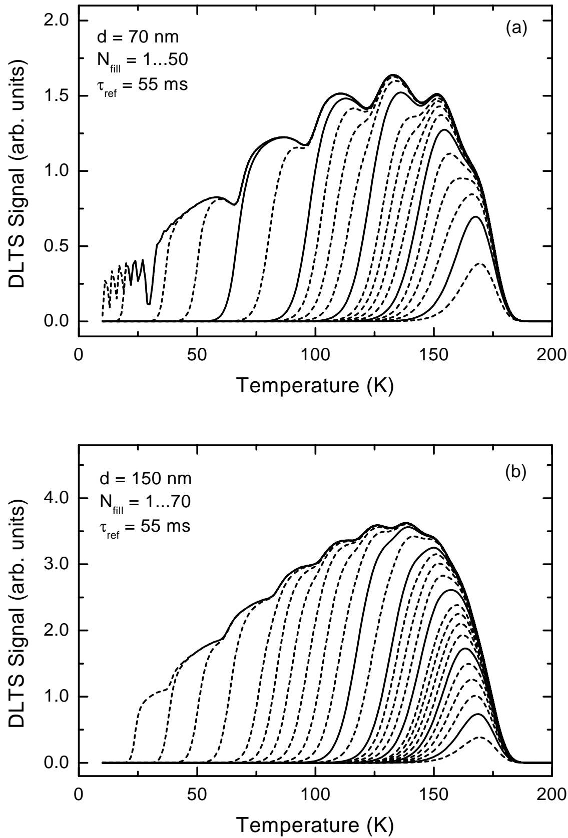

Figure 5.5: *Simulated DLTS spectra for Ge/Si QDs with different diameter and varying degree of filling from the microstate model described in Section 5.2. The reference time constant was* $\tau_{ref} = 55$ *ms. (a) QD diameter* $d = 70$ *nm, DLTS curves for filling with up to 50 holes; (b) QD diameter* $d = 150$ *nm, DLTS curves for filling with up to 70 holes. Solid lines were used for the first five "closed states", i.e. for* N_{fill} *=2, 6, 12, 20, and 30 holes.*

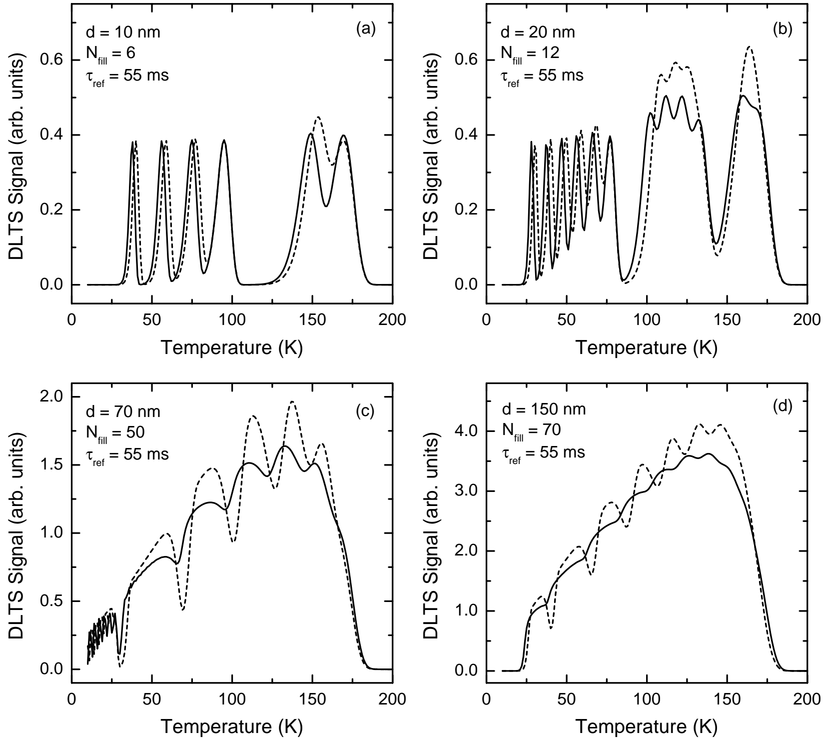

Figure 5.6: *Simulated DLTS spectra for Ge/Si QDs with different diameter generated by the microstate model described in Section 5.2 (solid lines) in comparison with the results of a conventional rate equation model (dashed lines). The reference time constant was* $\tau_{ref} = 55$ *ms. (a) QD diameter* $d = 10$ *nm and* $N_{fill} = 6$*; (b) QD diameter* $d = 20$ *nm and* $N_{fill} = 12$*; (c) QD diameter* $d = 70$ *nm and* $N_{fill} = 50$*; (d) QD diameter* $d = 150$ *nm and* $N_{fill} = 70$*.*

Summary

The carrier dynamics and the electronic properties of self-organized semiconductor quantum dots (QDs) have been studied with depletion-layer capacitance spectroscopy. For the first time, systematic studies of the carrier emission processes in self-organized QDs with time-resolved capacitance spectroscopy (also known as deep level transient spectroscopy – DLTS) were presented; InAs QDs in GaAs and Ge QDs in Si were examined.

In the first set of experiments, electron emission from a triple-layer of InAs/GaAs QDs was identified by comparison with reference samples without QDs. Further evidence was supplied by studying the dependence of the DLTS signal on reverse and pulse bias conditions. The experimental results demonstrate the importance of tunneling for the electron escape process. Besides direct tunneling from the QD ground state with a time constant in the order of 10 ms (for an electric field of about 4.5×10^6 V/m), thermally activated tunneling involving QD excited states was observed. The 94 meV activation energy of this process is hence attributed to the QD ground/excited state splitting. Good agreement with results from photoluminescence and an analysis of the static capacitance-voltage characteristic is found. The experimental results are furthermore in excellent agreement with numerically calculated QD levels obtained from eight-band $\mathbf{k}\cdot\mathbf{p}$ theory including strain and piezoelectricity.

A second study was performed on single-layer InAs/GaAs QDs in n- and p-doped matrices in order to investigate electron and hole escape processes. The DLTS measurements of electron emission exhibited the same features as for the triple-layer QDs and hence confirmed the previous results. Here, the activation energy of 82 meV is slightly lower reflecting a smaller quantization energy in the single-layer QDs. In contrast to electron emission, the hole escape process was found to be entirely due to thermal activation from the QD ground states to the GaAs valence band. The observed activation energy of 194 meV thus corresponds to the hole ground state energy. The suppression of

tunneling in the hole escape process is explained by the significantly larger effective mass of heavy holes compared to the effective mass of electrons. The QD electron and hole energy levels obtained from the DLTS measurements are in good agreement with results from photoluminescence, admittance spectroscopy, and theoretical predictions from eight-band $\mathbf{k}\cdot\mathbf{p}$ theory. From studying the hole emission rate as function of the reverse bias, a rather strong dependence on the electric field was observed, which can not be explained by the Poole-Frenkel effect (electric-field induced barrier-lowering). This is an indication of phonon-assisted tunneling, which may be exploited to study the carrier-phonon interaction in QDs.

The thermally activated emission of carriers from Ge QDs in Si was found to be dominated by many-particle effects. The band-discontinuity of Ge and Si is of type II; in this material system quantum confinement is hence only realized for holes. Due to the rather large QD dimensions (about 70 nm in diameter), the energy spectrum was found to be determined almost equally by quantization and Coulomb charging. The quantization energy was estimated to be about 12 meV and the Coulomb charging energy 5 meV (per hole). One thus expects that the QDs can be filled with more than 50 holes, which was confirmed by static capacitance-voltage measurements. From the DLTS measurements, an activation energy of about 350 meV was determined. This value is in good agreement with photoluminescence measurements and results from admittance spectroscopy. Measurements of reference samples without QDs did not give rise to any DLTS signal, and varying the reverse and pulse bias during the measurements allowed the identification of the QD layer as the source of the emitted charge. By varying the bias conditions, the influence of partial filling and emptying of the QDs on the emission process was revealed. For increasing filling of the QDs in the DLTS measurements, a decreasing apparent activation energy (down to 250 meV) was observed. This behaviour is explained by the observation of emission from many-particle states, in which part of the carriers in higher QD levels are significantly closer to the Si valence band than the QD ground states. The energy relative to the Si valence band edge is furthermore decreased by the Coulomb interaction of the confined holes. Using a two-dimensional harmonic oscillator model to describe the QD level structure, the carrier emission was modeled by a conventional rate equation approach. This simple model allowed the explanation of the observed DLTS spectra with good qualitative agreement.

Finally, a microstate model for the carrier dynamics in QDs was developed. From simulated DLTS spectra based on this model the strong dependence

of capacitance transient experiments on the QD level structure could be demonstrated.

In this work, the application of time-resolved capacitance spectroscopy to the investigation of self-organized QDs has been established. Based on this technique, the first studies of InAs/GaAs and Ge/Si QDs were performed. Their electronic properties and carrier emission mechanisms were elucidated by systematic investigations. Based on experimental results and theoretical considerations presented here, fundamental insights into the interdependence of many-particle effects and the carrier dynamics in QD systems were obtained.

Outlook

Naturally, when the application of a technology is introduced, there remain aspects requiring further investigations. Moreover, new experimental possibilities arise. Some of these are briefly outlined below.

The proper determination of capture cross-sections. Because of the very large capture cross-sections as obtained from Arrhenius plots, a direct measurement with help of a bias pulse-length variation is commonly not successful. Generating the carriers by illumination with light of an energy above the band gap of the matrix material, allows for a more subtle way to control the amount of charge provided for capturing into the QDs. The application of this method to conventional deep levels is described in, e.g. [Cha81, Bab87, Mei94, Dad99].

The techniques presented in this work are, of course, applicable to semiconductor QDs in arbitrary material systems, provided controlled doping and the formation of Schottky contacts or p-n diodes are feasible. Particularly in the case of Sb-based type-II heterostructures (e.g. GaSb/GaAs or InSb/GaAs) very large band discontinuities (and hence QD ground state energies) may be expected [Hat95, Hat98, Ben96a, Ben96b, Gla96, Hog98, Mag00, MK01]. QDs in these material systems are therefore very appealing for memory applications.

Capacitance transient spectroscopy is traditionally applied to study deep levels due to impurities and defects. The formation of QDs may also lead to the formation of defects due to dislocations [Fuj95, Dai97, Kri98, Bel00]. It is hence a logical approach to use capacitance spectroscopy to systematically study the defects associated with the QD growth. This now becomes feasible, since the ”pure” signature of carrier emission from the QDs is well understood.

The emission process of holes from InAs QDs in GaAs exhibits an enhanced dependence on the electric field, which is an indication of phonon-assisted tunneling. A detailed study of this effect may help to gather insight into

the coupling of bound QD states to phonons. It may be furthermore possible to identify relevant phonon modes.

The controlled charging of QDs with help of the external bias as revealed in the static capacitance measurements allows optical investigations of charged QDs. First experiments of this type were recently reported [War97, Böd99].

A very wide field of research becomes possible, if the strengths of optical experiments are combined with the power of capacitance spectroscopy. The depletion layer capacitance is a very sensitive measure for the amount of charge on the QDs and may hence serve as the detection meter in fundamental charge storage experiments. The wavelength of the incident light can serve as the ”tuning knob” for resonant charging of sub-ensembles of QDs. With this technique, wavelength-domain multiplexing [Mut95] and spectral-hole burning (see [Mas96, Mas99] and references therein) can hence be addressed. A significant advantage over the first experiments in this field [Ima95, Yus97, Fin98, Lun99] is the much simpler sample structure of depletion layer devices. Particularly in the case of type-II structures, the removal of one type of carriers after resonantly generating electron-hole pairs is very straightforward.

Appendix A

Experimental Details

A.1 Setup

The experimental setup is based on a CroyVac Helium constant flow cryostat with a CryoVac TIC 303M temperature controller. With this equipment one can stabilize temperatures between 10 K and 450 K with an accuracy of about ± 0.3 K. The capacitance is for static measurements determined with a HP4284A LCR meter with an internal voltage source, a measurement frequency between 20 Hz and 1 MHz, and an AC measurement signal amplitude of down to 5 mV. The accuracy of the measurement depends on the measurement frequency, the signal amplitude, and the integration time. For details see Reference [HP896].

For capacitance transient measurements a Boonton 7200 capacitance meter with an operation frequency of 1 MHz, a signal amplitude of 100 mV, and a rise time of about 50 μs is employed. The accuracy of the capacitance measurement is typically better than about 0.25% of the determined value. Reverse bias and superimposed pulses were externally supplied by a HP-8115A pulse generator. In order to allow operation in the most sensitive 2 pF range, a step-motor driven external capacitance correction (with a variable capacitor of 10 pF to 190 pF) is used to compensate the static sample capacitance after each change in the temperature and before transient recording.

The whole setup is controlled by a computer, which records the capacitance transients from the analog output of the capacitance meter after 12 bit A/D-conversion with up to about 30.000 points per transient and a minimum resolution of 5 μs. Typically 2000 points per transient with 105 μs resolu-

tion were used. Averaging of up to 100 transients was applied to increase the signal to noise ratio. Details on the data format used can be found in Reference [Lio99, Lio00]. A schematic layout of the experimental setup is shown in Figure A.1.

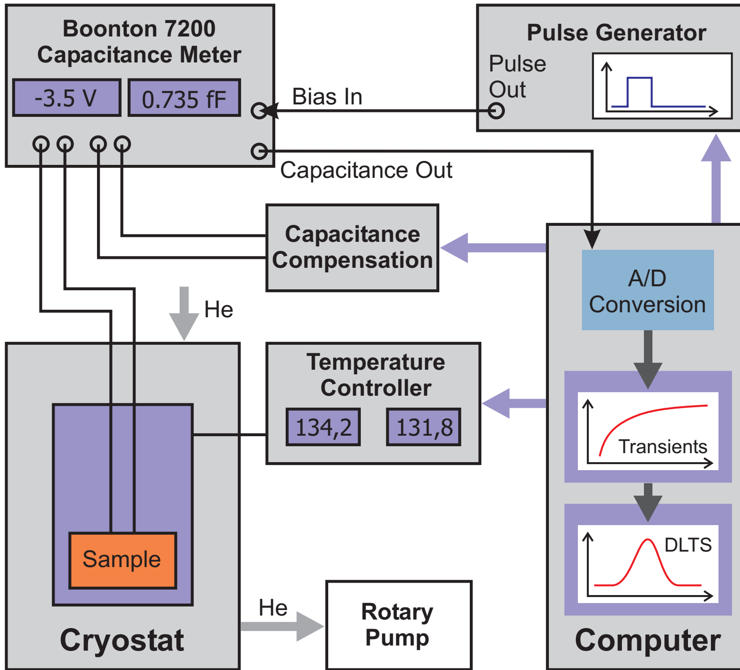

Figure A.1: *Experimental setup used for the DLTS measurements.*

A.2 Sample Processing

The GaAs samples were processed in the class 100 cleanroom of the "Institut für Festkörperphysik" of the "Technische Universität Berlin" using standard optical lithography with a Süss MJB3 mask aligner, wet chemical etching, and a Veeco metal evaporation system. The processing recipe for p-n diode samples is presented in the following.

p-n and n-p Diodes

Both sorts of devices were processed in almost the same way, except for the metals used to form Ohmic contacts. The whole process consists of the following steps:

- **Cleaning** – Rinse the sample for about 2 min in beakers filled with Aceton, Isopropanol $\times 2$, and H_2O.
- **Evaporation of back contact**
  - Mount sample on glass substrate with photoresist
  - Hotplate, 122°C, 10 min
  - Let sample cool, 3 min
  - HF(5%) dip, 5 sec
  - H_2O dip, 10 sec
  - H_2O dip, 10 sec
  - Dry with N_2
  - Metal evaporation (Section A.2)
- **Cleaning** – as above
- **Lithography: top contacts**
  - Spin photoresist MAP 1215 (3000 rnds/min, 30 sec)
  - Hotplate 85°C, 5 min
  - Let sample cool, 3 min
  - Exposure with mask, 79 mW/cm^2, 15 sec
  - Develop with MAD532:H_2O (1:1), $\geq$ 35 sec
  - H_2O dip, 10 sec
  - H_2O dip, 10 sec
  - Dry with N_2
- **Evaporation of top contacts** – as evaporation of back contacts, see above
- **Lift-off** in Aceton in ultrasonic bath (warm, if necessary)
- **Annealing** – 120 sec at 390°C in N_2 atmosphere
- **Cleaning** – as above
- **Lithography: mesas (MAN 410)**

  - Spin photoresist MAN 410 (3000 rnds/min, 30 sec)
  - Hotplate 85°C, 5 min
  - Let sample cool, 3 min
  - Exposure with mask, 79 mW/cm^2, $>$ 15 sec
  - Develop with MAD532:H_2O (1:1), $\geq$ 40 sec
  - H_2O dip, 10 sec
  - H_2O dip, 10 sec
  - Dry with N_2

- **OR: Lithography: mesas (AZ 5214E)**
  - Spin photoresist AZ 5214E (5000 rnds/min, 40 sec)
  - Hotplate 85°C, 5 min
  - Let sample cool, 3 min
  - Exposure with mask, 79 mW/cm^2, 15 sec
  - Hotplate 122°C, 5 min
  - Flood exposure, 79 mW/cm^2, 60 sec
  - Develop with AZ351B:H_2O (1:4), $\approx$ 25 sec, stir slowly
  - H_2O dip, 10 sec
  - H_2O dip, 10 sec
  - Dry with N_2

- **Wet chemical etching** – H_2O : H_2SO_4 : H_2O_2 (100:1:8), stir for $>$ 10 min (!)
  - Mount sample on glass substrate with photoresist
  - Hotplate, 122°C, 10 min
  - Let sample cool, 3 min
  - HF(5%) dip, 5 sec
  - H_2O dip, 10 sec
  - H_2O dip, 10 sec
  - Dry with N_2
  - Etch sample
  - H_2O dip, 10 sec
  - H_2O dip, 10 sec

- **Cleaning** – as above

Ohmic Contacts

For the formation of non-rectifying metal-semiconductor contacts, a standard procedure of evaporating metal with subsequent alloying is used. Depending on whether the material is n- or p-type, different layers of metals are used. They are given in the order of evaporation with their according thicknesses. After the evaporation, the samples were annealed in N_2 atmosphere to allow for diffusion of the metal into the semiconductor. The conditions used were: 120 sec at 390°C.

n-type GaAs

- 7.5 nm Ni
- 100 nm Au/Ge (88:12)
- 200 nm Au

p-type GaAs

- 5 nm Ni
- 50 nm Zn
- 200 nm Au

References

[Abs96] G. Abstreiter, P. Schittenhelm, C. Engel, E. Silveira, A. Zrenner, D. Meertens, and W. Jäger, *Growth and characterization of self-assembled Ge-rich islands on Si*, Semicond. Sci. Technol. **11**, 1521 (1996).

[Ana95] S. Anand, N. Carlsson, M.-E. Pistol, L. Samuelson, and W. Seifert, *Deep level transient spectroscopy of InP quantum dots*, Appl. Phys. Lett. **67** (20), 3016 (1995).

[Ana98] S. Anand, N. Carlsson, M.-E. Pistol, L. Samuelson, and W. Seifert, *Electrical characterization of InP/GaInP quantum dots by space charge spectroscopy*, J. Appl. Phys. **84** (7), 3747 (1998).

[Ara82] Y. Arakawa and H. Sakaki, *Multidimensional quantum well laser and temperature dependence of its threshold current*, Appl. Phys. Lett. **40**, 939 (1982).

[Ash92] R. C. Ashoori, H. L. Störmer, J. S. Weiner, L. N. Pfeiffer, S. J. Pearton, K. W. Baldwin, and K. W. West, *Single-Electron Capacitance Spectroscopy of Discrete Quantum Levels*, Phys. Rev. Lett. **68** (20), 3088 (1992).

[Ash93] R. C. Ashoori, H. L. Störmer, J. S. Weiner, L. N. Pfeiffer, K. W. Baldwin, and K. W. West, *N-Electron Ground State Energies of a Quantum Dot in Magnetic Field*, Phys. Rev. Lett. **71** (4), 613 (1993).

[Ash96] R. C. Ashoori, *Electrons in artificial atoms*, Nature **379**, 413 (1996).

[Asp00] T. Asperger, *Löchertransport in selbstorganisierten Germanium-Quantenpunkten*, Diplomarbeit, Technische Universität München (2000).

[Asp01] T. Asperger, C. Miesner, K. Brunner, and G. Abstreiter, *Space Charge Spectroscopy of Self Assembled Ge Quantum Dots in Si*, phys. stat. sol. (b) **224** (1), 237 (2001).

[Bab87] N. Baber, H. G. Grimmeis, M. Kleverman, P. Omling, and M. Z. Iqbal, *Characterization of silver-related deep levels in silicon*, J. Appl. Phys. **62** (7), 2853 (1987).

[Bab92] N. Baber, H. Scheffler, A. Ostmann, T. Wolf, and D. Bimberg, *Field effect on electron emission from the deep Ti donor level in InP*, Phys. Rev. B **45** (8), 4043 (1992).

[Bel00] A. E. Belyaev, S. T. Stoddart, P. M. Martin, P. C. Main, L. Eaves, and M. Henini, *Positively charged defects associated with self-assembled quantum dot formation*, Appl. Phys. Lett. **76** (24), 3570 (2000).

[Ben91] H. Benisty, C. M. Sotomayor-Torres, and C. Weisbuch, *Intrinsic mechanism for the poor luminescence properties of quantum-box systems*, Phys. Rev. B **44** (19), 10945 (1991).

[Ben96a] B. R. Bennet, R. Magno, and B. V. Shannabrook, *Molecular beam epitaxial growth of InSb, GaSb and AlSb nanometer-scale dots on GaAs*, Appl. Phys. Lett. **68** (4), 505 (1996).

[Ben96b] B. R. Bennet, B. V. Shannabrook, and R. Magno, *Phonons in self-assembled (In,Ga,Al)Sb quantum dots*, Appl. Phys. Lett. **68** (7), 958 (1996).

[Bim98] D. Bimberg, M. Grundmann, and N. N. Ledentsov, *Quantum Dot Heterostructures*, John Wiley & Sons, Chichester (1998).

[Blo92] P. Blood and J. W. Orton, *The Electrical Characterization of Semiconductors: Majority Carriers and Electron States*, Academic Press, London (1992).

[Boc90] U. Bockelmann and G. Bastard, *Phonon scattering and energy relaxation in two-, one-, and zero-dimensional electron gases*, Phys. Rev. B **42**, 8947 (1990).

[Boc92] U. Bockelmann and T. Egeler, *Electron relaxation in quantum dots by means of Auger processes*, Phys. Rev. B **46** (23), 15574 (1992).

[Böd99] M. C. Bödefeld, R. J. Warburton, K. Karrai, J. P. Kotthaus, G. Medeiros-Ribeiro, and P. M. Petroff, *Storage of electrons and holes in self-assembled InAs quantum dots*, Appl. Phys. Lett. **74** (13), 1839 (1999).

[Bog01] T. F. Boggess, L. Zhang, D. G. Deppe, D. L. Huffaker, and C. Cao, *Spectral engineering of carrier dynamics in In(Ga)As self-assembled quantum dots*, Appl. Phys. Lett. **78** (3), 276 (2001).

[Bou83] J. Bourgoin and M. Lannoo, *Point Defects in Semiconductors II - Experimental Aspects*, volume 35 of *Springer Series in Solid-State Sciences*, Springer, Berlin (1983).

[Bro96] P. N. Brounkov, T. Benyattou, and G. Guillot, *Simulation of the capacitance-voltage characteristics of a single-quantum-well structure based on the self-consistent solution of the Schrödinger and Poisson equations*, J. Appl. Phys. **80** (2), 864 (1996).

[Bro98] P. N. Brounkov, A. Polimeni, S. T. Stoddart, M. Henini, L. Eaves, P. C. Main, A. R. Kovsh, Y. G. Musikhin, and S. G. Konnikov, *Electronic structure of self-assembled InAs quantum dots in GaAs matrix*, Appl. Phys. Lett. **73** (8), 1092 (1998).

[Bru96] P. N. Brunkov, S. G. Konnikov, V. M. Ustinov, A. E. Zhukov, A. Y. Egorov, M. V. Maksimov, N. N. Ledentsov, and P. S. Kop'ev, *Capacitance spectroscopy of electron energy levels in InAs quantum dots in a GaAs matrix*, Semiconductors **30** (5), 492 (1996).

[Bru98] P. N. Brunkov, A. A. Suvorova, N. A. Bert, A. R. Kovsh, A. E. Zhukov, A. Y. Egorov, V. M. Ustinov, A. F. Tsatsul'nikov, N. N. Ledentsov, P. S. Kop'ev, S. G. Konnikov, L. Eaves, and P. S. Main, *Capacitance-voltage profiling of Au/n-GaAs Schottky barrier structures containing a layer of self-organized InAs quantum dots*, Semiconductors **32** (10), 1096 (1998).

[Bru99] P. N. Brunkov, A. R. Kovsh, V. M. Ustinov, Y. G. Musikhin, N. N. Ledentsov, S. G. Konnikov, A. Polimeni, A. Patan, P. C. Main, L. Eaves, and C. M. A. Kapteyn, *Emission of electrons from the ground and first excited states of self-organized InAs/GaAs quantum dot structures*, J. Electr. Mat. **28** (5), 486 (1999).

[Cha81] A. Chantre, G. Vincent, and D. Bois, *Deep-level optical spectroscopy in GaAs*, Phys. Rev. B **23** (10), 5335 (1981).

[Dab89] J. Dabrowski and M. Scheffler, *Isolated arsenic-antisite defect in GaAs and the properties of EL2*, Phys. Rev. B **40** (15), 10391 (1989).

[Dad97] A. Dadgar, R. Engelhardt, M. Kuttler, and D. Bimberg, *Capacitance transient study of the deep Fe acceptor in indium phosphide*, Phys. Rev. B **56** (16), 10241 (1997).

[Dad99] A. Dadgar, *MOCVD-Wachstum und elektrische Eigenschaften von Eisen und Platinmetallen im Indiumphosphid*, Mensch & Buch Verlag, Berlin (1999), [Dissertation, Technische Universität Berlin].

[Dai97] Y. T. Dai, J. C. Fan, Y. F. Chen, R. M. Lin, S. C. Lee, and H. H. Lin, *Temperature dependence of photoluminescence spectra in InAs/GaAs quantum dot superlattices with large thicknesses*, J. Appl. Phys. **82** (9), 4489 (1997).

[Day79] D. S. Day, M. Y. Tsai, B. G. Streetman, and D. V. Lang, *Deep-level-transient spectroscopy: System effects and data analysis*, J. Appl. Phys. **50** (8), 5093 (1979).

[Deb89] N. Debbar, D. Biswas, and P. Bhattacharya, *Conduction-band offsets in pseudomorphic InxGa$_{1-x}$As/Al$_{0.2}$Ga$_{0.8}$As quantum wells (0.07 $\leq x \leq$ 0.18) measured by deep-level transient spectroscopy*, Phys. Rev. B **40** (2), 1058 (1989).

[DiB68] B. DiBartolo, *Optical Interactions in Solids*, John Wiley & Sons, New York (1968).

[Dre94] H. Drexler, D. Leonard, W. Hansen, J. P. Kotthaus, and P. M. Petroff, *Spectroscopy of quantum levels in charge-tunable InGaAs quantum dots*, Phys. Rev. Lett. **73** (16), 2252 (1994).

[Eag90] D. J. Eaglesham and M. Cerullo, *Dislocation-Free Stranski-Krastanow Growth of Ge on Si (100)*, Phys. Rev. Lett. **64** (16), 1943 (1990).

[Faf94] S. Fafard, *Selective excitation of the photoluminescence and the energy levels of ultrasmall InGaAs/GaAs quantum dots*, Appl. Phys. Lett. **65** (11), 1388 (1994).

[Faf95] S. Fafard, R. Leon, D. Leonard, J. L. Merz, and P. M. Petroff, *Phonons and radiative recombination in self-assembled quantum dots*, Phys. Rev. B **52** (8), 5752 (1995).

[Fer99] R. Ferreira and G. Bastard, *Phonon-assisted capture and intradot Auger relaxation in quantum dots*, Appl. Phys. Lett. **74** (19), 2818 (1999).

[Fin98] J. J. Finley, M. Skalitz, M. Arzberger, A. Zrenner, G. Bhm, and G. Abstreiter, *Electrical detection of optically induced charge storage in self-assembled InAs quantum dots*, Appl. Phys. Lett. **73** (18), 2618 (1998).

[Fin99] J. J. Finley, M. Skalitz, M. Arzberger, A. Zrenner, G. Böhm, and G. Arzberger, *Optically induced persistent charge storage effects in self assembled InAs quantum dots*, Jpn. J. Appl. Phys. **38**, 531 (1999).

[Fre38] J. Frenkel, *On pre-breakdown phenomena in insulators and electronic semiconductors*, Phys. Rev. **54**, 647 (1938).

[Fri96] M. Fricke, A. Lorke, J. P. Kotthaus, G. Medeiros-Ribeiro, and P. M. Petroff, *Shell structure and electron-electron interaction in self-assembled InAs quantum dots*, Europhys. Lett. **36** (3), 197 (1996).

[Fry00a] P. W. Fry, J. J. Finley, L. R. Wilson, A. Lemaître, D. J. Mowbray, and M. S. Skolnick, *Electric-field-dependent carrier capture and escape in self-assembled InAs/GaAs quantum dots*, Appl. Phys. Lett. **77** (26), 4344 (2000).

[Fry00b] P. W. Fry, I. E. Itskevich, D. J. Mowbray, M. S. Skolnick, J. J. Finley, J. A. Barker, E. P. OReilly, L. R. Wilson, I. A. Larkin, P. A. Maksym, M. Hopkinson, M. Al-Khafaji, J. P. R. David, A. G. Cullis, G. Hill, and J. C. Clark, *Inverted Electron-Hole Alignment in InAs-GaAs Self-Assembled Quantum Dots*, Phys. Rev. Lett. **84** (4), 733 (2000).

[Fry00c] P. W. Fry, I. E. Itskevich, S. R. Parnell, J. J. Finley, L. R. Wilson, K. L. Schumacher, D. J. Mowbray, M. S. Skolnick, M. Al-Khafaji, A. G. Cullis, M. Hopkinson, J. C. Clark, and G. Hill, *Photocurrent spectroscopy of InAs/GaAs self-assembled quantum dots*, Phys. Rev. B **62** (24), 16784 (2000).

[Fry01] P. W. Fry, *Electronic properties of InAs/GaAs self-assembled quantum dots studied by photocurrent spectroscopy*, Physica E **9**, 106 (2001).

[Fuj95] H. Fujioka, E. R. Weber, and A. K. Verma, *Transient current study of low-temperature grown GaAs using an n-i-n structure*, Appl. Phys. Lett. **66** (21), 2834 (1995).

[Gib77] R. M. Gibb, G. J. Rees, B. W. Thomas, B. L. H. Wilson, B. Hamilton, D. R. Wright, and N. F. Mott, *A two stage model for deep level capture*, Phil. Mag. **36**, 1021 (1977).

[Gla96] E. R. Glaser, B. R. Bennet, B. V. Shannabrook, and R. Magno, *Photoluminescence studies of self-assembled InSb, GaSb, and AlSb quantum dot heterostructures*, Appl. Phys. Lett. **68** (25), 3614 (1996).

[Gri81] H. G. Grimmeiss and C. Ovrén, *Fundamentals of junction measurements in the study of deep energy levels in semiconductors*, J. Phys. E: Sci. Instrum. **14**, 1032 (1981).

[Gru95] M. Grundmann, O. Stier, and D. Bimberg, *InAs/GaAs Quantum Pyramids: Strain Distribution, Optical Phonons and Electronic Structure*, Phys. Rev. B **52** (16), 11969 (1995).

[Gru97] M. Grundmann and D. Bimberg, *Theory of random population for quantum dots*, Phys. Rev. B **55** (15), 9740 (1997).

[Gru00] M. Grundmann, *The present status of quantum dot lasers*, Physica E **5**, 167 (2000).

[Guh90] S. Guha, A. Madhukar, and K. C. Rajkumar, *Onset of incoherency and defect introduction in the initial stages of molecular beam epitaxical growth of highly strained* $In_xGa_{1x}As$ *on GaAs(100)*, Appl. Phys. Lett. **57** (20), 2110 (1990).

[Guo97] L. Guo, E. Leobandung, and S. Y. Chou, *A room-temperature silicon single-electron metaloxidesemiconductor memory with nanoscale floating-gate and ultranarrow channel*, Appl. Phys. Lett. **70** (7), 850 (1997).

[Har68] J. L. Hartke, *The Three-Dimensional Poole-Frenkel Effect*, J. Appl. Phys. **39**, 4871 (1968).

[Hat95] F. Hatami, N. N. Ledentsov, M. Grundmann, J. Bhrer, F. Heinrichsdorff, M. Beer, D. Bimberg, S. S. Ruvimov, P. Werner, U. Gsele, J. Heydenreich, U. Richter, S. V. Ivanov, B. Y. Meltser, P. S. Kop'ev, and Z. I. Alferov, *Radiative recombination in type-II GaSb/GaAs quantum dots*, Appl. Phys. Lett. **67** (5), 656 (1995).

[Hat98] F. Hatami, M. Grundmann, N. N. Ledentsov, F. Heinrichsdorff, R. Heitz, J. Böhrer, D. Bimberg, S. S. Ruvimov, P. Werner, V. M. Ustinov, P. S. Kop'ev, and Z. I. Alferov, *Carrier dynamics in type-II GaSb/GaAs quantum dots*, Phys. Rev. B **57** (8), 4635 (1998).

[Haw99] P. Hawker, A. J. Kent, and M. Henini, *Energy relaxation by photoexcited carriers in the InAs/GaAs quantum-dot system: Bolometric detection of strong acoustic-phonon emission*, Appl. Phys. Lett. **75** (24), 3832 (1999).

[Hed95] H. Hedemann, *Quantitative Analyse von Kapazitätstransientenspektren ausgedehnter Defekte in Halbleitern*, Cuvillier, Göttingen (1995), [Dissertation, Georg-August-Universität Göttingen].

[Hei96a] Y. Heiner, O. Stier, V. Türck, J. Vaschull, B. Sumpf, and A. Ostermeier, *Evolution strategies applied to least squares curve fitting of spectroscopic data*, Journal of Quantitative Spectroscopy and Radiative Transfer **56**, 769 (1996).

[Hei96b] F. Heinrichsdorff, A. Krost, M. Grundmann, D. Bimberg, A. Kosogov, and P. Werner, *Self-organization processes of InGaAs/GaAs quantum dots grown by metalorganic chemical vapor deposition*, Appl. Phys. Lett. **68**, 3284 (1996).

[Hei96c] R. Heitz, M. Grundmann, N. N. Ledentsov, L. Eckey, M. Veit, D. Bimberg, V. M. Ustinov, A. Y. Egorov, A. E. Zhukov, P. S. Kopev, and Z. I. Alferov, *Multiphonon-relaxation processes in self-organized InAs/GaAs quantum dots*, Appl. Phys. Lett. **68** (3), 361 (1996).

[Hei96d] R. Heitz, A. Kalburge, Q. Xie, M. Veit, M. Grundmann, P. Chen, A. Madhukar, and D. Bimberg, *Energy Relaxation in InAs/GaAs Quantum Dots*, in M. Scheffler and R. Zimmermann (eds.), *23rd International Conference on the Physics of Semiconductors*, volume 2, p. 1425, World Scientific, Berlin (1996).

[Hei97] R. Heitz, M. Veit, N. N. Ledentsov, A. Hoffmann, D. Bimberg, V. M. Ustinov, P. S. Kop'ev, and Z. I. Alferov, *Energy relaxation by multiphonon processes in InAs/GaAs quantum dots*, Phys. Rev. B **56** (16), 10435 (1997).

[Hei98a] F. Heinrichsdorff, *MOCVD growth and laser applications of In(Ga)As/GaAs quantum dots*, Mensch & Buch, Berlin (1998), [Dissertation, Technische Universität Berlin].

[Hei98b] R. Heitz, A. Kalburge, Q. Xie, M. Grundmann, P. Chen, A. Hoffmann, A. Madhukar, and D. Bimberg, *Excited states and energy relaxation in stacked InAs/GaAs quantum dots*, Phys. Rev. B **57** (15), 9050 (1998).

[Hei98c] R. Heitz, I. Mukhametzhanov, P. Chen, and A. Madhukar, *Excitation transfer in self-organized asymmetric quantum dot pairs*, Phys. Rev. B **58** (16), 10151 (1998).

[Hei99] R. Heitz, I. Mukhametzhanov, A. Madhukar, A. Hoffmann, and D. Bimberg, *Temperature Dependent Optical Properties of Self-Organized InAs/GaAs Quantum Dots*, J. Electron. Mat. **28** (5), 520 (1999).

[Hei00] D. Heinrich, J. Hoffmann, J. J. Finley, A. Zrenner, G. Bohm, and G. Abstreiter, *Optically-induced charge storage in self-assembled InAs quantum dots*, Thin Solid Films **380** (1-2), 192 (2000).

[Hoe72] B. Hoeneisen and C. A. Mead, *Fundamental limitations in microelectronics. I. MOS technology*, Solid-State Electronics **15** (7), 819 (1972).

[Hog98] R. A. Hogg, K. Suzuki, K. Tachibana, L. Finger, K. Hirakawa, and Y. Arakawa, *Optical spectroscopy of self-assembled type II GaSb/GaAs quantum dot structures grown by molecular beam epitaxy*, Appl. Phys. Lett. **72** (22), 2856 (1998).

[HP896] *HP 4284A Precision LCR Meter Operation Manual* (1996).

[Hua50] K. Huang and A. Rhys, *Theory of light absorption and non-radiative transitions in F-centers*, Proc. Roy. Soc. London, Ser. A **204**, 406 (1950).

[Ign01] I. V. Ignatiev, I. E. Kozin, V. G. Davydov, S. V. Nair, J.-S. Lee, H.-W. Ren, S. Sugou, and Y. Masumoto, *Phonon resonances in photoluminescence spectra of self-assembled quantum dots in an electric field*, Phys. Rev. B **63**, 075316 (2001).

[Ima95] K. Imamura, Y. Sugiyama, Y. Nakata, S. Muto, and S. Yokoyama, *New Optical Memory Structure Using Self-Assembled InAs Quantum Dots*, Jpn. J. Appl. Phys. **34**, L1445 (1995).

[Ino92] T. Inoshita and H. Sakaki, *Electron relaxation in a quantum dot: Significance of multiphonon processes*, Phys. Rev. B **46** (11), 7260 (1992).

[Irm83] K. Irmscher, H. Klose, and K. Maas, *Electric Field Enhanced Electron Emission from Gold Acceptor Level and A-Centre in Silicon*, phys. stat. sol. (a) **7**, K25 (1983).

[Jac98] L. Jacak, P. Hawrylak, and A. Wójs, *Quantum Dots*, Springer, Berlin (1998).

[Jia98] H. Jiang and J. Singh, *Self-Assembled Semiconductor Structures: Electronic and Optoelectronic Properties*, IEEE J. Quantum Electron. **34** (7), 1188 (1998).

[Kas93] M. A. Kastner, *Artificial Atoms*, Physics Today (Jan.), 24 (1993).

[Kei65] T. Keil, *Shapes of Impurity Absorption Bands in Solids*, Phys. Rev. **140** (2A), A601 (1965).

[Kim74] L. C. Kimerling, *Influence of deep traps on the measurement of free-carrier distributions in semiconductors by junction capacitance techniques*, J. Appl. Phys. **45** (4), 1839 (1974).

[Kim00] H. Kim, T. Noda, T. Kawazu, and H. Sakaki, *Control of Current Hysteresis Effects in a GaAs/n-AlGaAs Quantum Trap Field Effect Transistor with Embedded InAs Quantum Dots*, Jpn. J. Appl. Phys. **39**, 7100 (2000).

[Kir81] P. D. Kirchner, W. J. Schaff, G. N. Maracas, L. F. Eastman, T. I. . Chappell, and C. M. Ransom, *The analysis of exponential and nonexponential transients in deep-level transient spectroscopy*, J. Appl. Phys. **52** (11), 6462 (1981).

[Kir94] N. Kirstaedter, N. N. Ledentsov, M. Grundmann, D. Bimberg, V. M. Ustinov, S. S. Ruvimov, M. V. Maximov, P. S. Kop'ev, Z. I. Alferov, U. Richter,

P. Werner, U. Gosele, and J. Heydenreich, *Low threshold, large T_0 injection laser emission from (InGa)As quantum dots*, Electron. Lett. **30** (17), 1416 (1994).

[Kit80] C. Kittel and H. Kroemer, *Thermal Physics*, W. H. Freeman, San Francisco (1980).

[Koi00] K. Koike, K. Saitoh, S. Li, S. Sasa, M. Inoue, and M. Yano, *Room-temperature operation of a memory-effect AlGaAs/GaAsheterojunction field-effect transistor with self-assembled InAs nanodots*, Appl. Phys. Lett. **76** (11), 1464 (2000).

[Kor77] E. N. Korol, *Ionization of impurity states in semiconductors by an electric field*, Sov. Phys. Solid State **19** (8), 1327 (1977).

[Kri98] P. Krispin, J.-L. Lazzari, and H. Kostial, *Deep and shallow electronic states at ultrathin InAs insertions in GaAs investigated by capacitance spectroscopy*, J. Appl. Phys. **84** (11), 6135 (1998).

[Kro80] H. Kroemer, W.-Y. Chien, J. S. Harris, and D. D. Edwall, *Measurement of isotype heterojunction barriers by C-V profiling*, Appl. Phys. Lett. **36** (4), 295 (1980).

[Kuo99] D. M.-T. Kuo and Y.-C.Chang, *Dynamic behavior of electron tunneling and dark current in quantum-well systems under an electric field*, Phys. Rev. B **60** (23), 15957 (1999).

[Kuo00] D. M.-T. Kuo and Y.-C.Chang, *Electron tunneling rate in quantum dots under a uniform electric field*, Phys. Rev. B **61** (16), 11051 (2000).

[Lan74] D. V. Lang, *Deep-level transient spectroscopy: A new method to characterize traps in semiconductors*, J. Appl. Phys. **45** (7), 3023 (1974).

[Lan79a] D. V. Lang, *Space-Charge Spectroscopy in Semiconductors*, in P. Bräunlich (ed.), *Thermally Stimulated Relaxation in Solids*, volume 37 of *Topics in Applied Physics*, p. 93, Springer, Berlin (1979).

[Lan79b] D. V. Lang, R. A. Logan, and M. Jaros, *Trapping characteristics and a donor-complex (DX) model for the persistent-photoconductivity trapping center in Te-doped $Al_xGa_{1-x}As$*, Phys. Rev. B **19** (2), 1015 (1979).

[Lan81] M. Lannoo and J. Bourgoin, *Point Defects in Semiconductors I - Theoretical Aspects*, volume 22 of *Springer Series in Solid-State Sciences*, Springer, Berlin (1981).

[Lan87] D. V. Lang, *Measurement of band offsets by space charge spectroscopy*, in F. Capasso and G. Margaritondo (eds.), *Heterojunction band discontinuities - physics and device applications*, p. 377, North-Holland, Amsterdam (1987).

[LB882] *Landolt-Börnstein — Semiconductors: Physics of Group IV Elements and III-V Compounds*, volume III/17a, Springer, Berlin (1982).

[LB887] *Landolt-Börnstein — Semiconductors: Intrinsic Properties of Group IV Elements and II-V, II-VI and I-VII Compounds*, volume III/22a, Springer, Berlin (1987).

[Led96] N. N. Ledentsov, V. A. Shchukin, M. Grundmann, N. Kirstaedter, J. Böhrer, O. Schmidt, D. Bimberg, V. M. Ustinov, A. Y. Egorov, A. E. Zhukov, P. S. Kop'ev, S. V. Zaitsev, N. Y. Gordeev, Z. I. Alferov, A. I. Borovkov, A. O. Kosogov, S. S. Ruvimov, P. Werner, U. Gösele, and J. Heydenreich, *Direct formation of vertically coupled quantum dots in Stranski-Krastanow growth*, Phys. Rev. B **54** (12), 8743 (1996).

[Led00] N. N. Ledentsov, M. Grundmann, F. Heinrichsdorff, D. Bimberg, V. M. Ustinov, A. E. Zhukov, M. V. Maximov, Z. I. Alferov, and J. A. Lott, *Quantum-Dot Heterostructure Lasers*, IEEE Journal of Selected Topics in Quantum Electronics **6** (3), 439 (2000).

[Leo94] D. Leonard, K. Pond, and P. M. Petroff, *Critical layer thickness for self-assembled InAs islands on GaAs*, Phys. Rev. B **50**, 11687 (1994).

[Let91a] X. Letartre, D. Stiévenard, and E. Barbier, *Accurate determination of the conduction-band offset of a single quantum well using deep level transient spectroscopy*, Appl. Phys. Lett. **58** (10), 1047 (1991).

[Let91b] X. Letartre, D. Stiévenard, and E. Barbier, *Analytical calculation of the capacitance associated with a single quantum well located in a junction*, Appl. Phys. Lett. **69** (11), 7912 (1991).

[Let91c] X. Letartre, D. Stiévenard, and M. Lanoo, *Tunnel deep level transient spectroscopy on a single quantum well*, J. Appl. Phys. **69** (10), 7336 (1991).

[Lio99] M. Lion, *Deep Level Transient Spectroscopy an selbstorganisierten InAs/GaAs Quantenpunkten*, Studienarbeit, Technische Universität (1999).

[Lio00] M. Lion, *Optisch angeregte Kapzitätsspektroskopie an selbstorganisierten Quantenpunkten*, Diplomarbeit, Technische Universität (2000).

[Liu99] G. Liu, A. Stintz, H. Li, K. J. Malloy, and L. F. Lester, *Extremely low room-temperature threshold current density diode lasers using InAs dots in* $In_{0.15}Ga_{0.85}As$ *quantum well*, Electron. Lett. **35** (14), 1163 (1999).

[Liu00] N. Liu, J. Tersoff, O. Baklenov, J. A. L. Holmes, and C. K. Shih, *Nonuniform Composition Profile in* $In_{0.5}Ga_{0.5}As$ *Alloy Quantum Dots*, Phys. Rev. Lett. **84** (2), 334 (2000).

[Lu96] F. Lu, D. Gong, J. Wang, Q. Wang, H. Sun, and X. Wang, *Capacitance-voltage characteristics of a Schottky junction containing SiGe/Si quantum wells*, Phys. Rev. B **53** (8), 4623 (1996).

[Lun99] T. Lundstrom, W. Schoenfeld, H. Lee, and P. M. Petroff, *Exciton Storage in Semiconductor Self-Assembled QuantumDots*, Science **286** (Dec. 17), 2312 (1999).

[Luy99] R. J. Luyken, A. Lorke, A. O. Govorov, J. P. Kotthaus, G. Medeiros-Ribeiro, and P. M. Petroff, *The dynamics of tunneling into self-assembled InAs dots*, Appl. Phys. Lett. **74** (17), 2486 (1999).

[Mag00] R. Magno, B. R. Bennett, and E. R. Glaser, *Deep level transient capacitance measurements of GaSb self-assembled quantum dots*, J. Appl. Phys. **88** (10), 5843 (2000).

[Mar81] P. A. Martin, B. G. Streetman, and K. Hess, *Electric field enhanced emission from non-Coulombic traps in semiconductors*, J. Appl. Phys. **52** (12), 7409 (1981).

[Mar83] P. A. Martin, K. Meehan, P. Gavrilovic, K. Hess, N. Holonyak, and J. J. Coleman, *Transient capacitance spectroscoyp on large quantum well heterostructures*, J. Appl. Phys. **54** (8), 4689 (1983).

[Mar91] E. Martinet, E. Rosencher, F. Chevoir, J. Nagle, and P. Bois, *Direct determination of the electron-tunneling escape time from a GaAs/AlGaAs quantum well by transient-capacitance spectroscopy*, Phys. Rev. B **44** (7), 3157 (1991).

[Mas96] Y. Masumoto, *Persistent hole burning in semiconductor nanocrystals*, J. Lumin. **70**, 386 (1996).

[Mas99] Y. Masumoto, *Persistent Spectral-Hole-Burning in Semiconductor Quantum Dots and its Application to Spectroscopy*, Jpn. J. Appl. Phys. **38**, 570 (1999).

[ME80] S. Makram-Ebeid, *Effect of electric field on deep-level transients in GaAs and GaP*, J. Appl. Phys. **37** (5), 464 (1980).

[ME82a] S. Makram-Ebeid and M. Lannoo, *Electric-Field-Induced Phonon-Assisted Tunnel Ionization from Deep Levels in Semiconductors*, Phys. Rev. Lett. **48** (18), 1281 (1982).

[ME82b] S. Makram-Ebeid and M. Lannoo, *Quantum model for phonon-assisted tunnel ionization of deep levels in semiconductors*, Phys. Rev. B **25** (10), 6406 (1982).

[Mei94] E. Meijer, H. G. Grimmeiss, and L.-A. Ledebo, *Dynamics of capture from free-carrier tails in depletion regions and its consequences in junction experiments*, J. Appl. Phys. **55** (12), 4266 (1994).

[Mie00a] C. Miesner, T. Asperger, K. Brunner, and G. Abstreiter, *Capacitance-voltage and admittance spectroscopy of self-assembled Ge islands in Si*, Appl. Phys. Lett. **77** (17), 2704 (2000).

[Mie00b] C. Miesner, O. Röthig, K. Brunner, and G. Abstreiter, *Intra-valence band photocurrent spectroscopy of self-assembled Ge dots in Si*, Appl. Phys. Lett. **76** (8), 1027 (2000).

[Mie00c] C. Miesner, O. Röthig, K. Brunner, and G. Abstreiter, *Mid-infrared photocurrent measurements on self-assembled Ge dots in Si*, Physica E **7**, 146 (2000).

[Mie01] C. Miesner, *Intra-Valenzbandspektroskopie in SiGe-Nanostrukturen in Si*, Munich (2001), [Dissertation, Technische Universität München].

[Mil77] G. L. Miller, D. V. Lang, and L. C. Kimerling, *Capacitance Transient Spectroscopy*, Ann. Rev. Mat. Sci. **7**, 377 (1977).

[Mil97] B. T. Miller, W. Hansen, S. Manus, R. J. Luyken, A. Lorke, J. P. Kotthaus, S. Huant, G. Medeiros-Ribeiro, and P. M. Petroff, *Few-electron ground states of charge-tunable self-assembled quantum dots*, Phys. Rev. B **56** (11), 6764 (1997).

[MK01] L. Müller-Kirsch, R. Heitz, A. Schliwa, O. Stier, D. Bimberg, H. Kirmse, and W. Neumann, *Many-particle effects in type II quantum dots*, Appl. Phys. Lett. **78** (10), 1418 (2001).

[Mo90] Y.-W. Mo, D. E. Savage, B. S. Swartzentruber, and M. G. Lagally, *Kinetic pathway in Stranski-Krastanov growth of Ge on Si(001)*, Phys. Rev. Lett. **65** (8), 1020 (1990).

[Moo65] G. E. Moore, *Cramming more components onto integrated circuits*, Electronics **38** (8) (1965).

[Moo98] C. R. Moon, B.-D. Choe, S. D. Kwon, H. K. Shin, and H. Lim, *Electron distribution and capacitance-voltage characteristics of n-doped quantum wells*, J. Appl. Phys. **84** (5), 2673 (1998).

[MR95] G. Medeiros-Ribeiro, D. Leonard, and P. M. Petroff, *Electron and hole energy levels in InAs self-assembled quantum dots*, Appl. Phys. Lett. **66** (14), 1767 (1995).

[MR97a] G. Medeiros-Ribeiro, J. M. Garcia, and P. M. Petroff, *Charging dynamics of InAs self-assembled quantum dots*, Phys. Rev. B **56** (7), 3609 (1997).

[MR97b] G. Medeiros-Ribeiro, F. G. Pikus, P. M. Petroff, and A. L. Efros, *Single-electron charging and Coulomb interaction in InAs self-assembled quantum dot arrays*, Phys. Rev. B **55** (3), 1568 (1997).

[Muk98] I. Mukhametzhanov, R. Heitz, J. Zeng, P. Chen, and A. Madhukar, *Independent manipulation of density and size of stress-driven self-assembled quantum dots*, Appl. Phys. Lett. **73** (13), 1841 (1998).

[Mut95] S. Muto, *On a Possibility of Wavelength-Domain-Multiplication Memory Using Quantum Boxes*, Jpn. J. Appl. Phys. **34**, 210 (1995).

[Myb98] G. Myburg, F. D. Auret, W. E. Meyer, C. W. Louw, and M. J. v. Staden, *Summary of Schottky barrier height data on epitaxially grown n- and p-GaAs*, Thin Solid Films **325**, 181 (1998).

[Nak97] A. Nakajima, T. Futatsugi, K. Kosemura, T. Fukano, and N. Yokoyama, *Room temperature operation of Si single-electron memory with self-aligned floating dot gate*, Appl. Phys. Lett. **70** (13), 1742 (1997).

[Oku80] H. Okushi and Y. Tokumaru, *Isothermal capacitance transient spectroscopy for determination of deep level parameters*, Jpn. J. Appl. Phys. **19**, L335 (1980).

[Oml85] P. Omling, E. R. Weber, L. Montelius, H. Alexander, and J. Michel, *Electrical properties of dislocations and point defects in plastically deformed silicon*, Phys. Rev. B **32** (10), 6571 (1985).

[Pet00] H. Pettersson, C. Pryor, L. Landin, M.-E. Pistol, N. Carlsson, W. Seifert, and L. Samuelson, *Electrical and optical properties of self-assembled InAs quantum dots in InP studied by space-charge spectroscopy and photoluminescence*, Phys. Rev. B **61** (7), 4795 (2000).

[Pon84] D. Pons, *Accurate determination of the free carrier capture kinetics of deep traps by space-charge methods*, J. Appl. Phys. **55** (10), 3644 (1984).

[Qur92] U. S. Qurashi, M. Z. Iqbal, C. Delerue, and M. Lannoo, *Electric-field dependence of electron emission from the deep-level oxygen defect in GaP*, Phys. Rev. B **45** (23), 13331 (1992).

[Ray95] S. Raymond, S. Fafard, S. Charbonneau, R. Leon, D. Leonard, P. M. Petroff, and J. L. Merz, *Photocarrier recombination in* $Al_yIn_{1-y}As/Al_xGa_{1-x}As$ *self-assembled quantum dots*, Phys. Rev. B **52** (24), 17238 (1995).

[Rec72] I. Rechenberg, *Evolutionsstrategie – Optimierung technischer Systeme nach dem Prinzip der biologischen Evolution*, Frommann-Holzboog Verlag, Stuttgart (1972).

[Ree80] G. J. Rees, H. G. Grimmeiss, E. Janzen, and B. Skarstam, *Capture, emission and recombination at a deep level via an excited state*, J. Phys. C: Solid St. Phys. **13**, 6157 (1980).

[Rho88] E. H. Rhoderick and R. H. Williams, *Metal Semiconductor Contacts*, Oxford Science Publications, 2nd edition (1988).

[Ruv95] S. Ruvimov and K. Scheerschmidt, *TEM/HREM Visualization of nm-Scale Coherent InAs Islands (Quantum Dots) in a GaAs Matrix*, phys. stat. sol. (a) **150**, 471 (1995).

[Sau98] P. Sauvage, P. Boucaud, F. Glotin, R. Prazeres, J.-M. Ortega, A. Lemaître, J.-M. Gérard, and V. Thierry-Flieg, *Saturation of intraband absorption and electron relaxation time in n-doped InAs/GaAs self-assembled quantum dots*, Appl. Phys. Lett. **73** (26), 3818 (1998).

[Sch95] P. Schittenhelm, M. Gail, J. Brunner, J. F. Nützel, and G. Abstreiter, *Photoluminescence study of the crossover from two-dimensional to three-dimensional growth for Ge on Si(100)*, Appl. Phys. Lett. **67** (9), 1292 (1995).

[Sch96a] K. H. Schmidt, G. Medeiros-Ribeiro, M. Oestreich, P. M. Petroff, and G. H. Döhler, *Carrier relaxation and electronic structure in InAs self-assembled quantum dots*, Phys. Rev. B **54** (16), 11346 (1996).

[Sch96b] D. F. Schoeter, D. J. Griffiths, and P. C. Sercel, *Defect-assisted relaxation in quantum dots at low temperature*, Phys. Rev. B **54** (3), 1486 (1996).

[Sch98] K. H. Schmidt, G. Medeiros-Ribeiro, and P. M. Petroff, *Photoluminescence of charged InAs self-assembled quantum dots*, Phys. Rev. B **58** (7), 3597 (1998).

[Sch99] K. Schmalz, I. N. Yassievich, P. Schittenhelm, and G. Abstreiter, *Space-charge spectroscopy of self-assembled Ge-rich dots on Si grown by MBE*, Phys. Rev. B **60** (3), 1792 (1999).

[Shc99] V. A. Shchukin and D. Bimberg, *Spontaneous ordering of nanostructures on crystal surfaces*, Rev. Modern Physics **71**, 1125 (1999).

[Sin99] D. V. Singh, K. Rim, T. O. Mitchell, J. L. Hoyt, and J. F. Gibbons, *Admittance spectroscopy analysis of the conduction band offsets in Si/*$Si_{1-x-y}Ge_xC_y$ *and Si/*$Si_{1-y}C_y$ *heterostructures*, J. Appl. Phys. **85** (2), 985 (1999).

[Ste96] M. J. Steer, D. J. Mowbray, W. R. Tribe, M. S. Skolnick, M. D. Sturge, M. Hopkinson, A. G. Cullis, C. R. Whitehouse, and R. Murray, *Electronic energy levels and energy relaxation mechanisms in self-organized InAs/GaAs quantum dots*, Phys. Rev. B **54**, 17738 (1996).

[Sti99] O. Stier, M. Grundmann, and D. Bimberg, *Electronic and optical properties of strained quantum dots modeled by 8-band-k.p theory*, Phys. Rev. B **59**, 5688 (1999).

[Sti01a] O. Stier, *Electronic and Optical Properties of Quantum Dots and Wires*, volume 7 of *Berlin Studies in Solid State Physics*, Wissenschaft und Technik Verlag, Berlin (2001), [Dissertation, Technische Universität Berlin].

[Sti01b] O. Stier, A. Schliwa, R. Heitz, M. Grundmann, and D. Bimberg, *Stability of Biexcitons in Pyramidal InAs/GaAs Quantum Dots*, phys. stat. sol. (b) **224** (1), 115 (2001).

[Str38a] I. N. Stranski and L. Krastanow, *Die orientierte Ausscheidung von Ionenkristallen aufeinander vom Standpunkte der Kristallwachstumstheorie*, N. Jahrb. Min. Beil. Bd. (A) **74**, 304 (1938).

[Str38b] I. N. Stranski and L. Krastanow, *Zur Theorie der orientierten Ausscheidung von Ionenkristallen aufeinander*, Sitzungsber. Akad. Wiss. Wien, Math.-Naturwiss. K1, Abt. 2B **146**, 797 (1938).

[Sug76] T. Sugano, *Physical and Technological Limits in Size of Semiconductor Devices*, Jpn. J. Appl. Phys. **15**, 329 (1976).

[Sug98] Y. Sugiyama, Y. Nakata, S. Muto, T. Futatsugi, and N. Yokoyama, *Characteristics of Spectral-Hole Burning of InAs Self-Assembled Quantum Dots*, IEEE J. Sel. Topics in Quantum Electron. **4** (5), 880 (1998).

[Sun96] H. Sunamura, Y. Shiraki, and S. Fukatsu, *Growth mode transition and photoluminescence properties of $Si_{1x}Ge_x$/Si quantum well structures with high Ge composition*, Appl. Phys. Lett. **66** (8), 953 (1996).

[Sze81] S. M. Sze, *Physics of Semiconductor Devices*, John Wiley & Sons, New York, 2nd edition (1981).

[Sze85] S. M. Sze, *Semiconductor Devices - Physics and Technology*, John Wiley & Sons, New York (1985).

[Sze99] S. M. Sze, *Evolution of Nonvolatile Semiconductor Memory: From Floating-Gate Concept to Single-Electron Memory Cell*, in S. Luryi, J. Xu, and A. Zaslavsky (eds.), *Future Trends in Microelectronics*, p. 291, John Wiley & Sons, Inc. (1999).

[Tar96] S. Tarucha, D. G. Austing, T. Honda, R. J. v. d. Hage, and L. P. Kouwenhoven, *Shell Filling and Spin Effects in a Few Electron Quantum Dot*, Phys. Rev. Lett. **77** (17), 3613 (1996).

[Tiw96a] S. Tiwari, F. Rana, K. Chan, L. Shi, and H. Hanafi, *Single charge and confinement effects in nano-crystal memories*, Appl. Phys. Lett. **69** (9), 1232 (1996).

[Tiw96b] S. Tiwari, F. Rana, H. Hanafi, A. Hartstein, E. F. Crabbé, and K. Chan, *A silicon nanocrystal based memory*, Appl. Phys. Lett. **68** (10), 1377 (1996).

[Tod99] Y. Toda, O. Moriwaki, M. Nishioka, and Y. Arakawa, *Efficient Carrier Relaxation Mechanism in InGaAsyyyGaAs Self-Assembled Quantum Dots Based on the Existence of Continuum States*, Phys. Rev. Lett. **82** (20), 4114 (1999).

[Vin79] G. Vincent, A. Chantre, and D. Bois, *Electric field effect on the thermal emission of traps in semiconductor junctions*, J. Appl. Phys. **50** (8), 5484 (1979).

[Wal00] C. Walther, J. Bollmann, H. Kissel, H. Kirmse, W. Neumann, and W. T. Masselink, *Characterization of electron trap states due to InAs quantum dots in GaAs*, Appl. Phys. Lett. **76** (20), 2916 (2000).

[Wan94] Q. H. Wang, F. Lu, D. W. Gong, X. J. Chen, J. B. Wang, H. H. Sun, and X. Wang, *Interfacial defects in $Si_{1-x}Ge_x$/Si quantum wells detected by deep-level transient spectroscopy*, Phys. Rev. B **50** (24), 18226 (1994).

[Wan96] J. B. Wang, F. Lu, S. K. Zhang, B. Zhang, D. W. Gong, H. H. Sun, and X. Wang, *Analysis of capacitance-voltage characteristics of $Si_{1-x}Ge_x$/Si quantum-well structures*, Phys. Rev. B **54** (11), 7979 (1996).

[Wan99] L.-W. Wang, J. Kim, and A. Zunger, *Electronic structures of [110]-faceted self-assembled pyramidal InAs/GaAs quantum dots*, Phys. Rev. B **59** (8), 5678 (1999).

[War97] R. J. Warburton, C. S. Dürr, K. Karrai, J. P. Kotthaus, G. Medeiros-Ribeiro, and P. M. Petroff, *Charged excitons in self-assembled semiconductor quantum dots*, Phys. Rev. Lett. **79** (20), 5282 (1997).

[Wel97] J. J. Welser, S. Tiwari, S. Rishton, K. Y. Lee, and Y. Lee, *Room Temperature Operation of a Quantum-Dot Flash Memory*, IEEE Electron Device Letters **18** (6), 278 (1997).

[Wet00] R. Wetzler, A. Wacker, E. Schöll, C. M. A. Kapteyn, R. Heitz, and D. Bimberg, *Capacitance-voltage characteristics of InAs/GaAs quantum dots embedded in a pn structure*, Appl. Phys. Lett. **77** (11), 1671 (2000).

[Wet01] R. Wetzler, C. M. A. Kapteyn, R. Heitz, A. Wacker, E. Schöll, and D. Bimberg, *Capacitance Voltage Spectroscopy of Self-Organized InAs/GaAs Quantum Dots Embedded in a pn Diode*, phys. stat. sol. (b) **224** (1), 79 (2001).

[Wog97] U. Woggon, *Optical Properties of Semiconductor Nanostructures*, volume 136 of *Springer Tracts in Modern Physics*, Springer, Berlin (1997).

[Woj96] A. Wojs and P. Hawrylak, *Charging and infrared spectroscopy of self-assembled quantum dots in a magnetic field*, Phys. Rev. B **53** (16), 10841 (1996).

[Woj98] A. Wojs, P. Hawrylak, S. Fafard, and L. Jacak, *Theory of luminescence from highly excited self-assembled quantum dots*, Physica E **2**, 603 (1998).

[Wu97] W. Wu, J. R. Tucker, G. S. Solomon, and J. J. S. Harris, *Atom-resolved scanning tunneling microscopy of vertically ordered InAs quantum dots*, Appl. Phys. Lett. **71**, 1083 (1997).

[Yof01] A. D. Yoffe, *Semiconductor quantum dots and related systems: electronic, optical, luminescence and related properties of low dimensional systems*, Adv. in Phys. **50** (1), 1 (2001).

[Yu96] P. Y. Yu and M. Cardona, *Fundamentals of Semiconductors - Physics and Materials Properties*, Springer, Berlin (1996).

[Yus97] G. Yusa and H. Sakaki, *Trapping of photogenerated carriers by InAs quantum dots and persistent photoconductivity in novel GaAs/n-AlAs field-effect transistor structures*, Appl. Phys. Lett. **70** (3), 345 (1997).

[Yus98] G. Yusa and H. Sakaki, *Trapping of a single photogenerated hole by an InAs quantum dot in GaAs/n-AlGaAs quantum trap FET and its spectral response in the near-infrared regime*, Physica E **2**, 734 (1998).

[Zha98] S. K. Zhang, H. J. Zhu, F. Lu, Z. M. Jiang, and X. Wang, *Coulomb charging effect in self-assembled Ge quantum dots studied by admittance spectroscopy*, Phys. Rev. Lett. **80** (15), 3340 (1998).

[Zha99] S. K. Zhang, H. J. Zhu, F. Lu, Z. M. Jiang, and X. Wang, *Erratum: Coulomb charging effect in self-assembled Ge quantum dots studied by admittance spectroscopy*, Phys. Rev. Lett. **82** (12), 2622 (1999).

[Zha00] S. Zhang, F. Lu, Z. Jiang, and X. Wang, *Coulomb charging effect of holes in Ge quantum dots studied by deep level transient spectroscopy*, Thin Solid Films **369** (1-2), 65 (2000).

Publications

- *Carrier escape and level structure of InAs/GaAs quantum dots*
  C. M. A. Kapteyn, M. Lion, R. Heitz, D. Bimberg, P. Brunkov, B. V. Volovik, S. G. Konnikov, A. R. Kovsh, and V. M. Ustinov
  Proc. 25th Int. Conf. on the Physics of Semiconductors, Osaka, Japan, N. Miura and T. Ando eds., Springer, Berlin, 1045 (2001).
- *Fermi-filling of Ge quantum dots in Si*
  C. M. A. Kapteyn, R. Heitz, D. Bimberg, C. Miesner, T. Asperger, K. Brunner, and G. Abstreiter
  Proc. 25th Int. Conf. on the Physics of Semiconductors, Osaka, Japan, N. Miura and T. Ando eds., Springer, Berlin, 1053 (2001).
- *Capacitance-voltage characteristics of self-organized quantum dots embedded in a pn junction*
  R. Wetzler, C. M. A. Kapteyn, R. Heitz, A. Wacker, E. Schöll, and D. Bimberg
  Proc. 25th Int. Conf. on the Physics of Semiconductors, Osaka, Japan, N. Miura and T. Ando eds., Springer, Berlin, 1093 (2001).
- *Hole emission from Ge/Si quantum dots studied by time-resolved capacitance spectroscopy*
  C. M. A. Kapteyn, M. Lion, R. Heitz, D. Bimberg, C. Miesner, T. Asperger, K. Brunner, and G. Abstreiter
  phys. stat. sol. (b), **224** (1), 261 (2001).
- *Time-resolved capacitance spectroscopy of hole and electron levels in InAs/GaAs quantum dots*
  C. M. A. Kapteyn, M. Lion, R. Heitz, D. Bimberg, P. Brunkov, B. V. Volovik, S. G. Konnikov, A. R. Kovsh, and V. M. Ustinov
  phys. stat. sol. (b), **224** (1), 57 (2001).
- *Capacitance-voltage spectroscopy of self-organized InAs/GaAs quantum dots embedded in a pn diode*
  R. Wetzler, C. M. A. Kapteyn, R. Heitz, A. Wacker, E. Schöll, and D. Bimberg
  phys. stat. sol. (b), **224** (1), 79 (2001).

- *Comparison of hole and electron emission from InAs quantum dots*
  C. M. A. Kapteyn, M. Lion, R. Heitz, D. Bimberg, P. Brunkov, B. V. Volovik, S. G. Konnikov, A. R. Kovsh, and V. M. Ustinov
  Proc. 8th Int. Symp. ”Nanostructures: Physics and Technology”, St. Petersburg, Russia, 375 (2000).
- *Many-particle effects in Ge quantum dots investigated by time-resolved capacitance spectroscopy*
  C. M. A. Kapteyn, M. Lion, R. Heitz, D. Bimberg, C. Miesner, T. Asperger, K. Brunner, and G. Abstreiter
  Appl. Phys. Lett. **77** (25), 4169 (2000).
- *Capacitance-voltage characteristics of InAs/GaAs quantum dots embedded in a pn structure*
  R. Wetzler, A. Wacker, E. Schöll, C. M. A. Kapteyn, R. Heitz, and D. Bimberg
  Appl. Phys. Lett. **77** (11), 1671 (2000).
- *Hole and electron emission from InAs quantum dots*
  C. M. A. Kapteyn, M. Lion, R. Heitz, D. Bimberg, P. Brunkov, B. V. Volovik, S. G. Konnikov, A. R. Kovsh, and V. M. Ustinov
  Appl. Phys. Lett. **76** (12), 1573 (2000).
- *Carrier emission processes in InAs quantum dots*
  C. M. A. Kapteyn, M. Lion, F. Heinrichsdorff, R. Heitz, M. Grundmann, and D. Bimberg
  Physica E **7**, 388 (2000).
- *Electron escape from InAs quantum dots*
  C. M. A. Kapteyn, F. Heinrichsdorff, O. Stier, R. Heitz, M. Grundmann, N. D. Zakharov, D. Bimberg, and P. Werner
  Phys. Rev. B **60** (20), 14265 (1999).
- *Emission of electrons from the ground and first excited states in self-assembled InAs/GaAs quantum dot structures*
  P. N. Brunkov, A. R. Kovsh, V. M. Ustinov, Yu. G. Musikhin, N. N. Ledentsov, S. G. Konnikov, A. Polimeni, P. C. Main, L. Eaves, and C. M. A. Kapteyn
  J. Electron. Mater. **28**, 486 (1999).
- *Electron emission from InAs quantum dots*
  C. M. A. Kapteyn, F. Heinrichsdorff, O. Stier, M. Grundmann, and D. Bimberg
  Proc. 24th Int. Conf. on the Physics of Semiconductors, Jerusalem, Israel, D. Gershoni ed., World Scientific, Singapore, paper 1339 (1999).
- *Sample-specific conductance fluctuations modulated by the superconducting phase*
  S. G. den Hartog, C. M. A. Kapteyn, B. J. van Wees, T. M. Klapwijk, W. van der Graaf, and G. Borghs
  Physica B **249-251**, 485 (1998).

- *Transport in multi-terminal normal-superconductor devices: reciprocity relations, negative and nonlocal resistances, and reentrance of the proximity effect*
  S. G. den Hartog, C. M. A. Kapteyn, B. J. van Wees, T. M. Klapwijk, and G. Borghs
  Phys. Rev. Lett. **77** (24), 4954 (1996).

- *Phase coherent transport in a multi-terminal superconductor / two-dimensional electron gas quasiparticle interferometer*
  B. J. van Wees, S. G. den Hartog, C. M. A. Kapteyn, T. M. Klapwijk, and G. Borghs
  in "Correlated Fermions and Transport in Mesoscopic Systems", T. Martin, G. Montambaux and J. Tran Thanh Van eds., Editions Frontieres, Gif-sur-Yvette, 277 (1996).

- *Electron transport in multi-terminal 2DEG-superconductor devices*
  S. G. den Hartog, C. M. A. Kapteyn, B. J. van Wees, T. M. Klapwijk, and G. Borghs
  Czechoslovak Journal of Physics **46**, 2325 (1996).

- *Superconducting phase tuned sample-specific conductance fluctuations*
  S. G. den Hartog, C. M. A. Kapteyn, B. J. van Wees, T. M. Klapwijk, W. van der Graaf, and G. Borghs
  Physica B **227**, 229 (1996).

- *Sample-specific conductance fluctuations modulated by the superconducting phase*
  S. G. den Hartog, C. M. A. Kapteyn, B. J. van Wees, T. M. Klapwijk, W. van der Graaf, and G. Borghs
  Phys. Rev. Lett. **76** (24), 4592 (1996).

Acknowledgements

Science is teamwork and I feel indebted to many people who contributed significantly to the success of the work presented in this book – in one way or the other. I would like to thank some of them explicitly here, and I apologize to all those who should have also been mentioned.

First of all, I have to thank Prof. Bimberg for offering me to work in his group on such a fascinating topic and for his steady support of my research. To Robert Heitz I owe many fruitful discussions, well-founded critiques, and countless practical tips. Furthermore, I received a great deal of support and motivation from him. Without his contributions, the work would have evolved differently. I would like to express my gratitude to Prof. Marius Grundman for his kind availability for physical (and non-physical) questions. I have to thank Armin Dadgar for introducing me to the DLTS system, as well as his help and numerous hints concerning experimental techniques and equipment. I must thank Oliver Stier for calculations of the electronic states of ”my” QDs and his remarkable competence in all mathematical and numerical questions. Also Andrei Schliwa contributed with some calculations. There are too many things to thank my friend and colleague Volker Türck. So I resort to just mentioning here, the great scrambles we shared to the summit of Mt. Fuji and on the peaks of the Tateyama ridge, in the Japanese Alps, in the snow-storm last autumn.

For many PL measurements and his eagerness to contribute whenever possible, I would like to thank my fellow PhD candidate and ski champion Florian Guffart. To Sven Rodt I feel grateful, aside from his occasional life-saving supply of chocolate, for his tips concerning all kinds of software problems. In Alexander Weber I found a colleague to discuss physical questions, a companion for clever and funny lunch debates, and a fellow sufferer in the hardships of the life as a PhD candidate. The excellence Bernd Ludwig exhibited in developing electronic circuits for specialized applications, and his skills in examining and repairing defective pieces of equipment,

repeatedly amazed me. It was a pleasure working with him. Also Jörg Döhring and the crew from the mechanics workshop, who always did an excellent job, need to be mentioned in this context. I feel indebted to the students I was allowed to supervise, Maurice Lion and Jörg Ehehalt, not only for their immediate contributions to this work, but also for making me learn certain things they may not even have realized. I would also like to thank all the other present and former members of the group of Prof. Bimberg, with whom I was allowed to work. They made the atmosphere enjoyable, not only during several conference and skiing excursions, but also in the laboratory.

I enjoyed a fruitful cooperation with Reinhard Wetzler, Andreas Wacker, and Prof. Schöll from the Institute of Theoretical Physics. I furthermore owe gratitude to Prof. Schöll for preparing the second expert opinion on my thesis. For several samples of Ge QDs in Si and discussions on capacitance experiments I am grateful to Christian Miesner and Thomas Asperger from the group of Prof. Abstreiter of the "Walter-Schottky-Institut", Munich. I have to thank Oliver Schmid and Karl Eberl from the "Max-Planck-Institut für Festkörperphysik" in Stuttgart for their supply of samples and fruitful discussions. I had a productive cooperation with my colleague Pavel Brounkov from the "A.F. Ioffe Institute", St. Petersburg, who visited and worked with me for three months during the early stages of my work. Several scientists in other institutions supported me with invitations to hold seminar talks and by exhibiting remarkable interest in my work. I feel very thankful for this acknowledgement.

A personal grant over a period of three years from the "Studienstiftung des deutschen Volkes" and additional travel support in several cases is gratefully acknowledged. Furthermore, part of this work was funded by DFG in the framework of SFB 296 and by the INTAS-RFBR program 95-IN-618.

I owe to my family for their steady support and their continuous interest in the progress of my work. This work would not have been possible without many dear friends outside university who took care I would not loose touch with the "real world". And I am very grateful to so many special people with whom I met during the last years.

I would like to thank my "antipodean" friend Luke Gartlan for the strenuous task of scrupulously proofreading the manuscript and improving grammar, clarity, and language in numerous cases. The contents of the biggest part of this work must have been as cryptic as a secret language to him.

Thank you, Anna Maria Bellardi.